

# **Nanodelivery of Novel Inhibitors of ERCC1/XPF for Sensitizing Colorectal Cancer Cells to Platinum Drugs**

by

**Parnian Mehinrad**

A thesis submitted in partial fulfillment of the requirements for the degree of

Master of Science

in

Pharmaceutical Sciences

Faculty of Pharmacy and Pharmaceutical Sciences

University of Alberta

© Parnian Mehinrad, 2023

**Abstract:**

This project's long-term goal is to increase the efficacy of genotoxic therapeutics through the sensitization of cells to DNA-damaging therapy ahead of the treatment. The focus of this project was on the enhancement of platinum-based chemotherapeutics in colorectal cancer using colorectal cancer cell lines as models of the disease. For this purpose, a novel inhibitor of a DNA repair enzyme involved in the repair of DNA caused by platinum-based chemotherapeutics, i.e., small molecule inhibitors of ERCC1-XPF heterodimerization, namely A4 and pyronaridine were used. To reduce the systemic effect of ERCC1-XPF inhibitors, that can lead to the sensitization of normal cells as well as cancer cells to DNA-damaging chemotherapeutics nano delivery systems of A4 and pyronaridine were also developed. Inhibition of ERCC1/XPF, a heterodimeric enzyme complex with endonuclease activity that participates in the repair of DNA inter- and intra-strand crosslinks, by A4, pyronaridine, and their nano-formulations was hypothesized to make cells sensitive to DNA damage by platinum-based chemotherapeutics. The results of our studies led to the development of optimum polymer and lipid-based nano-formulations for delivery of A4 and pyronaridine, respectively, showing maximum encapsulation efficiency, <50 % drug release within 24 hrs, and average diameter of < 150 nm. Free and particularly encapsulated inhibitors of ERCC1/XPF were able to sensitize colorectal cancer cells to the cytotoxic effects of platinum-based chemotherapeutics under study at specific dose ratios. The sensitizing effect of ERCC1/XPF inhibitors and their encapsulated counterparts was more noticeable for carboplatin.

## Preface

**Chapter 2** briefly explains the chemosensitization of colorectal cancer with compound A4. Compound A4 was synthesized by Dr. Ahmed H.M. Elmenoufy while he was a Ph.D. student in Dr. West Lab in the faculty of chemistry. Section 2.2.2 explains the synthesis of A4 briefly. I performed the main experiments in this study and am responsible for the manuscript composition. Dr. West's Lab did the synthesis and purification of the A4 compound. Dr. David Jay performed the Proximity ligation assay (PLA) test described in the 2.2.7 section, and I provided the formulation that was tested. PLA assay was done under Dr. Weinfeld's supervision. Dr. Lavasanifar was the supervisor and the one who corrected the manuscript, while Dr. Weinfeld always helped us with his helpful notes and comments.

**Chapter 3** is focused on utilizing an antimalaria drug that is clinically available as a chemosensitizer in the colorectal cancer cell line. Dr. West's Lab figured out the potential of the pyronaridine compound. Most of the tests were carried out by me. Dr. Emami \_our previous Lab member and a visiting professor from the University of Esfahan performed parts of the release study and the stability assay. Also, he helped me with writing some parts of the manuscript. The rest of the manuscript is my original work, and it was supervised and corrected by Dr. Lavasanifar. Dr. Weinfeld always helped us with his helpful notes and comments.

## Dedication

✈ To Pouneh Gorji, Arash Pourzarabi, Nasim Rahmanifar, Elnaz Nabiyyi, and all other university students who were killed in the tragedy of flight PS752 before they ever had the chance to graduate.

## Acknowledgments

I am blessed with having extraordinary people in my life which without their help, I would never get here.

First and foremost, I would like to extend my sincere appreciation to my supervisor Dr. Afsaneh Lavasanifar. By giving me a chance to work under her supervision, not only she shaped me toward excellence and a far better version of myself but also gave me once in a lifetime opportunity to experience life in one of the best universities in Canada. As a woman, I could never ask for a better role model in my life. I take great pride in spending these years as a member of her group.

I would like to thank my supervisory committee members, Dr. Raimar Loebenberg and Dr. Hasan Uludag, for their helpful comments and suggestion over these years.

I would like to express my sincere appreciation for all the help and support that Dr. Weinfeld and Dr. West provided me.

I sincerely thank Dr. Farzad Kobarfard. Without his help, I would never be here. I will always cherish the memories of the time I had the pleasure of working with him. He will always be the example of the most successful yet very humble person I have ever met.

I am genuinely thankful to all the current and previous Lab mates. Dr. Vakili who helped me understand polymer chemistry and was an important support during my journey. Dr. Sam Sadat, who was not only my senior in the lab who taught me almost all the Lab techniques but also still supports me with his kind and supportive words. Dr. Waleed Mohammad Saeed, our previous postdoctoral fellow who taught me a lot and supported me during the first couple of months of my program. Dr. Igor Paiva the previous Ph.D. student and Postdoc who were like my big brother and taught me the importance of being dedicated and accurate while doing Lab work and Nasim Sarrami who is my friend, my teacher, my Lab-mate and more important the real-life example of how much you can learn from your peers. Also, the rest of my fabulous Lab mates, Helia Hosseini Nejad, Sirazum Munira, Tanin Shafati.

I acknowledge the funding agencies that have supported me during my master's program. Alberta cancer foundation, NMIN, and CIHR. Also, the faculty of graduate studies and research (FGSR) and the faculty of pharmacy and pharmaceutical sciences.

I would like to thank all my Friends. Without them, I would never survive this journey. Sara Sohrabi, Shayan Habibi, Ali Hejazi, Farnoosh Azour, Nikoo Aghaei, Bedir Tapkan, Liam Peet Pare, Milad Zamani, Afarin Nazarijou, Maryam Soufisiavash, Vida Goudarzi, Ardavan Mofidi and Jake Lee,

Lastly, a heartfelt thanks to my beloved family for always believing in me and supporting me through everything. My dear sister Pardis Mehinrad, my gorgeous mother, Azadeh Hezarkhani, and my hero and the wisest man that I know, my father, Abolfazl Mehinrad.

## Table of Contents

Chapter One: Introduction.....	1
1.1. Undefeated: Cancer .....	2
1.2. Treatment options: .....	3
1.3. Platinum-based drugs: .....	5
1.4. Chemotherapy and its shortcomings: .....	7
1.5. DNA Damages, How and why?.....	7
1.6. Major DNA repair and associated therapeutic resistance. ....	8
1.7. Nucleotide Excision Repair (NER):.....	9
1.8. ERCC1-XPF and the effect of blocking it with small molecules:.....	12
1.9. Nanotechnology in Cancer therapy: .....	13
1.10. Polymeric Micelle .....	14
1.11. Liposomal nano carriers .....	15
1.12. Rationale .....	17
1.13. Hypothesis.....	19
1.14. Objectives.....	20
Chapter Two: Nano-encapsulation of a novel inhibitors of ERCC1-XPF for targeted sensitization of colorectal cancer to platinum-based chemotherapeutics .....	21
2.1. Introduction.....	22
2.2. Material and Methods .....	24
2.2.1. Materials.....	24
2.2.2. Synthesis of A4 .....	25
2.2.3. Synthesis and characterization of polymers .....	25
2.2.4. Self-assembly of prepared block copolymers .....	27
2.2.5. Characterization of loaded and unloaded PMs.....	27
2.2.6. In Vitro drug release .....	28
2.2.7. Cell lines.....	29
2.2.8 Proximity ligation assay .....	29
2.2.9. Cytotoxicity Assay .....	30

2.2.10. Colony formation assay .....	30
2.2.11. Statistical Analysis.....	31
2.3. Results .....	31
2.3.1. Physicochemical Characterization of polymeric micellar formulations .....	31
2.3.2. In Vitro Drug Release .....	34
2.3.3. Proximity ligation Assay.....	35
2.3.4. In Vitro nonspecific cytotoxicity of A4 and its PEO-PBCL PM formulation against CRC cells .....	36
2.3.5. Sensitization of CRC cells to Carboplatin by A4 and its PEO-PBCL micellar formulation .....	38
2.3.6. Sensitization of CRC cells to Oxaliplatin by A4 and its PEO-PBCL micellar formulation .....	40
2.3.7. Colony forming Assay .....	41
2.4. Discussion:.....	54
Chapter Three: Repurposing pyronaridine as a novel inhibitor of heterodimeric ERCC1-XPF DNA endonuclease complex for target sensitization of colorectal cancer to platinum-based chemotherapeutics .....	57
3.1. Introduction.....	58
3.2. Material and Methods .....	60
3.2.1. Materials.....	60
3.2.2. Preparation of Pyronaridine-Loaded Liposomes.....	61
3.2.3. Encapsulation of Drugs in Liposomes.....	62
3.2.4. Characterization of loaded and unloaded liposomes .....	62
3.2.5. In vitro drug release.....	63
3.2.6. Liposome stability Assay.....	65
3.2.7. Cell lines.....	65
3.2.8. Assessing the Cell toxicity of Pyronaridine and determining its IC50 in colorectal cancer model .....	66
3.2.9. Assessing the Cell toxicity assay in Combenefit format .....	66
3.2.10. Colony formation assay .....	67
3.2.11. Statistical Analysis .....	67
3.3. Results .....	67



3.3.1. Optimization of the Liposomal formulation of pyronaridine .....	67
3.3.2. Stability of prepared liposomal formulations .....	70
3.3.3. Release Study.....	72
3.3.4. In vitro nonspecific cytotoxicity of Pyronaridine and its liposomal formulation against CRC cells:.....	75
3.3.5. Sensitization of CRC to Carboplatin by Pyronaridine and its liposomal formulation and assessing the possibility of synergism .....	76
3.3.6. Colony Forming Assay.....	80
3.4. Discussion.....	88
Chapter four: conclusion and future work .....	93
4.1. Conclusions.....	94
4.2. Future works .....	95
References: .....	96

## List of tables:

<b>Table 2.1:</b> Physicochemical characteristics of the self-assembled empty and A4 loaded block copolymer micelles (n=3).....	33
<b>Table 2.2:</b> The IC <sub>50</sub> (mean ± SD) of free A4 against colorectal cancer cell lines measured by MTT assay (n=3) .....	37
<b>Table 2.3:</b> The IC <sub>50</sub> of free A4 against colorectal cancer cell lines measured by MTT assay (n=3) .....	37
<b>Table 3.1:</b> Characteristics of pyronaridine-loaded liposomal formulations prepared from various phospholipids with an interior pH of 3.5. ....	68
<b>Table 3.2:</b> Characteristics of empty and pyronaridine-loaded liposomal formulations prepared from DSPC/DSPE-PEG and cholesterol with different interior pH.....	68
<b>Table 3.3:</b> The IC <sub>50</sub> (mean ± SD) of free PYD and LPY against colorectal cancer cell lines measured by MTT (n=3).....	75

## List of Figures

<b>Figure 1.1:</b> Chemical structure of platinum-based drugs.....	6
<b>Figure 1.2:</b> DNA damage and repair pathway. The figure demonstrates some common causes of DNA damage and the repair pathways (34) .....	9
<b>Figure 1.3:</b> A simplified model of Nucleotide Excision Repair (NER) pathway and its sub pathways. There are two sub-pathways in the recognition of the damage in the DNA A) GG-NER and B) TC-NER. There are 4 major steps in the NER pathway, 1. Recognition 2. verification 3. Excision 4. Gap filling that are demonstrated in simplified version (45).....	11
<b>Figure 1.4:</b> The schematic view of the polymeric micelles and example core, shell structure. Shell: Polyethylene glycol or PEO, Core: poly (D, L-lactide) or PDLA, poly ( $\alpha$ -benzyl carboxylate- $\epsilon$ -caprolactone) or PBCL and polycaprolactone or PCL .....	15
<b>Figure 1.5:</b> Schematic view of the liposomal formulation. Indicating different phospholipids incorporated in the project and a schematic demonstration of hydrophilic drug encapsulated in the core of the liposomes. ....	17
<b>Figure 1.6:</b> The chemical structure of ERCC1-XPF inhibitor known as A4 .....	18
<b>Figure 1.7:</b> The chemical structure of PYD an antimalaria drug which inhibits the interaction of ERCC1-XPF .....	19
<b>Figure 2.1:</b> HPLC chromatogram of <b>A4</b> , yielded a purity of 98%.....	32
<b>Figure 2.2:</b> TEM Pictures of PMs (loaded and unloaded with A4). Images were obtained at a magnification of 110,000x at 75kv.....	34
<b>Figure 2.3:</b> The in vitro release profile of A4 (mean $\pm$ SD, n=3) from the three polymeric micellar carriers vs. the release of free A4. ....	35
<b>Figure 2.4:</b> This figure indicates that A4 (2 $\mu$ M) loaded into PBCL was able to disrupt the XPF-ERCC1 dimer when loaded directly into SW620 cells. This action could not be replicated by PBCL alone, indicating that PM/A4 provided an appropriate vehicle to release A4 into SW620 cell and modified XPF-ERCC1 in situ.....	36
<b>Figure 2.5:</b> The comparison between the cytotoxicity of free and PEO-PBCL PM loaded A4 in three CRC cell lines following 24, 48, and 72 h incubation as determined by MTT assay ((n=3). 38	
<b>Figure 2.6:</b> Cytotoxicity of Carboplatin without and with A4 (Free or Polymeric micelles) at 72h incubation against A) HCT116 and B) SW620 cell line (n=3), There is a 4-hour time interval between the two treatments. * Shows statistically significant difference from control PM alone; * shows statistically significant from free A4 (Two-way ANOVA, Tukey's multiple comparison test) .....	39
<b>Figure 2.7:</b> Cytotoxicity of Oxaliplatin without and with A4 (free or polymeric micelles) at 72h incubation against A) HCT116 and B) Sw620 cell line (n=3). There is a 4-hour time interval between the two treatments. * Shows statistically significant difference from control PM alone;	

* shows statistically significant from free A4 (Two-way ANOVA, Tukey's multiple comparison test).....	41
<b>Figure 2.8:</b> The results of clonogenic assay following combination of A4 and A4 PM with carboplatin (3.125, 6.26, 12.5 $\mu$ M) or oxaliplatin (0.5, 1,2 $\mu$ M) against HCT116 (n=3).(* purple) Shows statistically significant difference from control PM alone; (* green) shows statistically significant from free A4 (Two-way ANOVA, Tukey's multiple comparison test).....	42
<b>Figure 2.9:</b> Clonogenic assay in SW620 cells treated with carboplatin (3.125, 6.25, 12.5 $\mu$ M) or oxaliplatin (0.5, 1,2 $\mu$ M) in the presence empty PMs or 0.0625, 0.5 $\mu$ M of free or PM loaded A4 (n=3) (* Purple) shows statistically significant difference from control PM alone; (* green) shows statistically significant from free A4 (Two-way ANOVA, Tukey's multiple comparison test).....	43
<b>Figure 2.10:</b> Clonogenic assay in HCT116, A4 (0.0625 $\mu$ M) and Carboplatin (3.125, 6.25, 12.5 $\mu$ M) (n=3) .....	45
<b>Figure 2.11:</b> Clonogenic assay in HCT116, A4 (0.0625 $\mu$ M) and Oxaliplatin (0.5, 1, 2) (n=3).....	46
<b>Figure 2.12:</b> Clonogenic assay in HCT116, A4 (0.5 $\mu$ M) and Carboplatin (3.125, 6.25, 12.5) (n=3) .....	47
<b>Figure 2.13:</b> Clonogenic assay in HCT116, A4 (0.5 $\mu$ M) and Oxaliplatin (0.5, 1, 2) (n=3).....	49
<b>Figure 2.14:</b> Clonogenic assay in SW620, A4 (0.0625 $\mu$ M) and Carboplatin (3.125, 6.25, 12.5) (n=3) .....	50
<b>Figure 2.15:</b> Clonogenic assay in SW620, A4 (0.0625 $\mu$ M) and Oxaliplatin (0.5, 1, 2) (n=3) .....	51
<b>Figure 2.16:</b> Clonogenic assay in SW620, A4 (0.5 $\mu$ M) and Carboplatin (3.125,6.25, 12.5) (n=3) 52	
<b>Figure 2.17:</b> Clonogenic assay in SW620, A4 (0.5 $\mu$ M) and Oxaliplatin (0.5, 1, 2) (n=3) .....	54
<b>Figure 3.1:</b> TEM pictures of DSPC with luminal pH of 3.5 Liposomal formulations (loaded and unloaded with pyronaridine). Images were obtained at 80 kV and two different magnifications of 18000x and 22000x and 89000x.....	69
<b>Figure 3.2:</b> Pyronaridine structure, showing the pKa of different protonable groups .....	70
<b>Figure 3.3:</b> Stability of DSPC-based liposomal formulations of pyronaridine in terms of <b>(A)</b> Average diameter, <b>(B)</b> Polydispersity index, and <b>(C)</b> Encapsulation efficiency formulations with different lumen pH (3.5 and 5) following storage at 22 or 4° C. ....	72
<b>Figure 3.4:</b> The effect of <b>(A)</b> phospholipid type and <b>(B)</b> interior pH of liposomal formulations on the in vitro release of pyronaridine. <b>(C)</b> The in vitro release profile of free versus encapsulated pyronaridine at set time points during 72h test. Release media: PBS+10 %BSA .....	74
<b>Figure 3.5:</b> The sigmoidal curves demonstrate half maximum inhibitory value (IC50) in <b>A)</b> HCT116 cell line free pyronaridine, <b>B)</b> liposomal formulation of pyronaridine, <b>C)</b> in SW620 cell line free pyronaridine, <b>D)</b> liposomal formulation of it .....	76
<b>Figure 3.6:</b> Combenefit format of presenting synergism data on <b>HCT116</b> cell line treated with <b>A)</b> Pyronaridine as free and <b>B)</b> liposomal formulation with <b>Carboplatin</b> . <b>C)</b> <b>HCT116</b> cell line treated with Pyronaridine as free and <b>D)</b> liposomal formulation in combination with <b>Oxaliplatin</b> .....	78

**Figure 3. 7:** Combeneft format of presenting synergism data on **SW620** cell line treated with **A)** Pyronaridine as free and **B)** liposomal formulation with **Carboplatin**. **C)** **SW620** cell line treated with Pyronaridine as free and **D)** liposomal formulation in combination with **Oxaliplatin**..... 79

**Figure 3. 8:** Clonogenic assay in HCT116 (0.15  $\mu$ M) and Carboplatin (3.125, 6.25, 12.5  $\mu$ M) (n=3). (\*Purple) Shows statistically significant differences from PBS as a control and PYD. \* Shows statistically significant difference from Lip as a control and LPY. (Two-way ANOVA, Tukey’s multiple comparison test)..... 81

**Figure 3. 9.** The results of clonogenic assay following combination of PYD (0.15, 0.6  $\mu$ M) and LPY with Carboplatin (3.125, .25, 12.5  $\mu$ M) and Oxaliplatin (0.5, 1, 2  $\mu$ M) against HCT116 and SW620. \* Shows statistically significant differences from the PBS as control and PYD. \* Shows statistically significant differences from the Lip as control and LPY. (Two-way ANOVA, Tukey’s multiple comparison test)..... 82

**Figure 3.10:** Clonogenic assay in HCT116, PYD (0.15  $\mu$ M) and Carboplatin (3.125, 6.25, 12.5  $\mu$ M) (n=3) ..... 84

**Figure 3.11:** Clonogenic assay in SW620, PYD (0.15  $\mu$ M) and Carboplatin (3.125, 6.25, 12.5  $\mu$ M) (n=3) ..... 85

**Figure 3.12:** Clonogenic assay in SW620, PYD (0.6  $\mu$ M) and Oxaliplatin (0.5, 1, 2  $\mu$ M) (n=3) ..... 87

**Figure 3.13:** Clonogenic assay in SW620, PYD (0.6  $\mu$ M) and Carboplatin (3.125, 6.25, 12.5  $\mu$ M) (n=3) ..... 88

## List of Abbreviations

°C, Celsius

μL, microliter

μM, micromolar

5-FU, 5-fluorouracil

BER, base excision repair

BSA, bovine serum albumin

CRC, Colorectal cancer

DLS, dynamic light scattering

DMEM, Dulbecco's Modified Eagle's Medium

DMSO, dimethyl sulfoxide

DNA, deoxy ribonucleic acid

DOPC, 1,2-dioleoyl-sn-glycero-3-phosphocholine

DP, degree of polymerization

DPPC, 1,2-dipalmitoyl-sn-glycero-3-phosphocholine

DSB, double strand break

DSPC, 1,2-distearoyl-sn-glycero-3-phosphocholine

DSPE-PEG (2000), 1,2-distearoyl-sn-glycero-3-phosphoethanolamine-N-[methoxy(polyethylene glycol)-2000]

EE, encapsulation efficiency

ERCC1, excision repair cross-complementation group 1

EPR, enhanced permeability and retention effect

FBS, fetal bovine serum

GG-NER, global-genome NER

h, hour

HhH2, helix-hairpin-helix

IC<sub>50</sub>, half maximal inhibitory concentration

In vitro, referring to the studies performed in living organisms

In vivo referring to the studies performed in cell culture

IR, ionizing radiation

K<sub>d</sub>, dissociation constant

LPY, liposomal pyronaridine

M, moles per liter

MeOH, methanol

Min, minute

mL, milliliter

MMC, mitomycin C

MMR, mismatch repair

MRT, mean release time

MTT, Thiazolyl Blue Tetrazolium Bromide

MW, molecular weight

MWCO, molecular weight cut-off

NER, nucleotide excision repair

nm, nanometer(s)

NMR, nuclear magnetic resonance

NP, nanoparticle

PBS, phosphate-buffered saline

PCL, poly( $\epsilon$ -caprolactone)

PDI, polydispersity index

PEG-400, polyethylene glycol-400

PEO, polyethylene oxide

PEO-*b*-PBCL, poly (ethylene oxide)-*b*-poly ( $\alpha$ -benzyl carboxylate- $\epsilon$ -caprolactone)

PEP-*b*-PCL, poly (ethylene oxide)-*b*-poly ( $\epsilon$ -caprolactone)

PLA, proximity ligation assay

PM, polymeric micelle

POPC, 1-palmitoyl-2-oleoyl-glycero-3-phosphocholine

PYD, pyronaridine

ROS, reactive oxygen species

SD, standard deviation

SDS, sodium dodecyl sulfate

SSB, single-strand break

TC-NER, transcription-coupled NER

TEM, transmission electron microscopy

THF, tetrahydrofuran

UV, ultraviolet



UV-vis, ultraviolet-visible

XP, xeroderma pigmentosum

ZP, zeta potential

# **Chapter One: Introduction**

## 1.1. Undefeated: Cancer

International Agency for Cancer Research states on its website that “One in five people worldwide develop cancer during their lifetime” (1). Right after cardiovascular diseases, cancer is the second leading cause of death globally. In 2020, 10 million individuals died because of cancer (2). Nowadays, we live in an era where access to appropriate healthcare has expanded, and global average living standards have increased. These policies have influenced the average life expectancy in most parts of the world. Even though these medical advancements have reduced communicable disease mortality rates internationally, cancer-related mortality has surged by about 40%. In the next 15 years, a further 60% increase is anticipated, with 13 million cancer fatalities predicted by 2030.

The key contributors to cancer-related mortality have also altered due to changes in disease diagnostics, the implementation of screening programs, and advances in therapeutics. Colorectal cancer (CRC) is the third most prevalent cancer (3). Over the past several years, the frequency of CRC has been drastically rising worldwide. According to estimates, 1.93 million new cases of CRC were diagnosed, and 0.94 million people died from CRC in 2020. Today more than 5.25 million individuals globally are affected by CRC, which is slightly fewer than breast cancer. This accounts for 7.79 million cancer cases (4).

Almost a decade ago, CRC was relatively uncommon, but today is a common malignancy in western countries, accounting for 10% of cancer-related deaths. Unhealthy dietary habits, inactivity, obesity, and aging populations are attributes of a surge in CRC cases (3).

The first step toward the treatment of the CRC patients is the diagnosis of the patients' clinical condition, the stage of CRC and whether the tumour is malignant. Different tests and modalities are used to define the patient's clinical condition (5).

In order to make the treatment as effective as possible, the treatment plan is tailored for each individual based on patient characteristics, tumor features and molecular profile of the cancer cell (5).

Due to various reasons CRC is much easier to be screened and treated in early stages compared to other malignancies. Firstly, CRC has a rather lengthy preclinical stage. Secondly to some extent it is easily detectable and treatable malignancy. Lastly endoscopic removal of the benign tumors and treatment of cancer in its early stages has a significant impact on the reduction of mortality from CRC (3).

Despite all that is mentioned above, about 10% of all cancers diagnosed each year, and cancer-related deaths globally are caused by CRC. Which is one of the major reasons why more effective treatment plans are essential (6).

## **1.2. Treatment options:**

The primary treatment method for those with non-metastatic CRC is surgery, which is carried out both as laparoscopic or open surgery (7–9). However, different factors such as patient's age and the staging of the cancer would limit the success of the surgery in CRC cure.

While the success in the treatment of non-metastatic colorectal cancer heavily depends on surgery and its quality, metastatic cases require a combination of different treatment approaches. In past twenty years, there has been a significant advancement in the systemic

treatment of patients with colorectal cancer. In non metastatic cases, colon cancer has no recognized neoadjuvant therapy. However, to lower the risk of local recurrence in rectal cancer, neoadjuvant radiation or chemoradiotherapy is advised for intermediate-stage and advanced-stage disease (10,11). Moreover, the success rate of surgery for non-metastatic colorectal cancer is considerably high and approximately only 5% of the patients would receive adjuvant chemotherapy. However, guidelines established by European and Japanese societies advised considering adjuvant therapy in high-risk cases, such as ones with poorly differentiated tumors (3,12).

Over the past two decades, there has been a considerable improvement in the survival of patients with metastatic colorectal cancer, and clinical trials have shown that a median overall survival of 30 months is achievable. The use of chemotherapeutics such as platinum based drugs, and irinotecan, the development of targeted therapies that target characteristics of the tumor or its microenvironment, and the adaptation of multidisciplinary approaches is responsible for this improvement in survival (3).

While around 80% of newly diagnosed CRC patients have localized tumor which is curative with surgery, adjuvant chemotherapy is recommended as a routine clinical practice (13). The rest of newly diagnosed population have metastatic melanomas that cannot be removed. Furthermore, around half of the patients experience a recurrence of the disease following surgical resection or develop metastasis mostly in liver or lung (14).

All that is mentioned above points to the fact that although surgery is the main curative option, chemotherapy must be given systematically to individuals with metastatic CRC (mCRC) in order to control their condition (15,16).

### **1.3. Platinum-based drugs:**

Platinum based drugs play a pivotal role as anti-tumor drugs in the treatment of different type of cancer. Cisplatin, the first generation of platinum- based chemotherapeutics showed a considerable efficacy in the clinical trials against a wide variety of solid tumors including ovarian, testicular, bladder, lung, head and neck and colorectal cancer right before it was realized that ototoxicity, dose dependent nephrotoxicity and cell resistance limit its overall efficacy. (17)

Due to the limitation that restricted the use of cisplatin, the next generation drug was developed. Carboplatin, a second generation of platinum-based drugs, with similar mechanism of action as the cisplatin drug was developed to overcome the limitations such as dose dependent nephrotoxicity of the first-generation drugs (17–19).

Carboplatin is less toxic and easier to administer in regular dosages. This is because the replacement of a more stable leaving group (cyclobutanedicarboxylate instead of chloride) in the chemical structure of carboplatin which led to an altered pharmacokinetic profile (20). Equal DNA adducts formation between carboplatin and cisplatin might partially account for these two drugs similar efficacies in treating most solid tumors (21).

In comparison to cisplatin, carboplatin demonstrated a significantly lower level of neurotoxicity, nausea and vomiting in the receiving patients.

Based on the Lexicomp, the drug data base, carboplatin is used in the treatment of advanced anal cancer, in combination with paclitaxel. "Target AUC 5 on day 1 every 4 weeks (in combination with paclitaxel) for 6 cycles or until disease progression or unacceptable toxicity (Rao 2020) or Target AUC 5 or 6 every 3 weeks (in combination with paclitaxel)"(22). Also, the combination of carboplatin and paclitaxel is used in the treatment of gastric cancer. "Target AUC 2 once weekly for 5 weeks (in combination with paclitaxel and concurrent radiation) prior to surgery or Target AUC 5 to 6 every 3 weeks (in combination with paclitaxel) " (23,24).

Oxaliplatin on the other hand not only is used for treatment of gastric cancer but also it used for the treatment of stage III colon cancer. Based on the same drug data base, Lexicomp, 85 mg/m<sup>2</sup> on day 1 every 2 weeks (in combination with infusional fluorouracil/leucovorin) for up to 12 cycles.

While both mentioned chemotherapeutic drugs show a limited success in colorectal cancer cases, the third-generation drug oxaliplatin- specifically in combination with 5-fluorouracil and leucovorin is the standard treatment protocol for CRC (25).

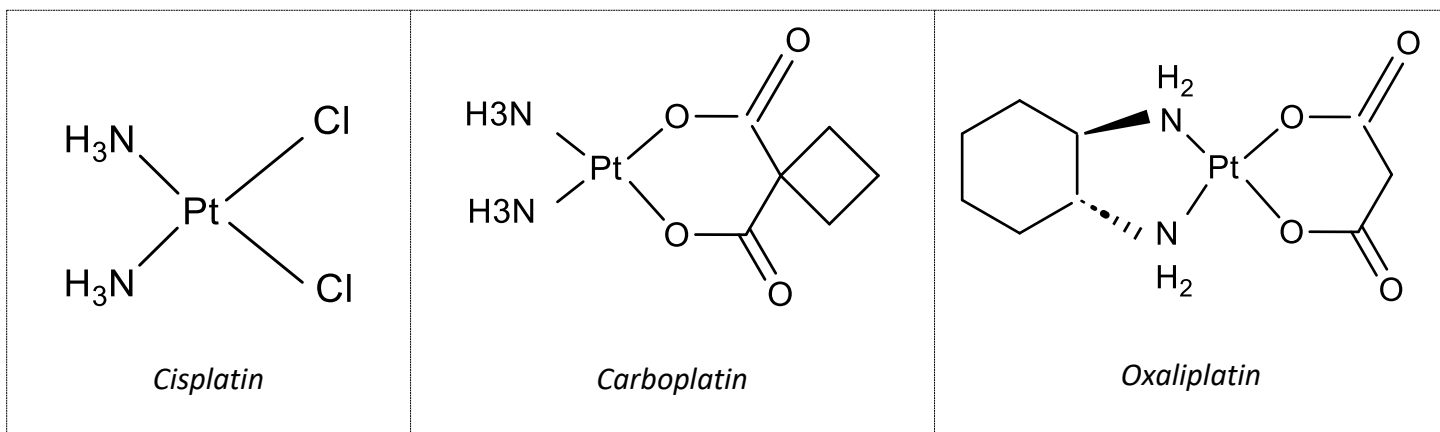


Figure 1.1: Chemical structure of platinum-based drugs

#### **1.4. Chemotherapy and its shortcomings:**

Despite being used to treat a variety of malignancies such as ovarian cancer and colorectal cancer, platinum chemotherapeutic drugs including carboplatin and oxaliplatin are hitting their limit due to the emergence of resistance. Chemo resistance, which could be either inherent or acquired occurs by many factors either inside or outside of the cancer cells

Numerous cellular adaptations, such as decreased uptake, inactivation by glutathione and other antioxidants, and increased levels of DNA repair and DNA tolerance are known to be responsible for resistance to platinum-based chemotherapeutics (26–28)

Cells use five different DNA repair pathways to protect their DNA from various lesions. Namely, nucleotide excision repair, mismatch repair, double strand break repair, base repair, and direct repair. The first two repair pathways (NER and MMR) seem to be the most significant DNA repair mechanisms known to be involved in the platinum chemoresistance. The mechanism of action of carboplatin is the formation of DNA adducts that result in intrastrand or interstrand cross-link, which disturb the structure of the DNA molecule and cause steric changes in the helix (26). An alteration in the DNA molecule's structure enables cell to recognize and repair DNA damage, which can keep the cell viable and lead to platinum resistance. (29,30).

#### **1.5. DNA Damages, How and why?**

The most significant molecule of our body, deoxyribonucleic acid (DNA), carries genetic information which is used to encode all living things. The DNA strands constantly endure different kinds of alterations and lesions. A part of these damages are results of regular metabolic activities that takes place inside of the cells and another part of the damages are due to numerous

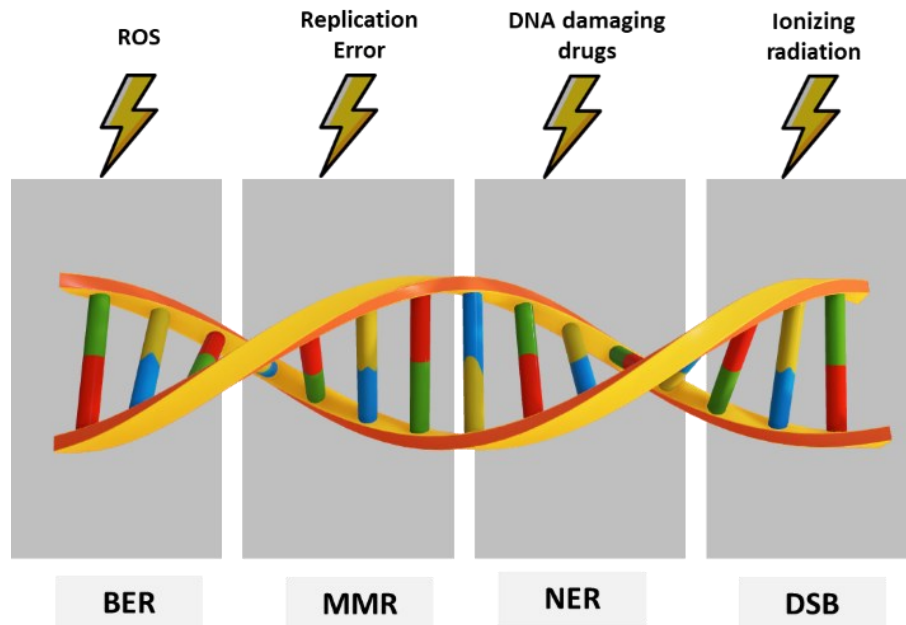


environmental and external variables such as damaging agents, atmospheric stressors, chemical, radiations, chemotherapeutics, and reactive oxygen species (ROS) that also contribute to the lesions that cells go through (31). As mentioned earlier, cells inherit different repair pathways to correct any mismatch or lesions that DNA go through.

### **1.6. Major DNA repair and associated therapeutic resistance.**

All cells have developed several repair mechanisms to correct lesions caused by chemicals and UV-radiations (32,33). Mammalian cells have four primary repair pathways namely, Nucleotide excision repair (NER), mismatch repair (MMR), base excision repair (BER) and double-strand break repair (34,35).

The underlying resistance mechanism to the genotoxic treatments that predominates in clinical situation cannot be determined with certainty. However, several experimental studies have shown that one of the primary underlying causes of resistance to radiotherapy and chemotherapy is increased DNA repair (32,36,37). The repair pathway that we focused on in these series of studies were the Nucleotide Excision Repair (NER) pathway.



*Figure 1.2: DNA damage and repair pathway. The figure demonstrates some common causes of DNA damage and the repair pathways (34)*

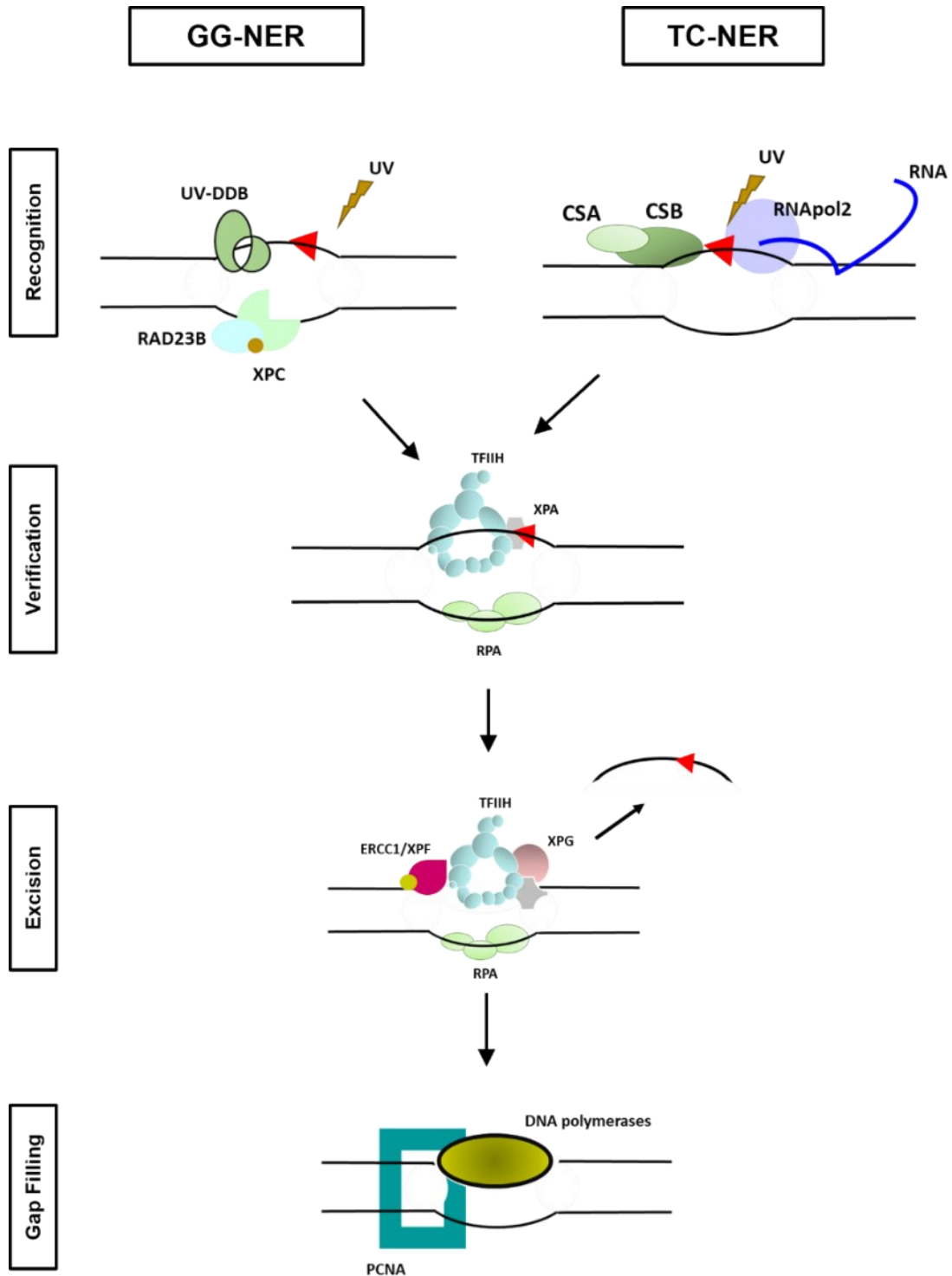
### 1.7. Nucleotide Excision Repair (NER):

It has been claimed that one of the primary causes of platinum resistance is DNA damage repair through the NER system (38). Mammals primarily employ nucleotide excision repair (NER) to remove bulky DNA lesions that could be produced by the UV radiations, environmental mutagens and certain cancer chemotherapeutic agents, and other environmental factors (38–40). NER is a very flexible repair pathway that can identify, confirm, and fix a wide variety of helix-distorting damages.

As it is shown in the **Figure 1.3**, a group of assembled repair proteins at the locations of the DNA damage mediate NER. Nucleotide Excision repair pathway, a fairly complicated mechanism, requires roughly thirty distinct proteins to carry out multi-steps of incise and patch process. (40–42). Global genome NER (GG-NER) and transcription-coupled NER (TC-NER) are two sub pathways which, through the action of damage recognition proteins, are involved in identifying the

damaged section. These two sub-pathways have same core mechanism but are distinguish from each other by how the lesions are detected (39). In contrast to GG-NER (Global genome Nucleotide Excision Repair) which removes damaged DNA from the whole genome, TC-NER (Transcription-coupled Nucleotide Excision Repair) performs a selective function in mending lesions found on the coding strand of genes that are being transcribed. (34,43)

Following the damage recognition by the proteins, the damaged DNA's backbone is excised by the sub-pathways with the aid of the excision and helicase proteins. The NER process is finished by ligating the nicks after both sides of the oligonucleotide have been removed and the nucleotide gap is filled. It is suggested that the process with which the DNA damage is bypassed, or the repair steps take place, will contribute to genomic instability and therapeutic resistance. (32,38,44).



*Figure 1.3: A simplified model of Nucleotide Excision Repair (NER) pathway and its sub pathways. There are two sub-pathways in the recognition of the damage in the DNA A) GG-NER and B) TC-NER. There are 4 major steps in the NER pathway, 1. Recognition 2. verification 3. Excision 4. Gap filling that are demonstrated in simplified version (45)*

## 1.8. ERCC1-XPF and the effect of blocking it with small molecules:

In mammalian cells, ERCC1-XPF protein complex functions as a 5'-3' structure-specific endonuclease and is engaged in several DNA pathways including Nucleotide excision repair pathway. It is essential for NER because it incises the damaged DNA strand at the 5' and 3' positions, respectively, to eliminate the pyrimidine-(6,4)- pyrimidone photoproducts (6-4PPs) and cyclobutene pyrimidine dimers (CPDs) brought on by UV irradiation. Additionally, the ERCC1-XPF heterodimer also plays a pivotal role in repair of chemically generated helix-distorting and bulky DNA lesions, which are all substrates for the NER pathway (34).

A total of 297 amino acids makes up the ERCC1 domain, which also includes a helix-hairpin-helix (HhH2) domain necessary for heterodimerization with XPF and a central region that interacts with DNA and the XPA protein but is not catalytically active. The XPF protein domain, on the other hand, consists of 916 amino acids and comprises important residues (FANCO) that are nuclease, helicase-like, and helix-hairpin-helix (HhH2) domains (34,46-48).

The Primary protein-protein interaction between ERCC1 and XPF is the development of a stable heterodimer complex by the heterodimerization of their hydrophobic C-terminal domains (47). Without the presence of XPF, it is expected that ERCC1 is unable to fold adequately in vitro, functioning as a scaffold for XPF during protein folding (47). Both proteins were demonstrated to be unstable in monomeric form and to instead aggregate once their hydrophobic interaction domains were exposed, which caused them to degrade quickly (34,47,48). It has been established that without dimerization, the protein complex derived from the catalytic domain of XPF lost its

ability to serve as an endonuclease. It has also been demonstrated that the catalytically inactive ERCC1 fragment is still necessary for the heterodimer complex activity (47).

The three ERCC1-XPF heterodimer targets with the highest therapeutic potentials are the XPA-binding domain necessary for the NER complex recruitment, the XPF endonuclease domain necessary for the ERCC1-XPF complex's catalytic activity, and the ERCC1-XPF interaction domain crucial for stability and catalytic activity are the three targets on the ERCC1-XPF heterodimer with the highest therapeutic potential.

### **1.9. Nanotechnology in Cancer therapy:**

A broad variety of nano-scaled drug carriers, often known as nanocarriers, have been created to enhance drug performance and overcome its pharmacokinetic resistance. Due to their small size and high surface area to volume ratio, nano-carriers exhibit properties distinct from those of bulk materials (49,50).

Nanocarriers are often designed to enable the delivery of medicinal or diagnostic agents to their site of action. Effective targeted delivery methods are expected to produce comparatively greater or more effective dosing at the targeted site while allowing for a lower systemic exposure of the drug. The growth of this discipline has been sparked by the anticipated advantages of decreased systemic adverse effects and concurrently better activity of the medications delivery by nanotechnology products (50,51).

Nanocarriers are known to be able to accumulate in the solid tumors passively due to the presence of leaky vasculature as well as impaired drainage of the lymphatic system. This mechanism which known as the enhanced permeation and retention (EPR) effect, is believed to

play a pivotal role in accumulation of nano sized carriers in tumors which is expected to enhance the exposure, thus specificity of encapsulated cargo within the nanocarrier for the tumor versus normal tissue. Targeted delivery is now a thriving area for nanomaterials and medicine delivery (52–58).

The nanoparticles must be able to avoid systemic identification and capture by the mononuclear phagocytic system in order to utilise the EPR effect for passive targeting. For this purpose, usually polyethylene glycol (PEG) modification of nano-carriers is used to lengthen nano-carrier stay in the blood circulation by avoiding immune system opsonization and clearance (50).

The development of a densely knit water network underlies the stealth effect of PEG chains. This will provide the nano-carrier with a hydrophilic surface that will inhibit adsorption of opsonins that may be recognized by the macrophages and mark the nanocarrier for uptake. PEG modification not only would prevent the nano carriers from being cleared by the immune system, prolonging their circulation duration which will eventually lead to enhanced their tumor accumulation, but also prevents particle aggregation (50,59–61).

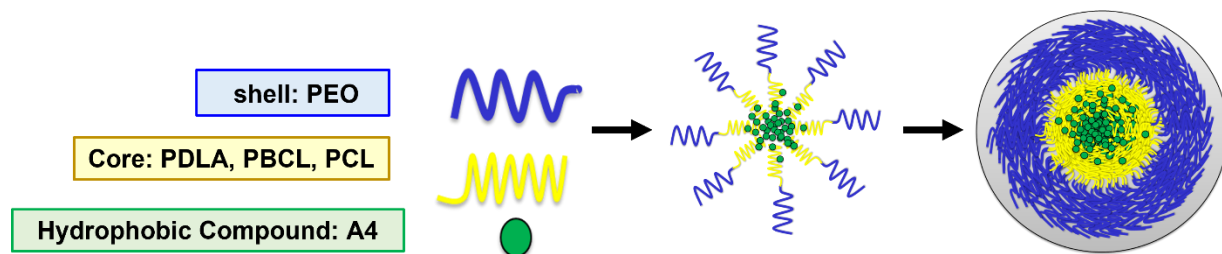
### **1.10. Polymeric Micelle**

Polymeric micelles have attracted a lot of attention as colloidal delivery methods that potentially meet the criteria for an optimal and flexible drug carrier. Polymeric micelles are usually spherical, core-shell nanostructures that are formed through the self-assembly of amphiphilic block copolymers in an aqueous environment They frequently employed for the solubilization of poorly water-soluble compounds and targeted drug delivery (50,62).

Their core is usually chemically manipulated to facilitate the encapsulation of water insoluble compounds, proteins, or DNA while the hydrophilic shell interfaces the biological fluid.

There are various reasons that would make the polymeric micelles a prime candidate for drug delivery. Firstly, their small size (<100nm) is anticipated to make it more probable for the particles to accumulate and distribute in the tumor adequately. Secondly their ability to encapsulate hydrophobic drugs has made polymeric micelles an excellent option for a vast group of compounds.

But above all due to the versatility of the choices for the core shell structure, polymeric micelles could be designed and created in a way that is suitable for the pathophysiology of the disease, physiochemical properties of the incorporated drug, the site of drug action, and the proposed route of administration (63).



*Figure 1.4: The schematic view of the polymeric micelles and example core, shell structure. Shell: Polyethylene glycol or PEO, Core: poly (D, L-lactide) or PDLA, poly ( $\alpha$ -benzyl carboxylate- $\epsilon$ -caprolactone) or PBCL and polycaprolactone or PCL*

### 1.11. Liposomal nano carriers

Lipid based nano-delivery systems have been the flagship of all the nanocarriers systems with many clinically available formulations in the market (64). Liposomes are microscopic spherical shaped vesicles composed of phospholipids bilayer. The property of the compound

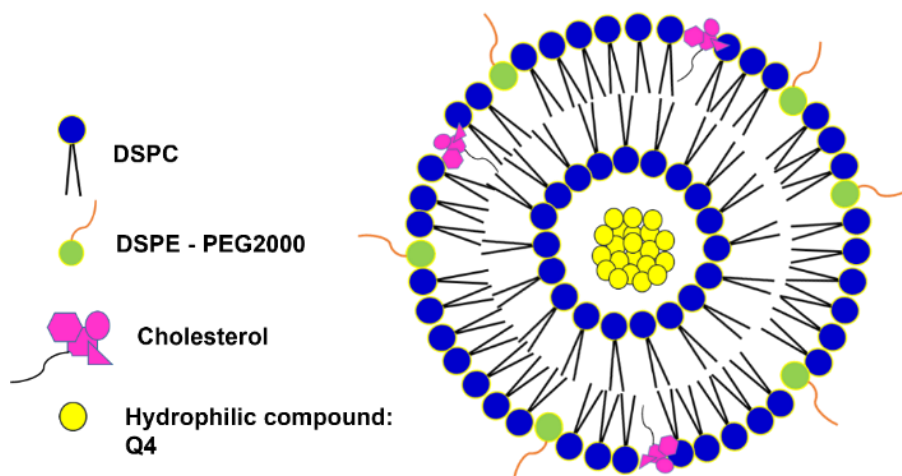


determines whether it is encapsulated in the core, the lipid bilayer or the interface between the two (65,66).

Compounds that are lipophilic are often integrated directly into the lipid bilayer, whereas drugs that are hydrophilic are typically contained within the central aqueous core. Following the general concept of any nano-delivery system, the loaded compound will take on the pharmacokinetic characteristics of the carrier rather than the free agent, which would make it more probable to accumulate in the tumor and distribute in the tissue (65–69).

Development of pegylated liposomes (STEALTH liposomes) were achieved after realizing that incorporation of polyethylene glycol causes the liposomes to remain the blood circulation longer which would increase the chance of them to accumulate in the site of action (66,67,70).

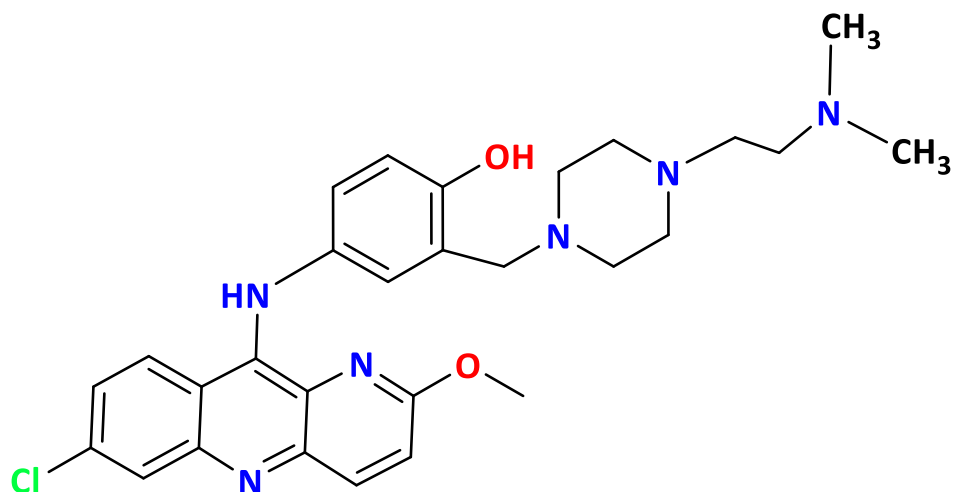
Considering that the major role of the compounds that are studied in this project are chemosensitization of the cancer cells to the effect of chemotherapy, the mutual factor in rationalizing the use of nanoparticles is the increase of tumor specificity of the chemosensitizer compounds so that the normal cells do not become sensitized to the effect of chemotherapy.



*Figure 1.5: Schematic view of the liposomal formulation. Indicating different phospholipids incorporated in the project and a schematic demonstration of hydrophilic drug encapsulated in the core of the liposomes.*

## 1.12. Rationale

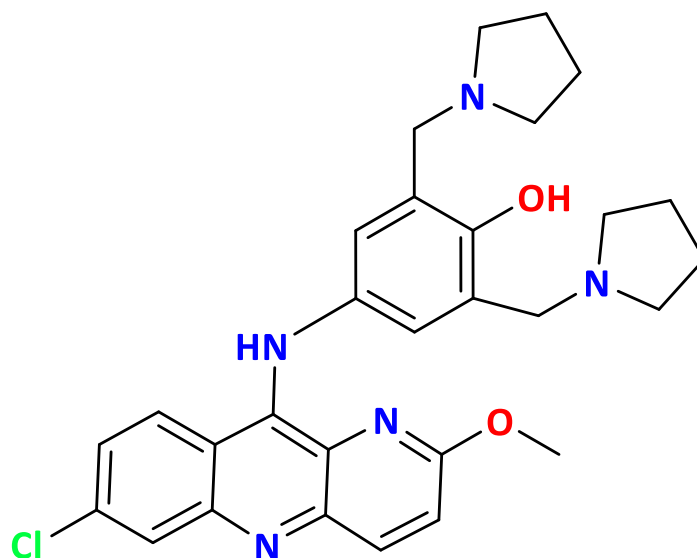
ERCC1-XPF is proven to be a key enzyme in the NER pathway which is involved in the repair of the damages that has been done to the DNA of the cells following radiation or treatment with DNA damaging agents such as platinum based chemotherapeutics or cyclophosphamide. (71). Based on the previous studies it has been proven that the inhibition of the interaction between the ERCC1 and XPF is able to sensitize the cell to the effect of genotoxic therapeutics. (47,48). Different generations of inhibitors of ERCC1/XPF dimerization has been developed as chemo and radio-sensitizing compounds by our collaborators, Dr Fred West and Dr Michael Weinfeld (71). Among all the synthesized compounds, Compound 4 (A4) were shown to be a potent inhibitor of ERCC1-XPF ( $IC_{50} = 0.33 \pm 0.12 \mu\text{M}$  and  $K_d 100 \pm 5$ ) (71). Considering that the A4 compound is water insoluble, in order to tackle the solubility issue and at the same time increase its tumor specificity, encapsulation of the compound in nanocarriers is proposed (71).



*Figure 1.6: The chemical structure of ERCC1-XPF inhibitor known as A4*

Considering the water insolubility of the compound and the previous success that polymeric micelles had in delivery of hydrophobic compounds, they are the prime nanocarrier candidates for the delivery of A4. (63)

While studying and synthesizing these series of compounds, the research group of Dr. Frank West's identified a chemically close structure to that of A4: i.e., an antimalaria drug, known as pyronaridine (**PYD**), as a potential ERCC1/XPF inhibitor (72). Based the recent studies not only PYD has demonstrated chemotherapeutic activity but also it has been shown to be a modulator of P-glycoprotein (73). Considering that PYD is water soluble, the main goal of its encapsulation is to increase its specificity and potency. For this purpose, the proposed nanocarrier was a liposomal delivery system with components similar to that of Doxil<sup>®</sup> formulation.



*Figure 1.7: The chemical structure of PYD an antimalaria drug which inhibits the interaction of ERCC1-XPF*

### 1.13. Hypothesis

**Project one:** Encapsulation of A4 (a water-insoluble inhibitor of XPF enzyme) in properly designed polymeric nano-carriers will enhance the aqueous solubility level of the drug, slowdown its release while keeping the chemo-sensitizing activity of this ERCC1/XPF inhibitor intact.

**Project two:** Liposomal formulation of pyronaridine (LPY) slowdown its release while keeping the chemo-sensitizing activity of this ERCC1/XPF inhibitor intact.

#### **1.14. Objectives**

- 1- To select the proper polymeric drug delivery system for A4
- 2- To examine the anti-cancer activity of the free and encapsulated drug in colorectal cancer model in combination with platinum drugs.
- 3- To develop and optimize liposomal formulation (Lpy) of PYD for passive tumor targeting
- 4- To examine the anti-cancer activity of the free and encapsulated drug in colorectal cancer model in combination with platinum drugs.

**Chapter Two: Nano-encapsulation of a novel inhibitors of ERCC1-XPF for targeted sensitization of colorectal cancer to platinum-based chemotherapeutics**

## 2.1. Introduction

Colorectal cancer is the third most diagnosed cancer, with 1.8 million cases worldwide. It is the second leading cause of cancer deaths, with a global annual rate of 850000 deaths (4,74). Based on the pattern of population growth and aging, it is anticipated that by 2040, 3.2 million new CRC cases will be diagnosed globally. While surgery is the most curative option for nonmetastatic cases, the patient outcome of treatment strongly depends on many factors, including the staging of cancer. Chemotherapy and radiotherapy could be employed to decrease the size of the tumor before surgery so that surgery would be possible (3).

Platinum drugs are used for the treatment of many types of cancers, such as ovarian, breast, lung, and colorectal cancer (28,75). The mechanism of action of platinum drugs is to bind to the DNA of a cell and form DNA adducts which will lead to intrastrand or interstrand cross-links. These cross-links will result in the disruption of the structure of DNA molecules. Both oxaliplatin and carboplatin cause DNA lesions which will finally lead to apoptosis of the cells. (26,29,76,77). However, the use of platinum-based drugs as chemotherapeutics has been associated with chemoresistance and dose-dependent adverse side effects. Chemoresistance to platinum drugs is shown to be associated with several underlying mechanisms, including decreased cellular uptake (78), accelerated detoxification (79), and enhanced DNA repair (29,75).

Although treating cancer cells with platinum DNA-damaging agents could result in lesions to the DNA of the cell followed by its apoptosis but it would also result in activation of many DNA repairing mechanisms such as Nucleotide Excision Repair pathway (NER) leading to resistance to

the effect of DNA damaging agents. Previous studies shows that NER pathway is a key pathway in defining the sensitivity of cancer to the effect of platinum-based drugs (26,76,77).

ERCC1-XPF is a heterodimeric enzyme which has a key role in NER pathway (80). In this structure ERCC1 is considered catalytically inactive and its main role is to stabilize XPF, while XPF has the endonuclease activity (81,82). ERCC1-XPF is an attractive target for sensitization of cancer to platinum based chemotherapeutics, due to the availability of its crystal structure and the availability of multiple binding sites on the protein that can be accessed by small molecule inhibitors (71).

Inhibition of XPF by small molecules, can prevent its dimerization with ERCC1 leading to rapid degradation of either protein and eventual sensitization of cancer cells to the effects to DNA damaging agents such as platinum-based chemotherapeutics (46,48).

Our research group have been focusing on synthesizing different small molecule inhibitors of ERCC1/XPF dimerization with the aim of sensitizing cancer cells to the effect of DNA damaging cancer therapeutics. A4 is one of these small ERCC1/XPF inhibitors developed by our team showing significant sensitization of colorectal cancer cells to cyclophosphamide and UV radiation in previous studies (71,83–85).

While preliminary results on A4 are promising, poor water solubility and lack of specificity to cancer cells would limit its further use for more thorough studies on this compound. To overcome these shortcomings, in the present research, we developed a polymeric micellar formulation of A4 that can increase the soluble levels of this ERCC1/XPF inhibitor. We then assessed the physicochemical properties of the developed formulation and its activity in combination with two



platinum-based chemotherapeutics in colorectal cancer cell lines. Nano-drug delivery systems of appropriate size and surface properties are known to accumulate in the solid tumor (52). Polymeric micellar formulations that are the subject of this study, have shown great potential in solubilisation of poorly soluble drugs and/or targeted delivery of the accommodated cargos in previous studies (63).

The results pointed to the potential of polymeric micellar formulations of A4 were able to not only enhance solubilized drug A4 levels, but to slow down its release and at the same time maintain activity of A4 in the inhibition of ERCC1/XPF in colorectal cancer cells and show synergy in combination with carboplatin.

## **2.2. Material and Methods**

### **2.2.1. Materials**

Methoxy-polyethylene oxide (mPEO) (average molecular weight of 5000 g/mol) bovine serum albumin (BSA), and research-grade organic solvents were purchased from Sigma (St. Louis, Mo, USA). L-lactide (98%) was purchased from Alfa Aesar, Lancashire (UK). D-Lactide (98%) was a generous gift from Purac, Schiedam, Netherlands.  $\epsilon$ -Caprolactone was purchased from Lancaster synthesis (UK).  $\alpha$ -Benzyl carboxylate- $\epsilon$ -caprolactone monomer was synthesized by 'Alberta Research Chemicals Inc.' (Edmonton, AB, Canada), according to a previously published procedure (86). Stannous octoate was purchased from Sigma Aldrich, purified, and dehydrated by toluene azeotropic distillation, which was followed by vacuum distillation. Cell culture media DMEM, fetal bovine serum (FBS), and penicillin-streptomycin were purchased from GIBCO. Spectra/Por dialysis tubing (MWCO, 3.4kDA) was purchased from Spectrum Laboratories (Rancho

Dominguez, CA)

### 2.2.2. Synthesis of A4

Synthesis of compound A4 was achieved through a one-pot sequential addition reaction in 3 steps as previously reported by our collaborator and shown in Figure 1A (Ref: J. Med. Chem. 2019, 62, 17, 7684–7696). Mannich reaction of *p*-acetamidophenol with formaldehyde and appropriate secondary amine in 2-propanol was carried out under reflux for 12 h. The solvent and excess of the unreacted formaldehyde from the resulting mixture was removed under vacuum and without isolating the compound, the resulting viscous residue was treated with 6 M HCl to deacetylate the acetamido group to furnish the primary amine as depicted for intermediate 1 in Figure 1B. Afterwards, an equimolar amount of 6,9-dichloro-2-methoxyacridine was added, affording after heating compound A4 in good yield after isolation and purification. The reaction sequence in synthesis is general, facile, and reproducible. The synthesized compound A4 were characterized by <sup>1</sup>H NMR, <sup>13</sup>C NMR, HRMS, IR and the purity of A4 was determined by HPLC (≥98% purity) as shown in **Figure 2.1**

### 2.2.3. Synthesis and characterization of polymers

#### 2.2.3.1. PEO-*b*-PBCL

The PEO-*b*-PBCL diblock copolymer was synthesized as it was described before (86). Briefly, the ring-opening polymerization of the 2.325 g of  $\alpha$ -benzyl carboxylate- $\epsilon$ -caprolactone (Mw:248 g/mol) was initiated with 1.25 g of PEO (methoxy polyethylene oxide) (Mw:5000 g/mol) using 4 drops of stannous octoate, as the catalyst. The reaction was conducted in a 10 mL ampule containing all the reactants and sealed under a vacuum. The reaction proceeded at 140 °C for 4 hours. The synthesized polymer was then purified through dissolving the product in

dichloromethane (DCM), precipitation with hexane at cold temperature (-20 C) for 10 minutes. The resulting precipitant was then washed by following the use of the DCM/hexane addition and cooling process for 5 to 10 times.

After purification, the synthesized diblock copolymer was characterized by  $^1\text{H}$  NMR (600 MHz Avance III- Bruker, East Milton, ON, Canada) using deuterated chloroform ( $\text{CDCl}_3$ ), as solvent. The area under the curve for peaks at 3.580 and 5.079 ppm related to PEG (polyethylene glycol) and  $\alpha$ -benzyl-carboxylate- $\epsilon$ -caprolactone groups in the polymer structure, respectively, were used to measure the molecular weight and degree of polymerization (Dp) of the hydrophobic block in the polymer assuming an average DP of 144 for the PEO block.

#### 2.2.3.2. *PEO-b-PCL*

The synthesis of *PEO-b-PCL* was carried out as described before (86). briefly a typical reaction, 1.25g methoxy polyethylene oxide (Mw:5000 g/mol) was reacted with 1.255g of  $\epsilon$ -caprolactone (Mw:114.4). The ampule was then sealed under a vacuum and kept in an oven with a temperature of 140 °C for 6 hours. The polymer was characterized by  $^1\text{H}$  NMR (600 MHz Avance III- Bruker, East Milton, ON, Canada) using deuterated chloroform ( $\text{CDCl}_3$ ), as solvent. The area under the curve for peaks at 3.664 and 4.079 ppm related to PEG (polyethylene glycol and caprolactone groups and  $\epsilon$ -caprolactone in the polymer structure were used to measure the molecular weight and the DP of the hydrophobic block in the polymer assuming an average DP of 144 for the PEO block.

#### 2.2.3.3. *PEO-PDLA (50-50)*

The synthesis of *PEO-PDLA (50-50)* was also carried out as described before (62,86). Polyethylene oxide (Mw:5000 g/mol) was the initiator and a 50:50 mixture of L-lactide and D-

lactide were used as monomers in this reaction (62). Briefly, MePEO (0.6 g) was reacted with a 50-50 ratio of L-lactide and D-lactide (total weight of 0.7g, 0.35g of D-lactide, and 0.35g of L-lactide) in an ampule. Stannous Octoate (5-6 drops) was used as the catalyst. The ampule was then sealed under a vacuum and kept in an oven with a temperature of 140 °C for 6 hours. The synthesized polymer was then purified as described above. The purified polymer was characterized by <sup>1</sup>H NMR (600 MHz Avance III- Bruker, East Milton, ON, Canada) using deuterated chloroform (CDCl<sub>3</sub>), as solvent. The area under the curve for peaks at 3.581 and 5.101 ppm related to PEG (polyethylene glycol and D, L Lactide groups in the polymer structure were used to measure the molecular weight and DP of the hydrophobic block in the polymer assuming an average DP of 144 for the PEO block.

#### **2.2.4. Self-assembly of prepared block copolymers**

A cosolvent evaporation method was used to prepare empty or drug-loaded polymeric micelles (PMs) (62,87). A4 and diblock copolymers were dissolved in 0.6 mL of acetone. The mixture was then added dropwise to 3 mL of double-distilled water. The remaining acetone evaporated under the fume hood overnight while stirring, using a magnetic bar. The PM dispersion was centrifuged at 11600 x g for 5 min. This was followed by filtration of the PMs using a 0.22µm MF-Millipore™ Membrane. (Syringe-driven Filter Unit, Millex, 33mm).

#### **2.2.5. Characterization of loaded and unloaded PMs**

The average size (Z-average), polydispersity index (PDI), and zeta potential (ZP) of the prepared PMs were assessed using dynamic light scattering (DLS) Malvern Zetasizer 3000 (Malvern Instruments Ltd., Malvern, UK). A4 has an absorbance at 470 nm. This was used to measure the amount of loaded drug using a plate reader (Synergy H1 Hybrid Reader Biotek,

Software Gene5 1.11) based on a calibration curve of the drug in a DMSO: water 50:50 solution. The prepared PMs dispersion in aqueous media was diluted with the same volume of DMSO to disrupt the PMs, and the concentration of A4 was measured by UV spectroscopy as described above. The A4 loading and loading efficiency were calculated based on the following equations.

$$A4 \text{ loading (\%)} = \frac{\text{Weight of the encapsulated A4 in PMs}}{\text{Total weight of the polymer in PMs}} \times 100$$

$$A4 \text{ Encapsulation efficiency (\%)} = \frac{\text{Weight of the encapsulated A4}}{\text{Initial weight of the A4 added}} \times 100$$

The stability of the PMs in terms of the potential for aggregation or drug leakage was assessed (88). For this purpose, the PMs were kept in a fridge and at room temperature for 20 days. The shape morphology, loading, and encapsulation efficiency of the drug during the storage period were assessed. The morphology of the prepared PMs was checked with TEM as described before (89). Briefly, PM samples in water (0.17 mg/mL) were transferred to a copper-coated grid and incubated at room temperature for 15s. The water was dried with a piece of Whatman paper. The samples were then stained using a 2% phosphotungstic acid solution. The excess stain was removed with filter paper after 2 minutes. The prepared TEM (Transmission Electron Microscopy) specimens were then analyzed in a Morgagni 268 TEM microscope (Philips/field emission). The inserted camera was Gatan a CCD camera.

#### **2.2.6. In Vitro drug release**

The *in vitro* release of loaded A4 from PMs was assessed using the equilibrium dialysis technique (n=3). Each dialysis bag (Spectrapor dialysis tubing, MWCO=3.5 kDa, Spectrum Laboratories, Rancho Dominguez, CA, USA.) was filled with 3mL of the PM formulation of A4 in

water. Each bag was immersed in 300 mL of the release solution containing double distilled water and 10 % BSA. The media was changed after 12h. At selected time points (0, 2, 4, 6, 8, 24 h) 200  $\mu$ L of samples were taken from inside the dialysis bags and replaced with fresh water. The A4 concentration remaining in the dialysis bags was quantified using a plate reader at 470 nm as described above (Synergy H1 Hybrid Reader Biotek, Software Gene5 1.11) (89). The drug concentration remaining in the bag was subtracted from the total drug concentration and used as the released drug concentration.

### **2.2.7. Cell lines**

Three cell lines HCT116, HT-29, and SW620 were initially purchased from American Type Culture Collection (ATCC) by Dr. Weinfeld's Lab and lent to us. The cells were grown in DMEM supplemented with 10% FBS and 1% penicillin-streptomycin (90).

### **2.2.8 Proximity ligation assay**

The interaction and disruption of ERCC1-XPF heterodimer is assessed after being treated with 2  $\mu$ M of A4 compound. Proximity ligation assay was performed as explained before (85,91,92). As a brief explanation, 30,000 SW620 cells were seeded in an 8 well Nun Lab-Tek chamber slide system. The slides were incubated for 24 hours prior to the treatment. After adding the treatments, cells were incubated for 24 hours and then processed for protein proximity analysis using the Duolink assay (Olink Bioscience, Uppsala, Sweden) with and ERCC1 antibody (FL-297, 1/100; Santa cruz biotechnology, Santa Cruz, CA, USA) and XPF antibody (LS-C173159, 1/100; LifeSpan BioSciences, Seattle, WA). The Samples were then fixed and stained with DAPI. Later then the cells were visualized with ZEISS Axio Scan.Z1 slide scanner (ZEISS, Oberkochen,

Germany). The nuclei of the cells are shown as blue dots. The red dots are presenting the interaction between ERCC1, and XPF and they were analyzed with ImageJ software (LOCI, University of Wisconsin, USA). Results are determined as mean values from two experiments conducted independently.

### **2.2.9. Cytotoxicity Assay**

The 3-(4,5-dimethylthiazol-2-yl)-2,5-diphenyl-2H-tetrazolium bromide (MTT) assay was used to assess the cytotoxicity of the A4 (free or as PEO-PBCL PM formulation) alone or in combination with platinum-based drugs, carboplatin, and Oxaliplatin, against HCT116, HT29, and SW620 cells. Briefly,  $2 \times 10^3$  cells were seeded in 96 well plates. The plates were kept in the incubator overnight so that the cells would adhere to the plates. The day after cells were treated with different concentrations of A4 and platinum-based drugs using a 4-hour time interval between treatments. The cytotoxicity was assessed at 24, 48, and 72h after incubation with the second treatment. After incubation, 20  $\mu$ L of MTT solution (5 mg/mL) was added to the plates and incubated with the cells for 2hs. Then the culture media was removed and replaced with 100  $\mu$ L of DMSO to dissolve all the crystals. The percentage of cell viability was calculated based on the amount of light absorption of dissolved crystals at 570 nm for A4/platinum treated cells compared to media treated cells (93).

### **2.2.10. Colony formation assay**

For HCT116 cells in combination with chemotherapeutics, 100 cells were seeded. After seeding the plates were kept in the incubator overnight for cells to adhere to the petri dish. Cells were then treated with the A4 (free or in PEO-PBCL PMs) first, and after a 4-hour period, they received different concentrations of carboplatin or oxaliplatin. The media was changed after

3 days. At the endpoint of the study, the cells were fixed with freezing cold methanol and stained with 0.5% crystal violet solution. The colonies were counted afterward. The plating efficiency was then calculated (94).

$$(\textit{Plating efficiency}) = \frac{\textit{Number of counted colonies}}{\textit{Number of Seeded Cells}}$$

### **2.2.11. Statistical Analysis**

All experiments were repeated at least three times, and the data are shown as mean  $\pm$  standard deviation (SD). The significant difference was assessed with One-way or two-way ANOVA followed by Tukey's post-hoc analysis. Statistical analysis was carried out using Graph Pad Prism 9 Software (GraphPad Software Inc., La Jolla, CA, USA). If a significant difference was seen between groups, groups were compared using the Mann-Whitney U test. A value of  $p \leq 0.05$  were considered significantly different in all the experiments.

## **2.3. Results**

### **2.3.1. Physicochemical Characterization of polymeric micellar formulations**

The structure of the three-block copolymers and degree of polymerization (DP) of the hydrophobic block was assessed using  $^1\text{H}$  NMR (Figure S1) (86). The data showed a DP of 42, 32, and 35, for the hydrophobic block in PEO-PCL, PEO-PBCL, and PEO-PDLA copolymers, respectively. The physicochemical characteristics of the assembled PMs with or without A4 loading, including their average diameter, polydispersity index, encapsulation efficiency, and loading content, are listed in **Table 2.1**.

The average size of all PMs was below 100 nm, and all formulations showed a relatively narrow polydispersity index (below 0.25). The size of all three PMs after A4 loading seemed to be smaller



( $p < 0.05$ ), which could be the result of hydrophobic interaction between the hydrophobic A4 and the core of the PMs. Among all the formulations, PEO-PBCL demonstrated the smallest size while PEO-PCL size changed the most after A4 loading. Also, the smallest loaded PMs were formed by PEO-PBCL which had the highest encapsulation efficiency for A4 ( $83.06 \pm 5.83 \%$ ) at the same time.

The size of PMs obtained by TEM microscopy was assessed with Image J software. The sizes that were obtained by the TEM microscopy were considerably smaller than the ones obtained with DLS. Between the three different formulations, PEO-PBCL was demonstrating less difference in size between the two methods.

The mean zeta potential of empty PMs is negative at -5 to -9 mV. However, the mean zeta potential shifted toward positive mV after A4 was loaded inside the carriers.

Overall, among all the carriers, PEO-PBCL PMs has shown the best loading, smallest average diameter and PDI.

HPLC chromatogram of A4 measured at 210 and 254 nm:

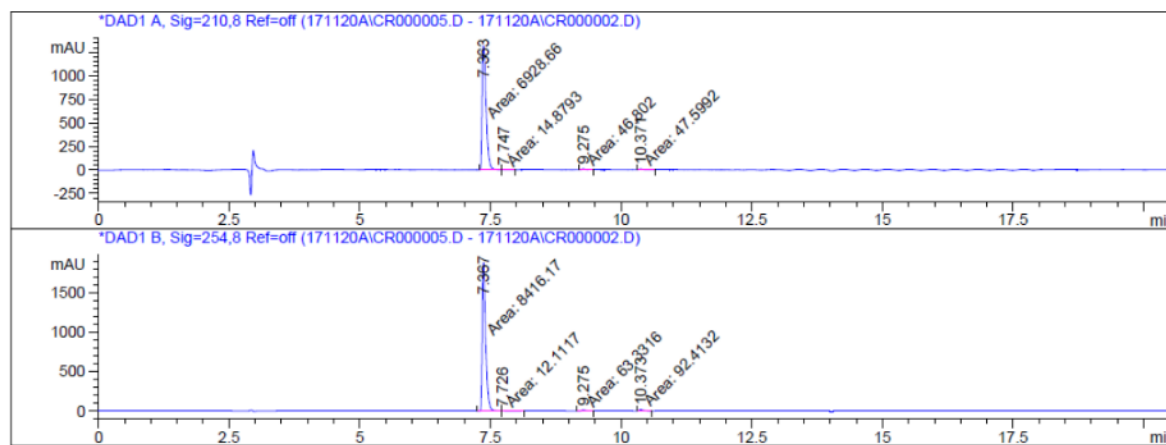


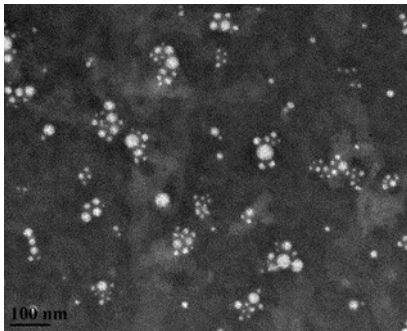
Figure 2.1: HPLC chromatogram of A4, yielded a purity of 98%.

**Table 2.1:** Physicochemical characteristics of the self-assembled empty and A4 loaded block copolymer micelles (n=3)

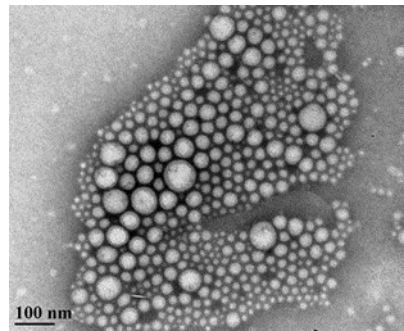
PM formulation	Average diameter $\pm$ SD <sup>b</sup>	PDI $\pm$ SD <sup>b</sup>	Average diameter $\pm$ SD (nm) <sup>c</sup>	Zeta potential	Loading content (w/w%)	Encapsulation Efficiency (%)
PEO <sub>144</sub> -b-PCL <sub>44</sub> <sup>a</sup>	61.60 $\pm$ 0.41	0.240 $\pm$ 0.007	30.51 $\pm$ 8.1	-9.5 $\pm$ 0.23	-	-
PEO <sub>144</sub> -b-PCL <sub>44</sub> /A4	55.71 $\pm$ 0.38 <sup>d</sup>	0.105 $\pm$ 0.015	35.591 $\pm$ 13.39	<b>4.76 <math>\pm</math> 0.1</b>	7.64 $\pm$ 0.33	69.45 $\pm$ 9.04
PEO <sub>144</sub> -b-PBCL <sub>32</sub>	46.37 $\pm$ 0.25	<b>0.220 <math>\pm</math> 0.070</b>	32.931 $\pm$ 10.1	-7.58 $\pm$ 0.069	-	-
PEO <sub>144</sub> -b-PBCL <sub>32</sub> /A4	39.73 $\pm$ 0.32 <sup>d</sup>	<b>0.120 <math>\pm</math> 0.008</b>	<b>31.0 <math>\pm</math> 9.27</b>	<b>3.35 <math>\pm</math> 0.48</b>	<b>11.48 <math>\pm</math> 0.37<sup>e</sup></b>	<b>83.06 <math>\pm</math> 5.83<sup>e</sup></b>
PEO <sub>144</sub> -b-PDLA <sub>35</sub>	79.12 $\pm$ 0.43	0.178 $\pm$ 0.008	32.61 $\pm$ 13.98	-5.5 $\pm$ 0.04	-	-
PEO <sub>144</sub> -b-PDLA <sub>35</sub> /A4	68.12 $\pm$ 0.11 <sup>d</sup>	0.099 $\pm$ 0.013	27.963 $\pm$ 10.56	<b>3.32 <math>\pm</math> 0.17</b>	7.56 $\pm$ 0.86	75.65 $\pm$ 8.66

- a) The subscript number shows the DP of the block in the copolymer structure
- b) based on DLS data.
- c) based on TEM data
- d) Differences were considered significant if  $p \leq 0.05$ , following unpaired student's t test comparison between the free and loaded polymeric micelles or
- e) Differences were considered significant at  $*p \leq 0.05$  (one-way ANOVA multiple comparison test following Tukey's method)

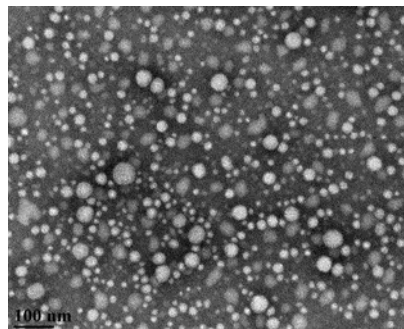
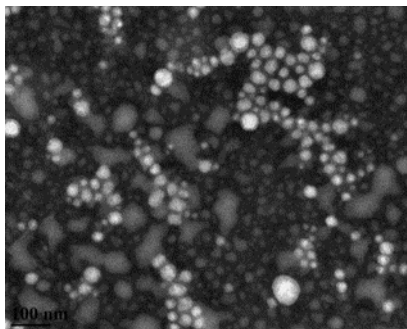
The morphology of the polymeric micelles was investigated with the help of TEM for both loaded and unloaded PMs, where the spherical shape of PMs was confirmed.

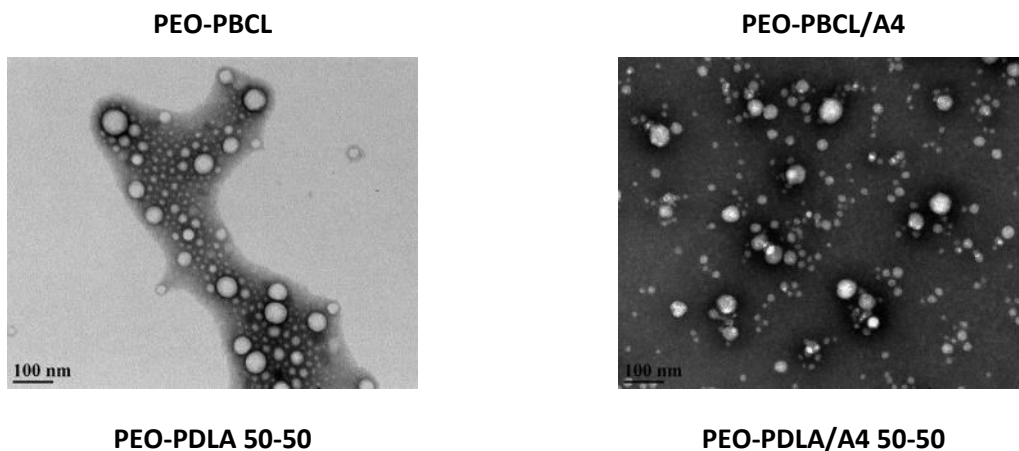


PEO-PCL



PEO-PCL/A4





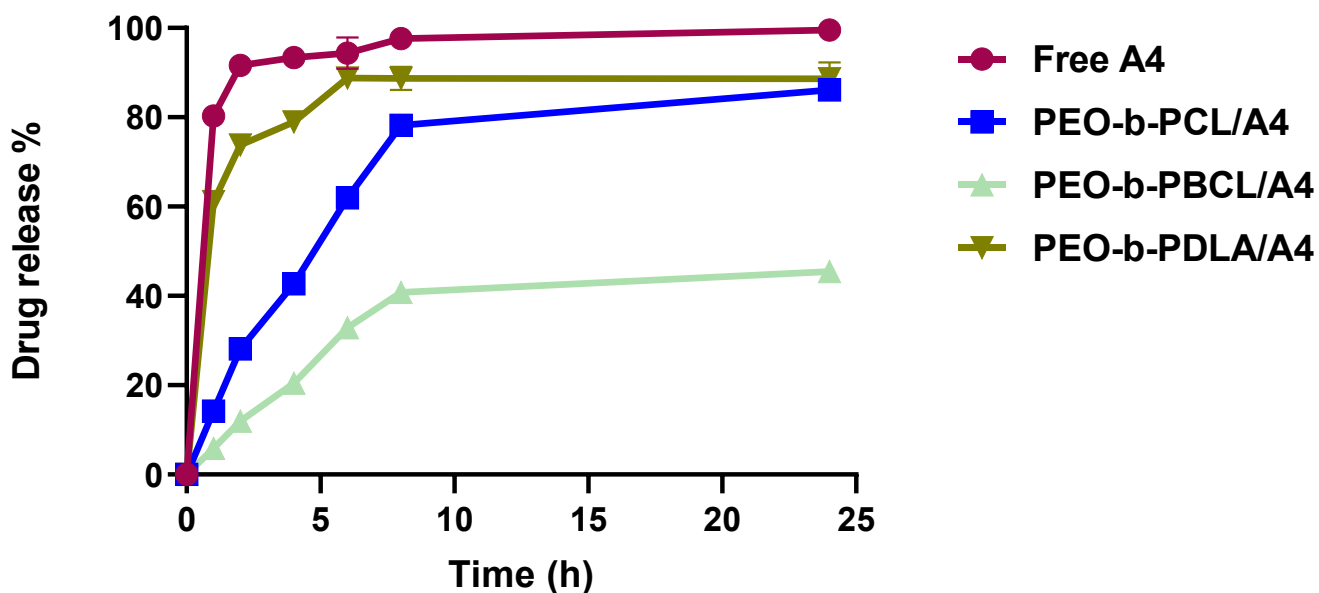
*Figure 2.2: TEM Pictures of PMs (loaded and unloaded with A4). Images were obtained at a magnification of 110,000x at 75kv.*

### 2.3.2. In Vitro Drug Release

**Figure 2.3** shows the release profile of free A4 versus the three developed formulations. During the first 4 hours of the study, more than 90% of the free A4 (93.4%) was released from the dialysis bag (MWCO = 3.5kDa). In contrast, only 20.43% of the drug in the PEO-PBCL formulation was released from the carrier and into the release media at the same time point. The two other formulations, PEO-PDLA and PEO-PCL PMs, were able to slow down the release to 78.97% and 42.68% after 4hs. After 24 hours about 45% of the drug was released from the PEO-PBCL PMs. While PEO-PDLA and PEO-PCL micelles released > 80 % of their A4 content within 24 hrs. Overall, among the formulations under study, the kinetics of drug release from the fastest to slowest followed this order: free A4 > PEO-PDLA/A4 > PEO-PCL/A4 > PEO-PBCL/A4.

Overall, the PEO-PBCL PMs provide the smallest PM formulations of A4 with the highest encapsulation and slowest release profile. As a result, all further studies were done, Using PEO-

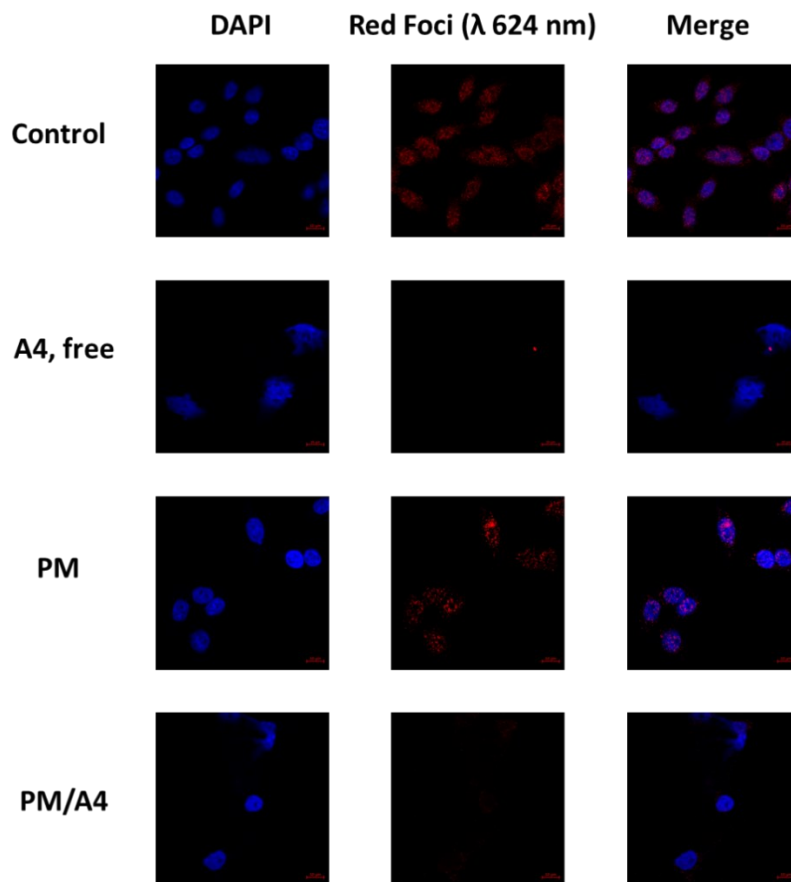
PBCL as the nano-carrier.



*Figure 2.3: The in vitro release profile of A4 (mean  $\pm$  SD, n=3) from the three polymeric micellar carriers vs. the release of free A4.*

### 2.3.3. Proximity ligation Assay

We investigated to see whether A4 compound has the ability to inhibit the interaction between ERCC1 and XPF protein in SW620 cell line. **Figure 2.4** shows that A4 compound significantly reduced the number of fluorescent foci resulting from dimerized ERCC1-XPF in comparison to the single foci visualized with cells only treated with control.



**Figure 2.4:** This figure indicates that A4 (2  $\mu$ M) loaded into PBCL was able to disrupt the XPF-ERCC1 dimer when loaded directly into SW620 cells. This action could not be replicated by PBCL alone, indicating that PM/A4 provided an appropriate vehicle to release A4 into SW620 cell and modified XPF-ERCC1 in situ.

### 2.3.4. In Vitro nonspecific cytotoxicity of A4 and its PEO-PBCL PM formulation against CRC cells

The level of A4 cytotoxicity against three different CRC cell lines, HCT116, SW620, and HT-29, following incubation for 24, 48, and 72h was assessed by MTT assay. Data is shown in **Figure 2.5**, and the IC<sub>50</sub> values are demonstrated in **Table 2.2**.

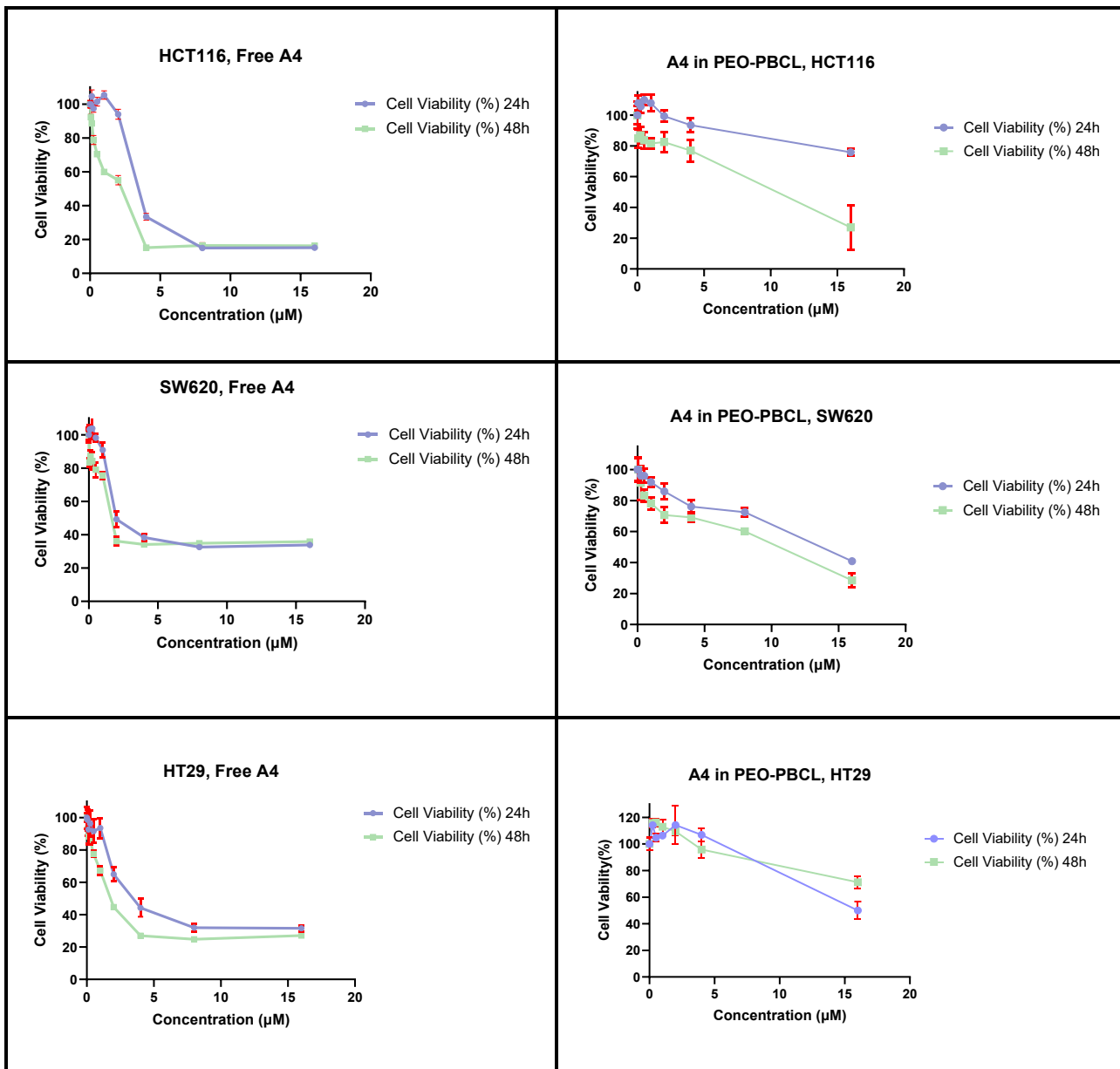
*Table 2.2: The IC<sub>50</sub> (mean ± SD) of free A4 against colorectal cancer cell lines measured by MTT assay (n=3)*

Free A4	IC <sub>50</sub> in HCT116 (μM)	IC <sub>50</sub> in SW620 (μM)	IC <sub>50</sub> in HT29 (μM)
24h	3.127 ± 0.04	1.286 ± 0.03	2.183 ± 0.139
48h	1.56 ± 0.05	1.248 ± 0.06	1.297 ± 0.07
72h	1.59 ± 0.06	0.4810 ± 0.02	0.495 ± 0.02

*Table 2.3: The IC<sub>50</sub> of free A4 against colorectal cancer cell lines measured by MTT assay (n=3)*

PM/A4	IC <sub>50</sub> in HCT116 (μM)	IC <sub>50</sub> in SW620 (μM)	IC <sub>50</sub> in HT29 (μM)
24h	> 16 μM	(8-16) μM	(8-16) μM
48h	(8-16) μM	(8-16) μM	> 16 μM

The nonspecific cytotoxicity of A4 seemed to increase as its incubation time was enhanced. However, in general, the nano-formulation seemed to reduce the nonspecific toxicity of A4 against all three cancer cell lines. Considering that HT-29 showed a considerably lower level of sensitivity to the effect of A4 compound, the rest of the studies were done on the two other cell lines. The empty micelles were not cytotoxic and did not show any decrease in the level of toxicity. (Also the amount of absorbance was deducted from all the wells).

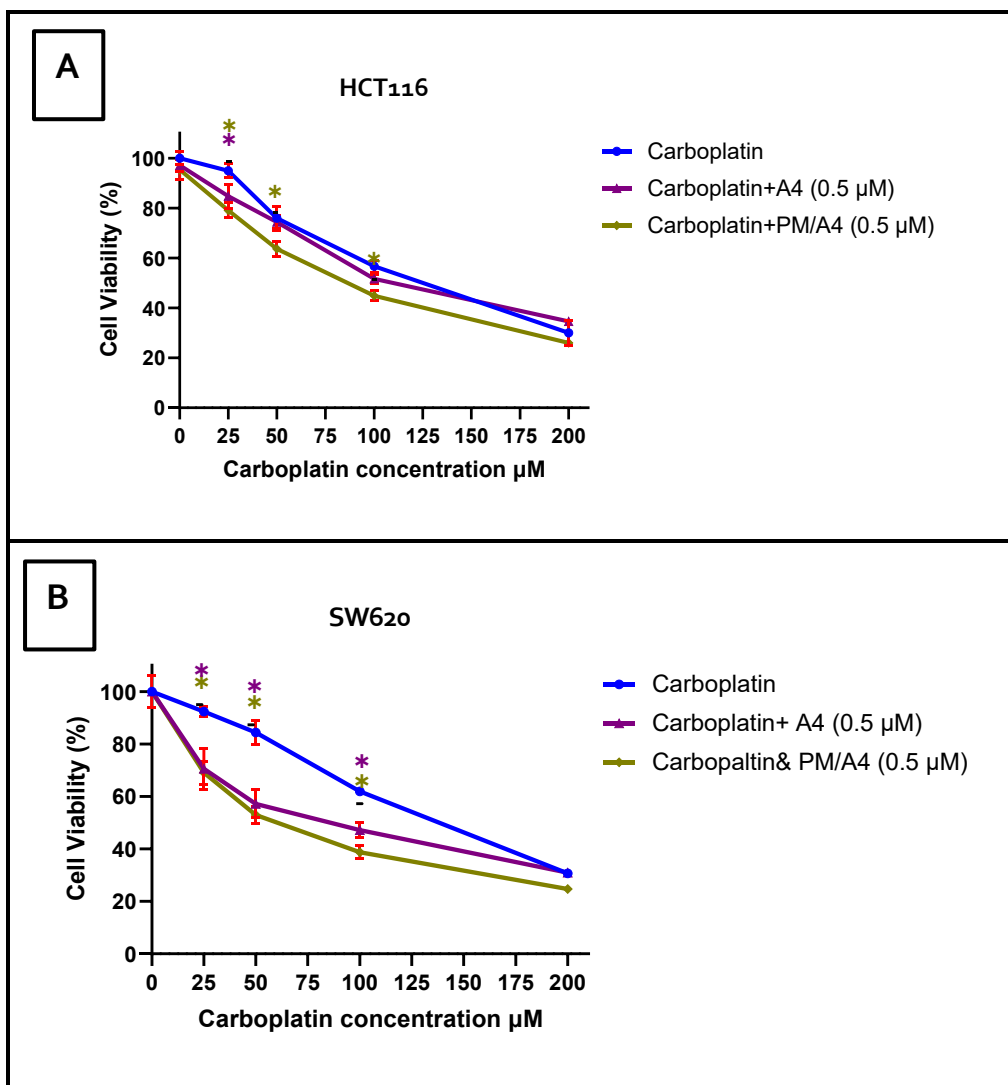


**Figure 2.5:** The comparison between the cytotoxicity of free and PEO-PBCL PM loaded A4 in three CRC cell lines following 24, 48, and 72 h incubation as determined by MTT assay ((n=3).

### 2.3.5. Sensitization of CRC cells to Carboplatin by A4 and its PEO-PBCL micellar formulation

In this series of studies, A4 was applied 4h prior to platinum drug treatment, and its function as a chemosensitizer was evaluated. The study was performed using A4 concentrations below the IC50 of this compound as a single agent in the two cell lines **A)** HCT116 and **B)** SW620

under study, i.e., 0.25 and 0.5  $\mu\text{M}$  of A4 either as free or PEO-PBCL PM formulation. (Figure 2.6.)



**Figure 2.6:** Cytotoxicity of Carboplatin without and with A4 (Free or Polymeric micelles) at 72h incubation against A) HCT116 and B) SW620 cell line (n=3), There is a 4-hour time interval between the two treatments. \* Shows statistically significant difference from control PM alone; \* shows statistically significant from free A4 (Two-way ANOVA, Tukey's multiple comparison test)

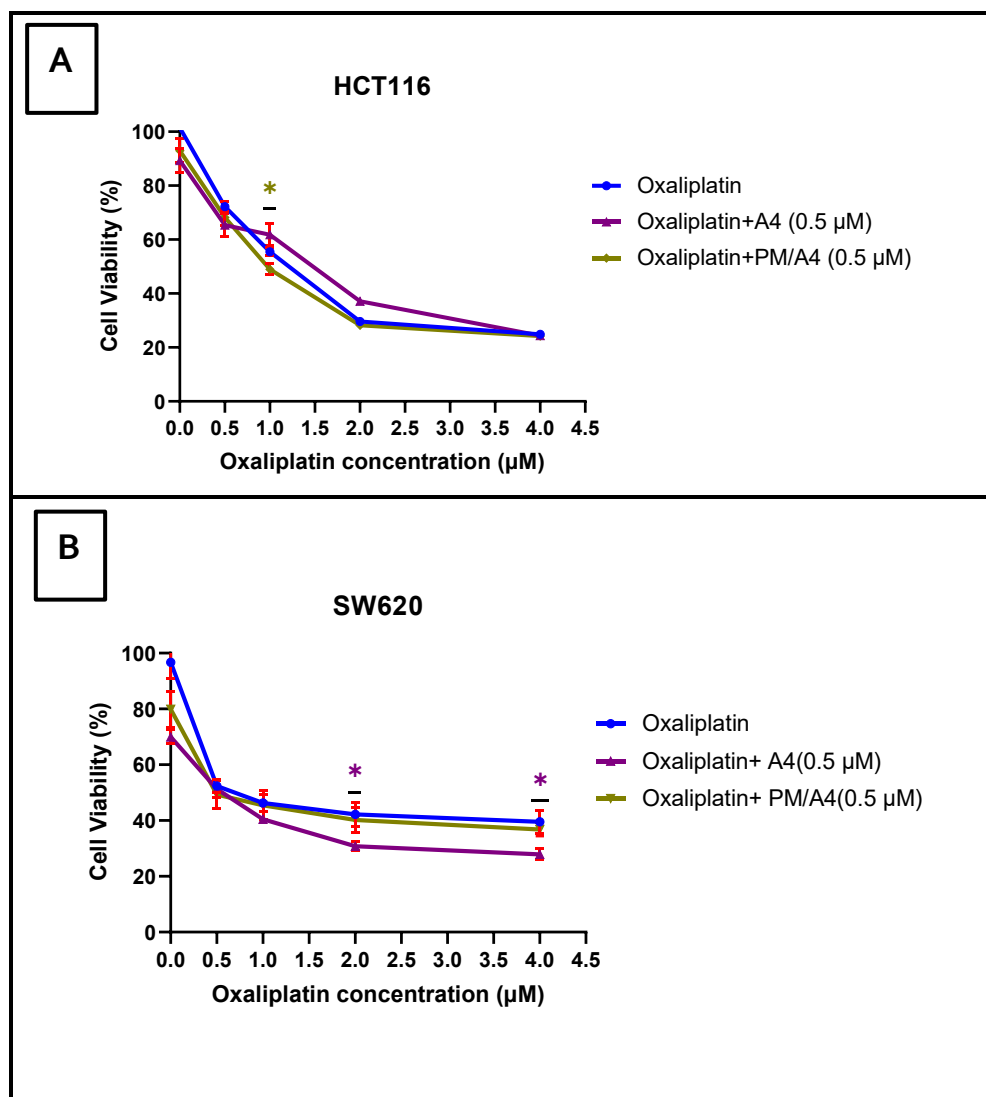
The results showed a chemo-sensitizing activity when 0.5  $\mu\text{M}$  concentrations of A4, particularly as a PM formulation, was combined with carboplatin in both CRC cells under study **Figure 2.6** on



the other hand, 0.25  $\mu\text{M}$  of A4, while showing a minor effect in combination with the chemotherapeutic, was not as effective as 0.5  $\mu\text{M}$  A4 as a chemosensitizer.

### 2.3.6. Sensitization of CRC cells to Oxaliplatin by A4 and its PEO-PBCL micellar formulation

The chemo-sensitizing effect of A4 in combination with another platinum chemotherapeutic agent, i.e., Oxaliplatin, is assessed as well. The data showed the cell lines under study to be much more sensitive to the effects of oxaliplatin alone than carboplatin. (Figure 2.7.)



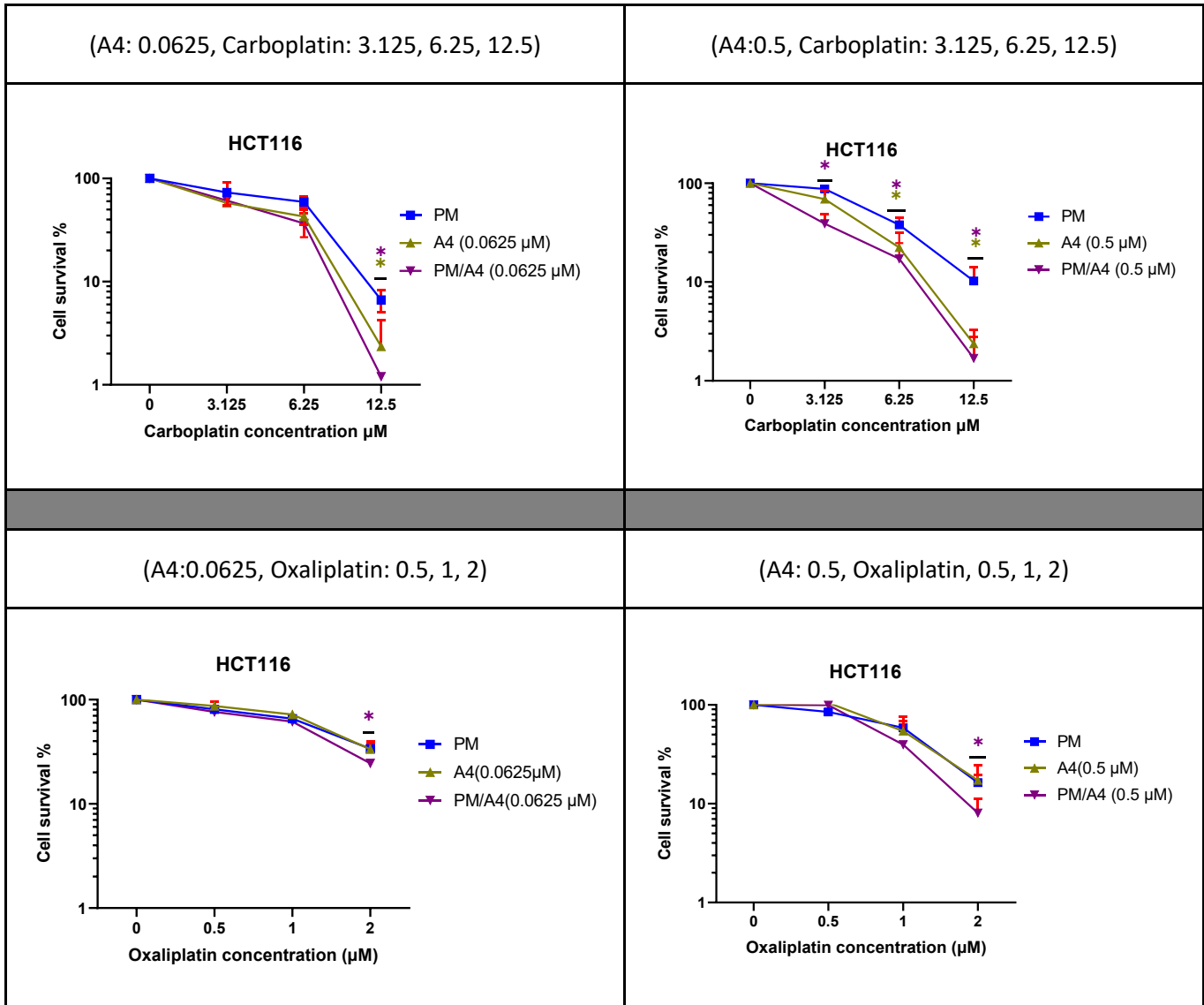
*Figure 2.7: Cytotoxicity of Oxaliplatin without and with A4 (free or polymeric micelles) at 72h incubation against A) HCT116 and B) Sw620 cell line (n=3). There is a 4-hour time interval between the two treatments. \* Shows statistically significant difference from control PM alone; \* shows statistically significant from free A4 (Two-way ANOVA, Tukey's multiple comparison test)*

Overall, A4 and its PM formulations were less effective as chemosensitizers when combined with Oxaliplatin.

### **2.3.7. Colony forming Assay**

#### **2.3.7.1. HCT116**

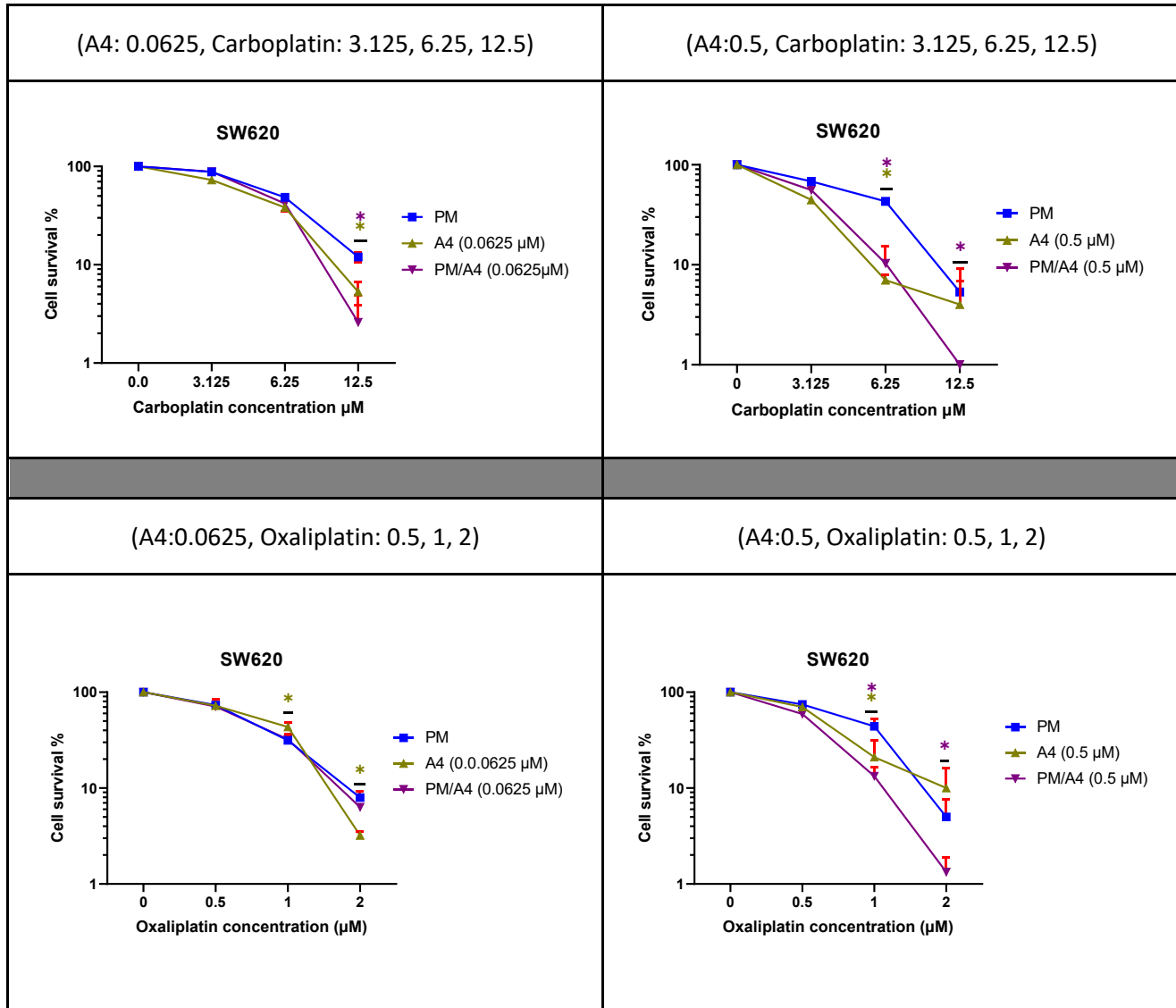
In the HCT116 cell line, the combination of A4 and carboplatin has shown more promising results as the combination of either free or PM A4 led to lower surviving fraction of the HCT116 cells at both 0.0626 and 0.5  $\mu$ M A4 concentration. Meanwhile, in this cell line, the combination of A4 and oxaliplatin did not show promising result and increasing the concentration of PM A4 only led to a negligible improvement in cytotoxicity in combination with the highest concentration of oxaliplatin under study. (Two-way ANOVA, Tukey's multiple comparison test) (n=3) (**Figure 2.8.**)



**Figure 2.8:** The results of clonogenic assay following combination of A4 and A4 PM with carboplatin (3.125, 6.26, 12.5  $\mu\text{M}$ ) or oxaliplatin (0.5, 1, 2  $\mu\text{M}$ ) against HCT116 (n=3). (\* purple) Shows statistically significant difference from control PM alone; (\* green) shows statistically significant from free A4 (Two-way ANOVA, Tukey's multiple comparison test)

### 2.3.7.2. SW620

In SW620 cell, the combination of A4 and PM/A4 seemed to enhance the cytotoxic effects of both carboplatin and oxaliplatin. This effect was still more consistent in combination of either free or PM A4 with carboplatin. Combination of PM A4 has shown to increase the cytotoxic activity of oxaliplatin against SW620 cells when higher concentrations of A4 were used (0.5  $\mu\text{M}$ ) (Two-way ANOVA, Tukey's multiple comparison test) (n=3) (**Figure 2.9.**)



**Figure 2.9:** Clonogenic assay in SW620 cells treated with carboplatin (3.125, 6.25, 12.5  $\mu\text{M}$ ) or oxaliplatin (0.5, 1, 2  $\mu\text{M}$ ) in the presence empty PMs or 0.0625, 0.5  $\mu\text{M}$  of free or PM loaded A4 ( $n=3$ ) (\* Purple) shows statistically significant difference from control PM alone; (\* green) shows statistically significant from free A4 (Two-way ANOVA, Tukey's multiple comparison test)

# HCT116 Colony Pictures

A4:0.0625, Carboplatin:3.125, 6.25, 12.5  $\mu$ M

HCT116	DMSO <1 %	A4 (0.0625)	PM	PM/A4 (0.0625)
Carboplatin: 0 $\mu$ M				
Carboplatin: 3.125 $\mu$ M				
Carboplatin: 6.25 $\mu$ M				

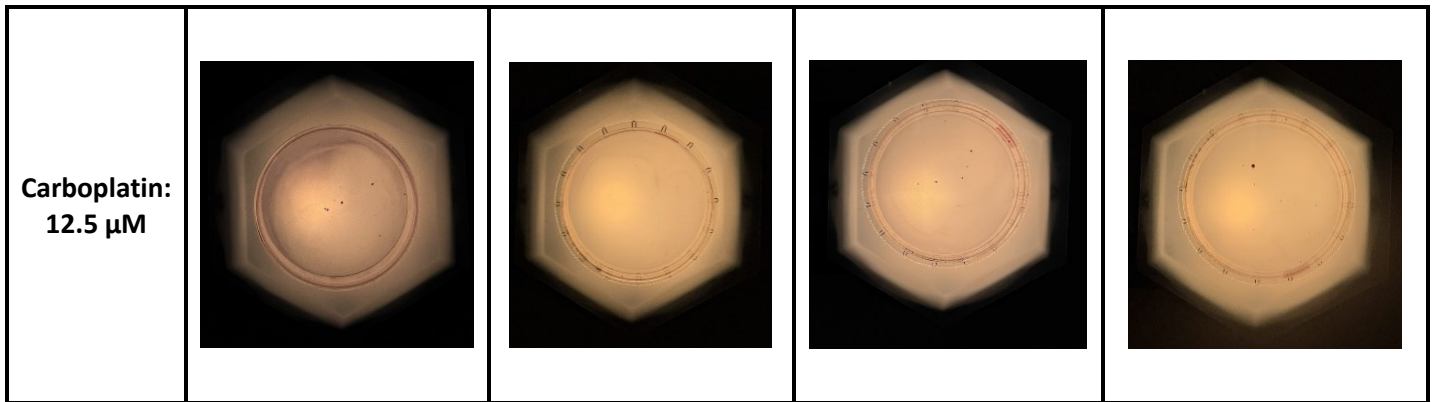
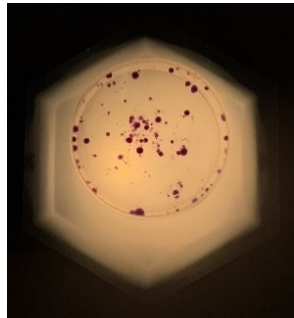
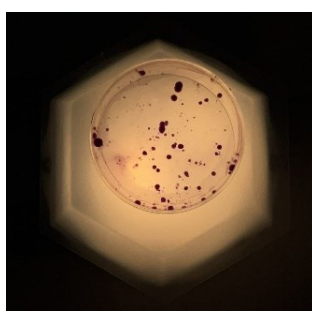
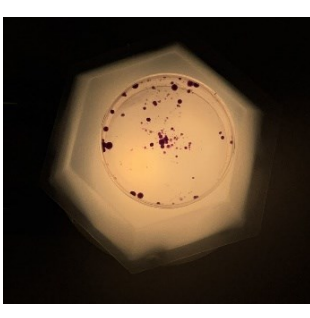
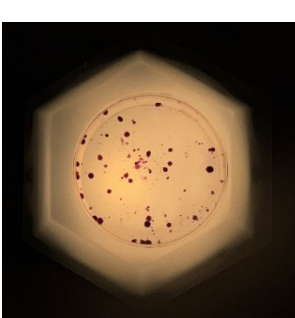
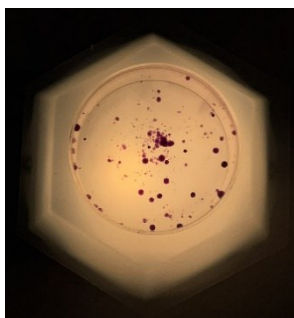
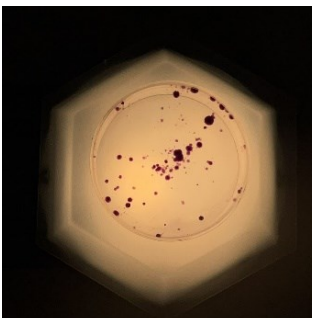
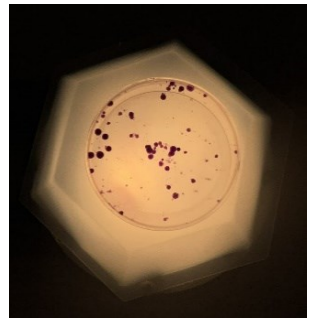
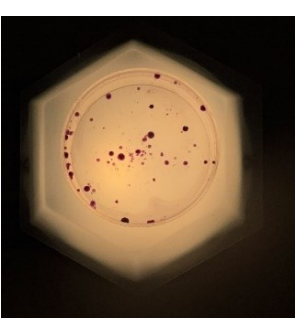


Figure 2.10: Clonogenic assay in HCT116, A4 (0.0625  $\mu$ M) and Carboplatin (3.125, 6.25, 12.5  $\mu$ M) (n=3)

**A4:0.0625, Oxaliplatin :0.5, 1, 2  $\mu$ M**

HCT116	DMSO<1%	A4 (0.0625)	PM	PM/A4 (0.0625)
<p><b>Oxaliplatin: 0 <math>\mu</math>M</b></p>				
<p><b>Oxaliplatin: 0.5 <math>\mu</math>M</b></p>				

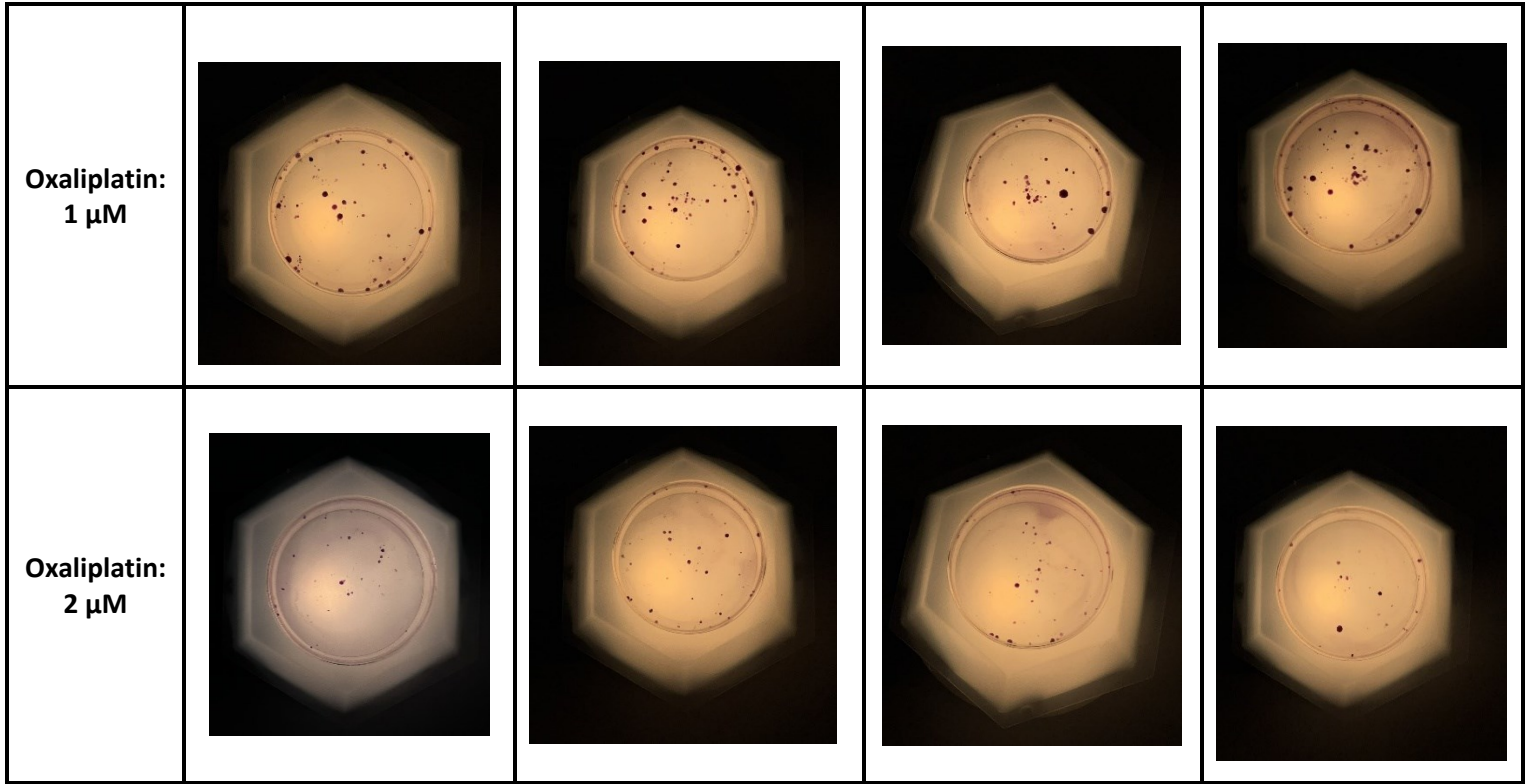
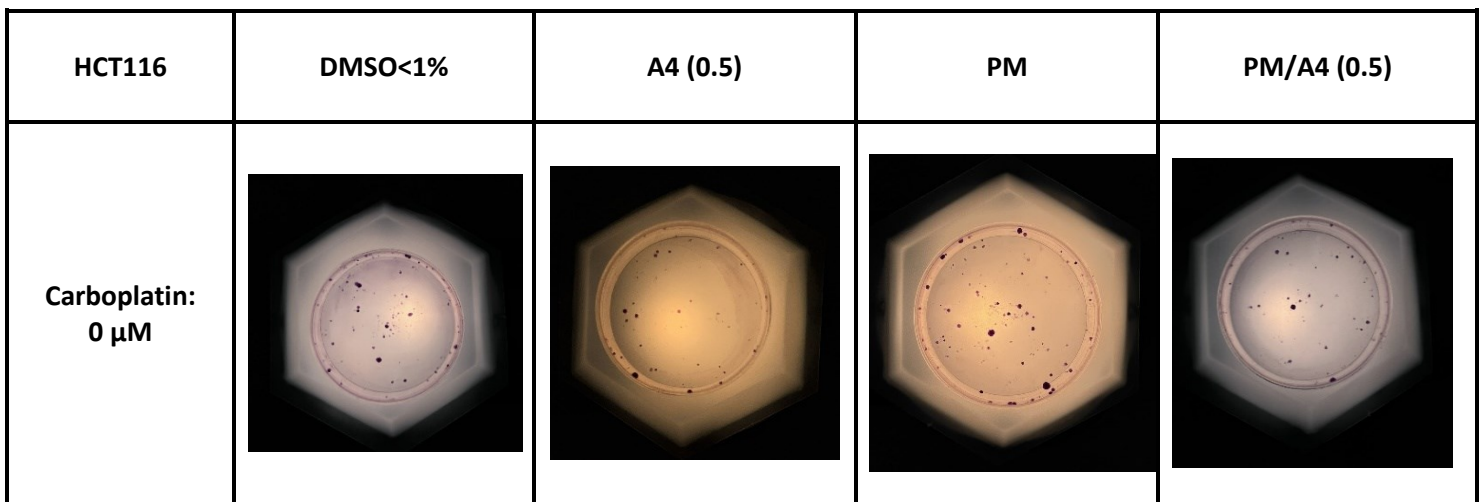
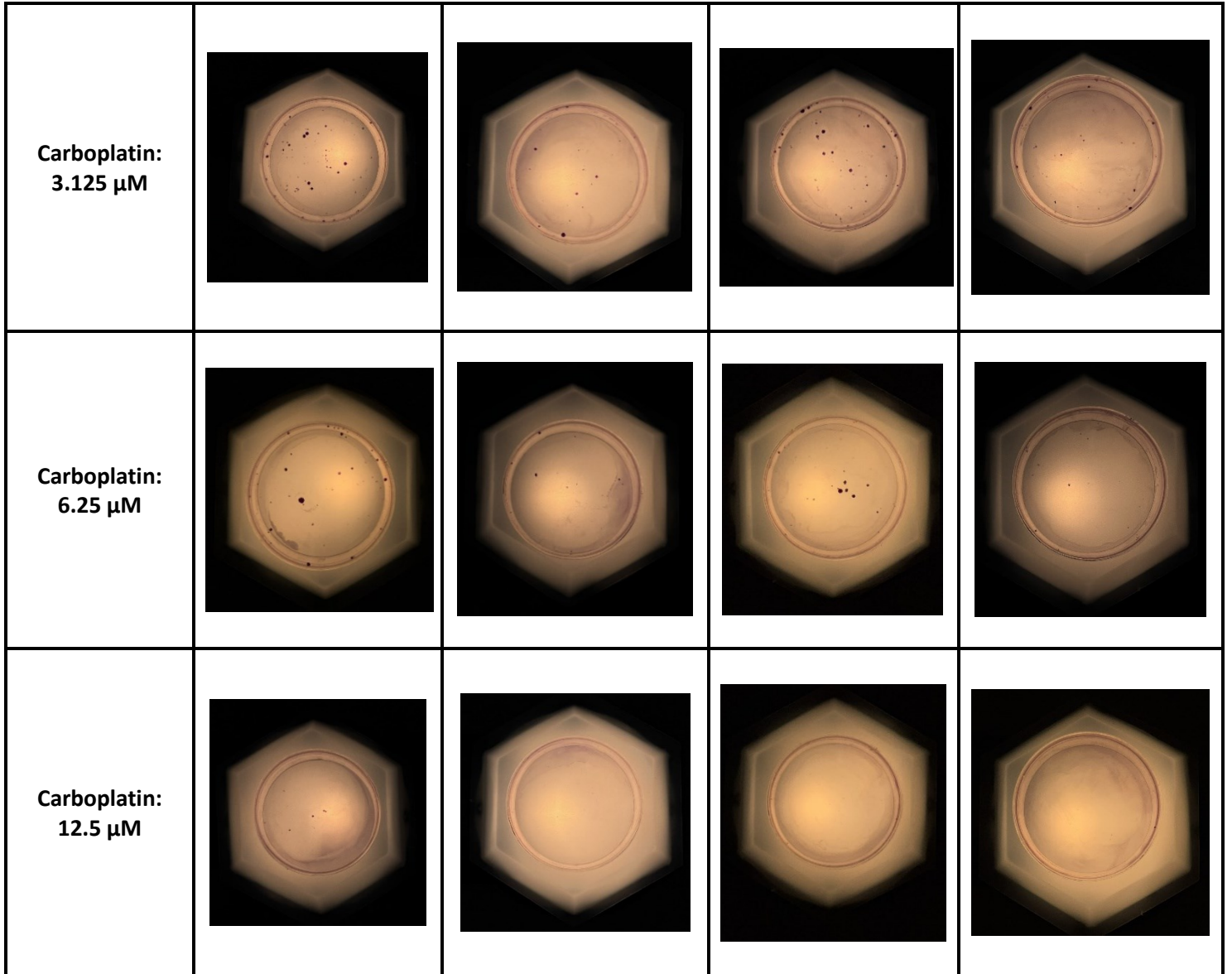


Figure 2.11: Clonogenic assay in HCT116, A4 (0.0625  $\mu$ M) and Oxaliplatin (0.5, 1, 2) (n=3)

A4:0.5, Carboplatin:3.125, 6.25, 12.5  $\mu$ M

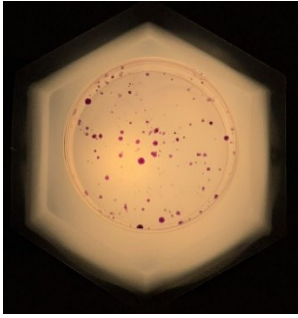
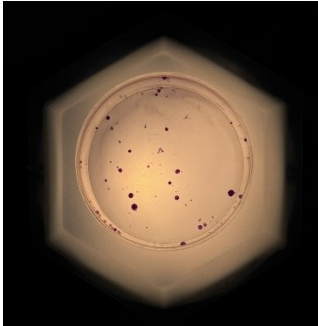
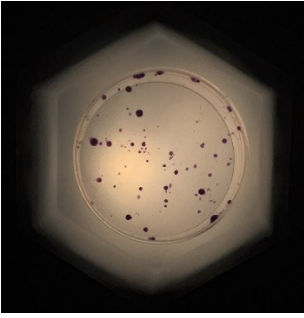
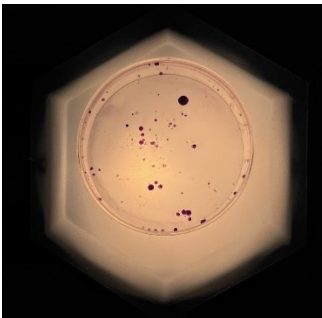
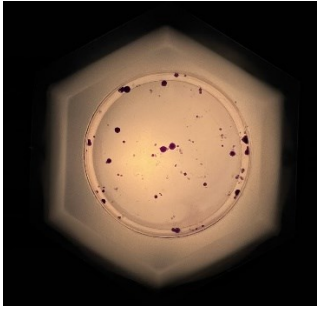
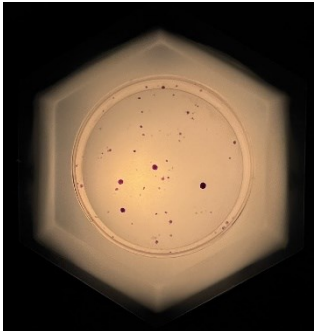
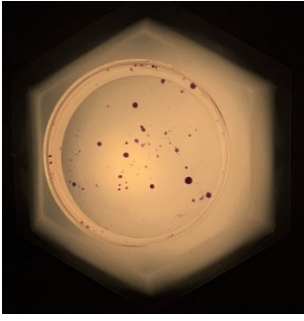
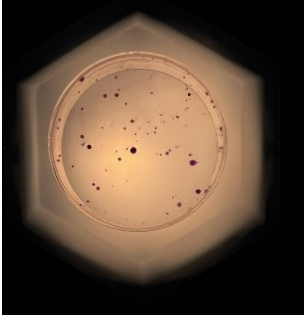
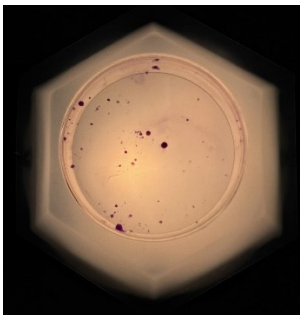
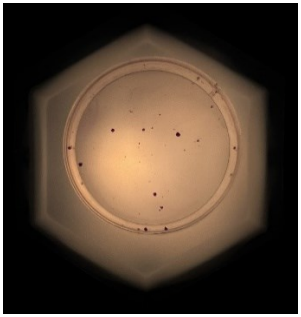
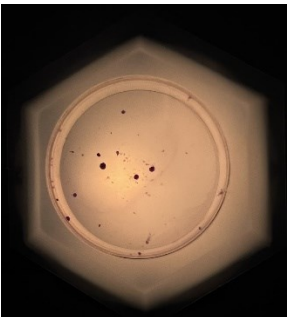
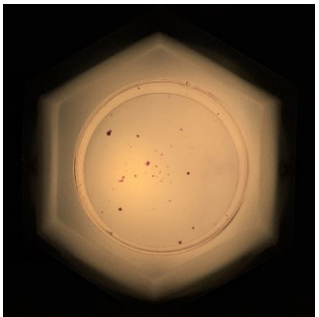




*Figure 2.12: Clonogenic assay in HCT116, A4 (0.5  $\mu$ M) and Carboplatin (3.125, 6.25, 12.5) (n=3)*



A4:0.5  $\mu\text{M}$ , Oxaliplatin :0.5, 1, 2  $\mu\text{M}$

HCT116	DMSO<1%	A4 (0.5)	PM	PM/A4 (0.5)
Oxaliplatin: 0 $\mu\text{M}$				
Oxaliplatin: 0.5 $\mu\text{M}$				
Oxaliplatin: 1 $\mu\text{M}$				

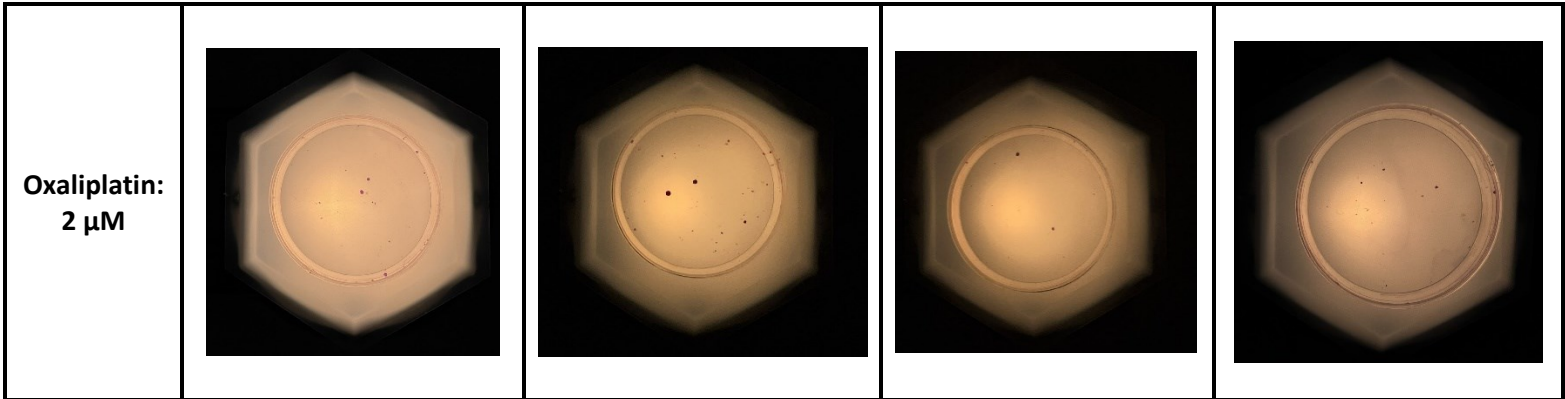
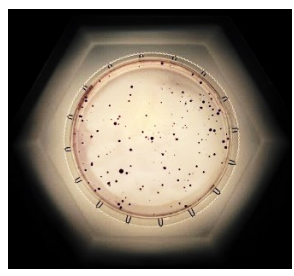
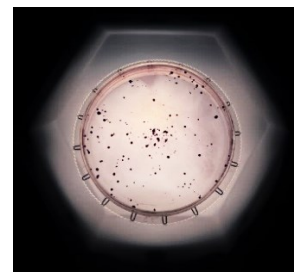
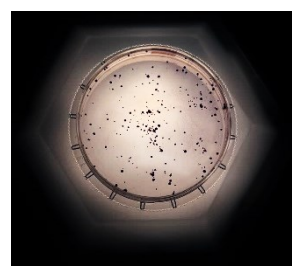
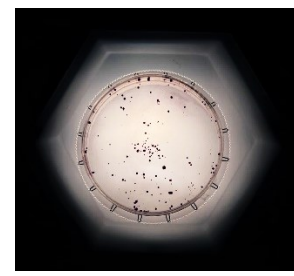
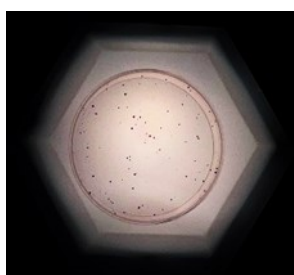
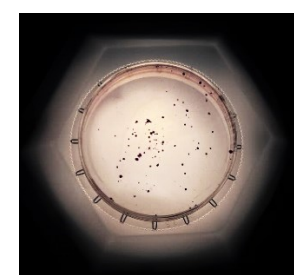
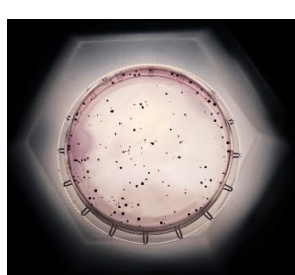
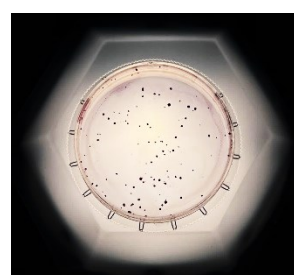


Figure 2.13: Clonogenic assay in HCT116, A4 (0.5  $\mu$ M) and Oxaliplatin (0.5, 1, 2) (n=3)

**SW620 Colony pictures**

**A4:0.0625  $\mu$ M, Carboplatin: 3.125, 6.25, 12.5  $\mu$ M**

SW620	DMSO<1%	A4 (0.0625)	PM	PM/A4 (0.0625)
<p><b>Carboplatin: 0 <math>\mu</math>M</b></p>				
<p><b>Carboplatin: 3.125 <math>\mu</math>M</b></p>				

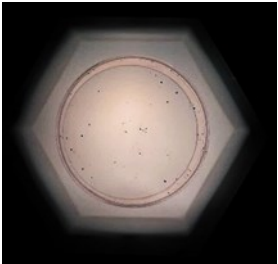
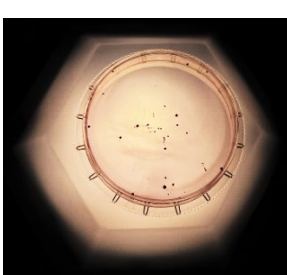
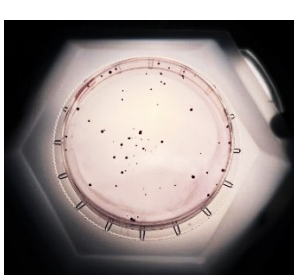
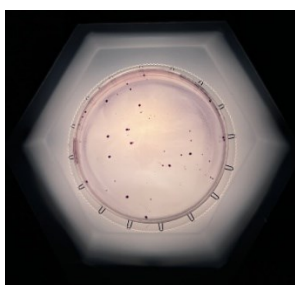
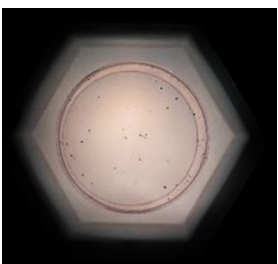

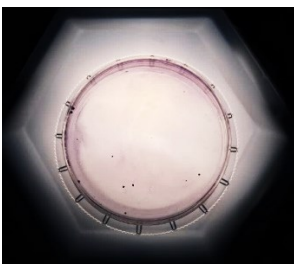
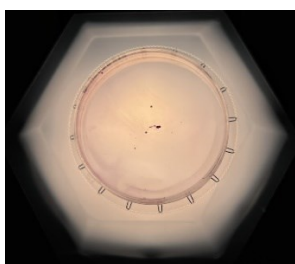
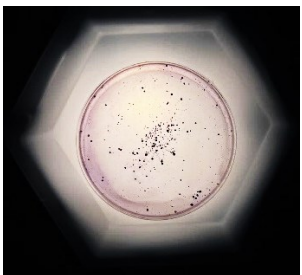
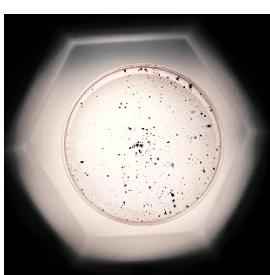
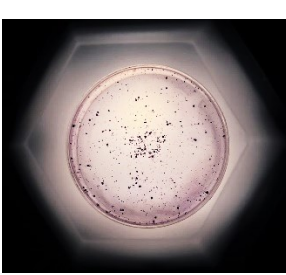
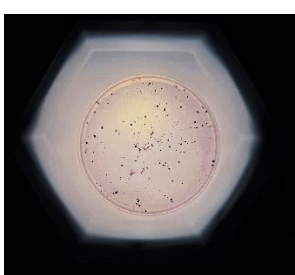
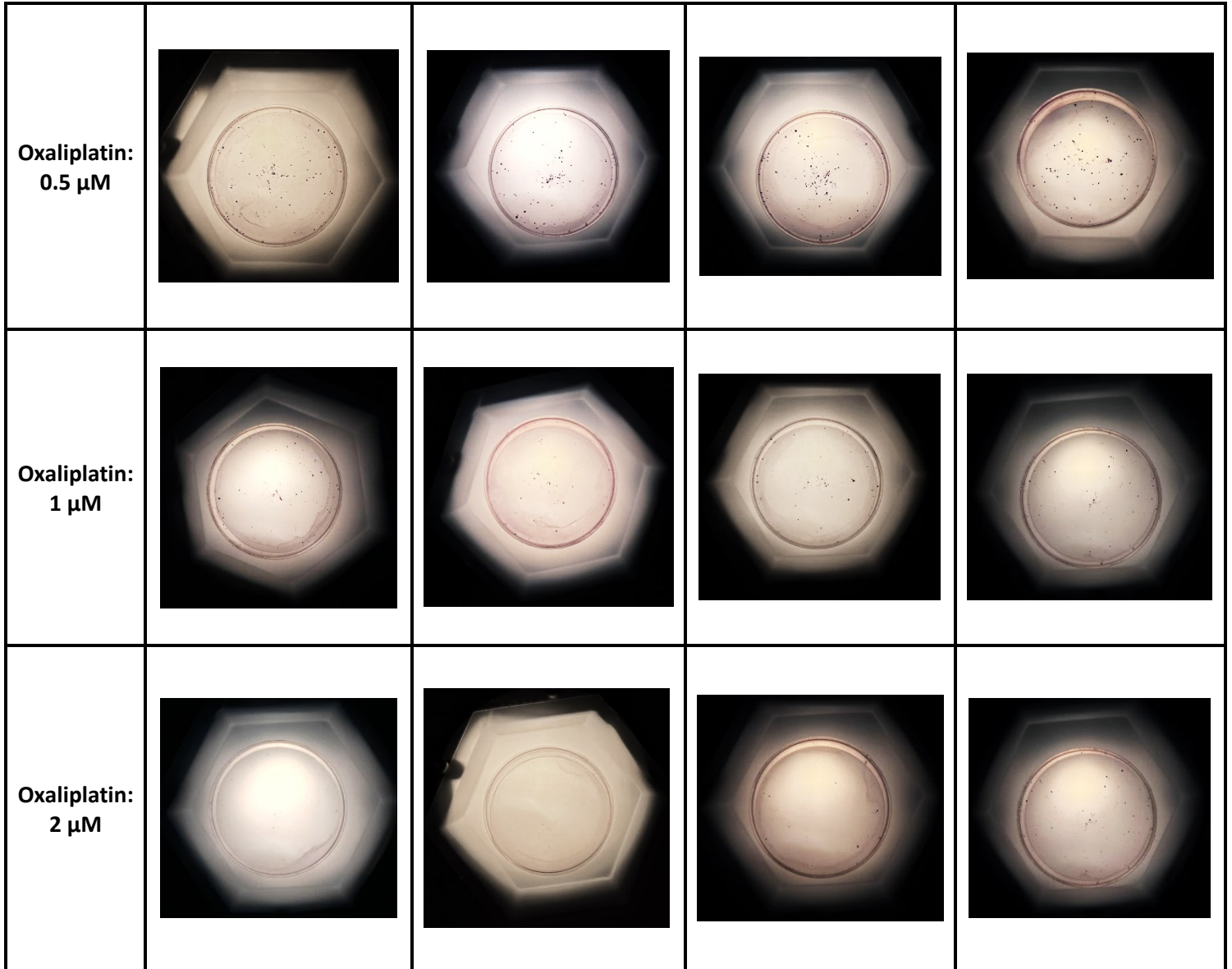
<b>Carboplatin: 6.25 <math>\mu\text{M}</math></b>				
<b>Carboplatin: 12.5 <math>\mu\text{M}</math></b>				

Figure 2.14: Clonogenic assay in SW620, A4 (0.0625  $\mu\text{M}$ ) and Carboplatin (3.125, 6.25, 12.5) (n=3)

A4:0.0625  $\mu\text{M}$ , Ox: 0.5, 1, 2  $\mu\text{M}$

SW620	DMSO<1%	A4 (0.0625)	PM	PM/A4 (0.0625)
<b>Oxaliplatin: 0 <math>\mu\text{M}</math></b>				



*Figure 2.15: Clonogenic assay in SW620, A4 (0.0625  $\mu\text{M}$ ) and Oxaliplatin (0.5, 1, 2) (n=3)*

**A4: 0.5  $\mu\text{M}$ , Carboplatin 3.125, 6.25, 12.5  $\mu\text{M}$**

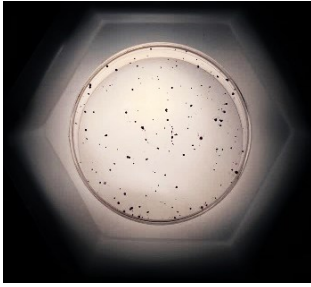

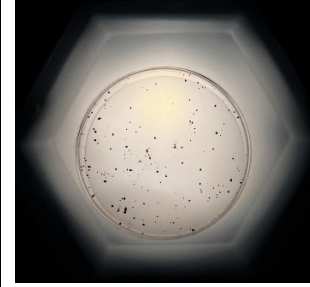

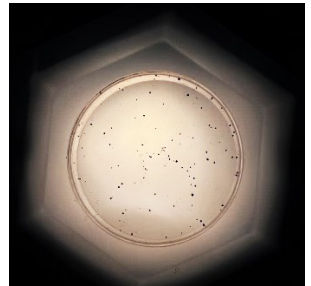

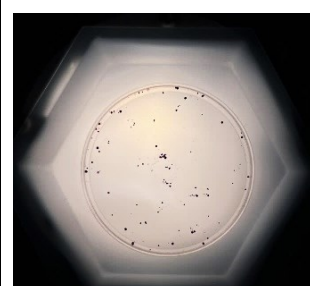

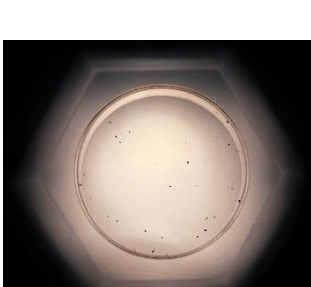

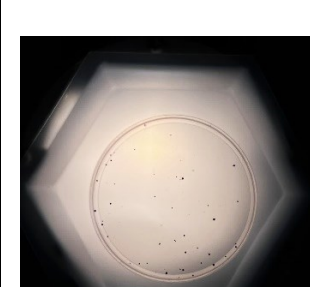
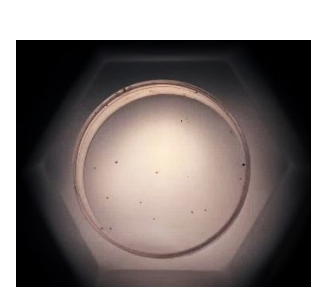
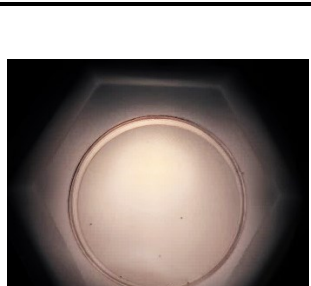
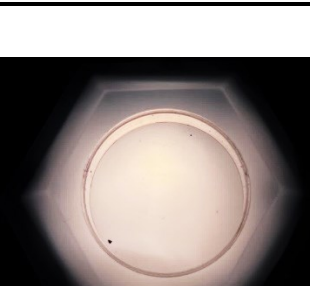
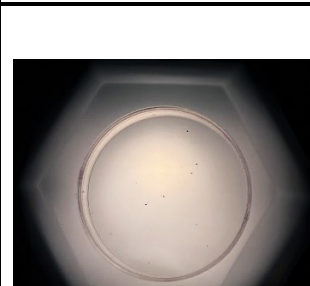
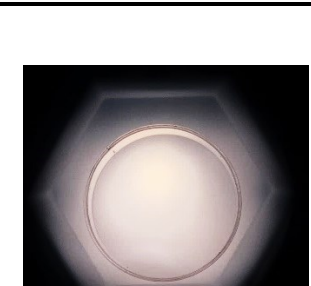

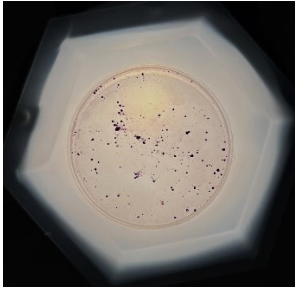
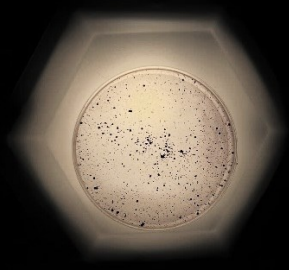
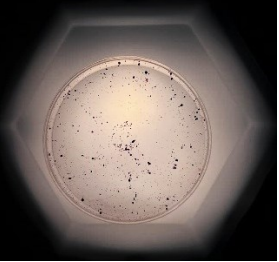
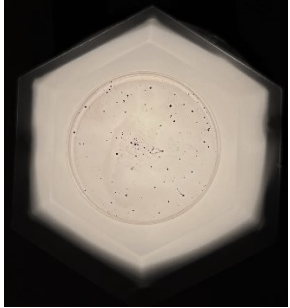
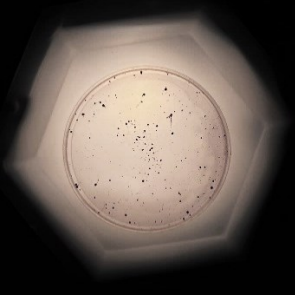
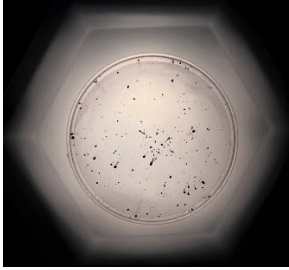
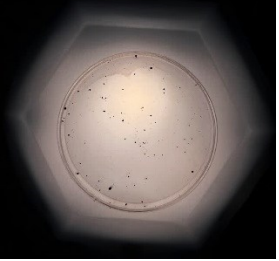

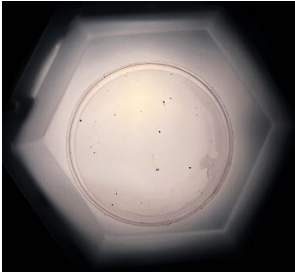
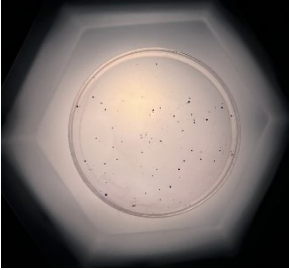
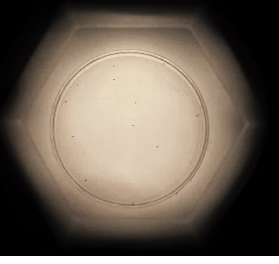
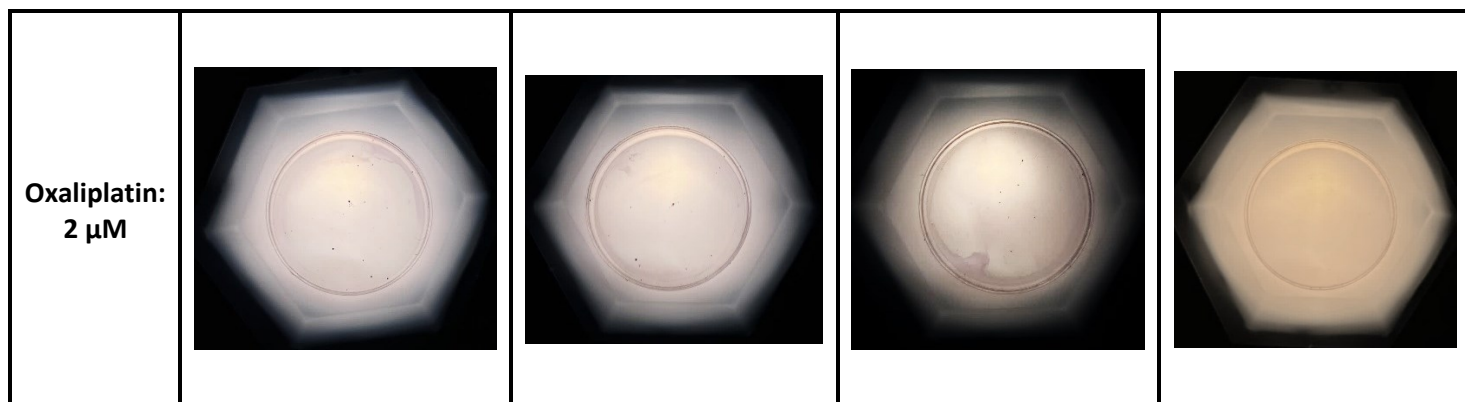
SW620	DMSO<1%	A4 (0.5)	PM	PM/A4 (0.5)
Carboplatin: 0 $\mu\text{M}$				
Carboplatin: 3.125 $\mu\text{M}$				
Carboplatin: 6.25 $\mu\text{M}$				
Carboplatin: 12.5 $\mu\text{M}$				

Figure 2.16: Clonogenic assay in SW620, A4 (0.5  $\mu\text{M}$ ) and Carboplatin (3.125, 6.25, 12.5) (n=3)

A4: 0.5  $\mu$ M, Oxaliplatin: 0.5, 1, 2  $\mu$ M

SW620	DMSO<1%	A4 (0.5)	PM	PM/A4 (0.5)
Oxaliplatin: 0 $\mu$ M				
Oxaliplatin: 0.5 $\mu$ M				
Oxaliplatin: 1 $\mu$ M				



*Figure 2.17: Clonogenic assay in SW620, A4 (0.5  $\mu$ M) and Oxaliplatin (0.5, 1, 2) (n=3)*

#### **2.4. Discussion:**

Inhibitors of DNA repair can make cancer cells sensitive to the effects of DNA damaging therapeutics but may have the same effect on normal cells. Development of nanocarrier for targeted delivery of novel inhibitors of DNA repair enzyme, ERCC1/XPF was pursued in this study to reduce the chance of their side effects on normal cells, particularly when combined with DNA damaging agents. This study aimed to design a polymeric micellar formulation for the A4 compound, which would tackle the poor water solubility of the compound while showing promise in enhancing its delivery to colorectal cancer cells for targeted sensitization of cancer over normal cells to the effect of platinum-based compounds.

Carboplatin and Oxaliplatin, as two of the chemotherapeutic agents with the capability of damaging the DNA of the cells, have been used in the treatment of many types of cancer, including colorectal cancer (28,75). However, drug resistance, high toxicity, and side effects that most patients suffer from, can hinder their activity in increasing patient outcome (29,75,95). In this study, we followed two main objectives. First, to find the most desirable polymeric micellar

for the A4 compound that would tackle this compound's poor water solubility offering the highest A4 encapsulation efficiency and slowest release profile in biologically relevant release media. Second, to assess the cytotoxicity activity of the free and encapsulated drug in colorectal cancer model in combination with platinum drugs. Such formulations are expected to provide pharmacologically relevant drug doses and a potential tumor targeted drug delivery profile for future animal studies.

Among all three developed PM formulations, PMs based on PEO-*b*-PBCL demonstrated the best loading efficiency for A4 while reducing its release rate better than the other formulations at the same time (**Table 2.1.** and **Figure 2.3.**). These desirable physicochemical characteristics, such as smaller size, higher loading content and the slower release of A4 from this structure, is attributed to the presence of pendent  $\alpha$ -benzyl carboxylate group on PCL. The PEO-*b*-PBCL, with  $\alpha$ -benzyl carboxylate, has a higher hydrophobicity than other block copolymers under study. The higher loading of A4 in the PBCL containing micelles could be due to hydrophobic interactions between the drug and the core-forming block. This has been shown in both DLS and TEM data. In general, the TEM revealed smaller average diameters for the micellar formulations compared to DLS, which was expected due to the dry nature of the samples in the TEM measurements.

The same hydrophobic interaction can be the reason for the retainment of  $\sim 50\%$  of the drug content in the PEO-PBCL micellar formulation after 24 hours of release study in the biologically relevant media.

The results of cytotoxicity study revealed, cytotoxic activity for A4 monotherapy in the three human colorectal cancer cell lines under study, although the HCT116 cells appeared to be less



sensitive to this effect compared to the other two cell lines. In addition, the PEO-PBCL micellar formulation of A4 was able to lower the non-specific toxicity of A4 in all three CRC cell lines under study, in vitro (**Figure 2.5.**). This could be attributed to slow release of A4 from the micellar formulation.

In colony forming assay, when combined with platinum-based DNA damaging agents, A4 at a low concentration of 0.0625  $\mu\text{M}$  showed to sensitize both cell lines to the anticancer activity of carboplatin, but not that of oxaliplatin. Higher concentrations of A4 (0.5  $\mu\text{M}$ ) were needed to see its sensitizing effects for oxaliplatin in both cell lines, however. Besides, the PM formulation of A4 was more effective as a chemo-sensitizer when combined with oxaliplatin, while both free and PM/A4 showed similar activity in sensitization of CRC cell lines to carboplatin. Similar trend was observed in MTT assay, where the chemo-sensitizing activity of A4 was more noticeable in combination with carboplatin particularly in SW620 cells. Similar to colony forming assay, in MTT assay only PMA4 showed sensitizing activity in combination with oxaliplatin in SW620 cells, as well.

#### Conclusions:

The results points to PM A4 as a nano-formulation for this novel inhibitor of ERCC1/XPF capable of sensitization of CRC cells to the anticancer activity of platinum-based chemotherapeutics.

**Chapter Three: Repurposing pyronaridine as a novel inhibitor of heterodimeric ERCC1-XPF DNA endonuclease complex for target sensitization of colorectal cancer to platinum-based chemotherapeutics**

### 3.1. Introduction

Colorectal cancer is the third most diagnosed cancer worldwide and the fourth cause of cancer death around the world. While regular screening has helped to decrease colorectal cancer mortality in some parts of the world, it is anticipated that by 2035 due to factors such as population growth and aging, there will be 60 and 71 % growth in the number of colon and rectal cancers, respectively (96). Surgery is the main curative option for individuals with colorectal cancer that has not spread beyond the colon (97–99). In some cases, chemotherapy is used before the surgery in a neoadjuvant setting to enhance the chance of treatment success. In addition, in metastatic cases, chemotherapy would be the major course of treatment to reduce tumor load and even tumor stage. This highlights the importance of chemotherapy in the management of colorectal cancer (98,100–103).

Even though platinum-based drugs, alone and combined with other chemotherapeutic agents, have been used to treat various malignancies, including ovarian, bladder, head and neck, and colorectal cancer, response to this treatment is limited (26). In order to exert their effects, platinum drugs must attach to a cell's DNA and create DNA adducts. These adducts then cause intrastrand or interstrand cross-links. As a result of these cross-links, DNA molecules' structural integrity will be compromised. Both carboplatin and oxaliplatin damage DNA, which ultimately causes cell death (26,29,76,77). Different mechanisms, including decreased cellular uptake (78), increased drug efflux, and enhanced DNA repair mechanisms (29,75), can lead to chemoresistance against the effectiveness of platinum based chemotherapeutics. Adverse side effects such as neurotoxicity is another limiting factor hindering the effective use of platinum based chemotherapy in clinic (26–28).

In spite of the fact that the damages that are done to the DNA of the cells by DNA damaging agents could eventually result in cells apoptosis, it can also result in the activation of many DNA repair mechanisms including Nucleotide excision repair pathway (NER) leading to chemotherapeutic resistance. Based on previous studies it was demonstrated that blocking this pathway with small molecules can increase the sensitivity of cancer cells to the effect of certain genotoxic treatments (26,76,77).

The heterodimeric enzyme, ERCC1-XPF is essential for the NER pathway. The primary function of ERCC1 in this structure, which is thought to be catalytically inactive, is to bind to XPF while XPF has endonuclease activity (81,82). Due to its crystal structure and availability of several binding sites on the protein that may be targeted by small molecule inhibitors, ERCC1-XPF is a desirable target for the sensitization of cancer to platinum based chemotherapeutic (71).

Our research group have been focusing on the development of small molecules that can block the active sites of XPF protein, preventing its dimerization with ERCC1. This was shown to result in the sensitization of many cancer cell types to the effect of platinum based chemotherapeutics (71).

While investing a wide number of compounds, West et al. found a clinically available antimalaria drug, i.e., pyronaridine, with a very similar structure to lead ERCC1/XPF inhibitors developed by their group (including A4 compounds that was used in the previous chapter).

Pyronaridine, has been studied for its cytotoxic effects for almost a decade now (104). It is a water-soluble compound that can be found in the form of tetraphosphate salt (105). Our recent data using Proximity ligation Assay (PLA assay) has confirmed the ability of pyronaridine as an

inhibitor of ERCC1/XPF dimerization at 2 $\mu$ M (91). It was shown to inhibit the catalytic activity of ERCC1/XPF at levels like that of A4 and act as a radiosensitizer in combination with ionizing radiation.

Although our preliminary results confirmed the potential of pyronaridine as a chemosensitizer through inhibition of ERCC1/XPF dimerization, lack of cancer specificity is still a concern for systemic co-administration of this compound with chemotherapeutic agents. To overcome this problem, we proposed developing nanocarriers of pyronaridine that can direct this chemo and radio sensitizer to solid tumors by enhanced permeation and retention (EPR) effect.

Considering the water solubility of this compound, liposomal delivery system was proposed for the nano-encapsulation of pyronaridine (106). Liposomal encapsulation of PYD by remote loading in liposomes (DOPC, DSPE-PEG2000, Cholesterol) with an interior of citrate buffer has been reported in the literature before (107). Here we conducted the modification of the lipid composition and change in the interior pH of the liposomes, in order to define the optimum formulation for in vivo testing. At the same time the potential of PYD and its liposomal formulation as chemosensitizers in combination with two platinum chemotherapeutics, carboplatin and oxaliplatin, in colorectal cancer cells was assessed, *in vitro* (107).

## **3.2. Material and Methods**

### **3.2.1. Materials**

Pyronaridine tetraphosphate was purchased from abcam, United Kingdom. Lipids including 1,2-Distearoyl-*sn*-glycero-3-phosphocholine (**DSPC**), 1,2-distearoyl-*sn*-glycero-3-phosphoethanolamine-*N*-[methoxy(polyethyleneglycol)-2000] (**DSPE-PEG**), Cholesterol, 1,2-

Dioleoyl-*sn*-glycero-3-phosphocholine (**DOPC**), 1-palmitoyl-2-oleoyl-*sn*-glycero-3-phosphocholine (**POPC**), 1,2-dipalmitoyl-*sn*-glycero-3-phosphocholine (**DPPC**), were all purchased from Avanti Polar Lipid, Inc. (Alabaster, AL, USA). Sodium Dodecyl Sulfate (electrophoresis purity reagent) was bought from Bio-RAD. All the research grade solvents were purchased from sigma (St. Louis, Mo, USA). Spectra/Por dialysis tubing (MWCO, 3.4KDA) was purchased from Spectrum Laboratories (Rancho Dominguez, CA). Cell culture media DMEM, fetal bovine serum (FBS), and penicillin-streptomycin were purchased from GIBCO (108).

### **3.2.2. Preparation of Pyronaridine-Loaded Liposomes**

Liposomes were made with a thin lipid film hydration method. For the preparation of liposomes DSPC, DOPC POPC or DPPC were mixed with DSPE-PEG and cholesterol at a molar ratio of 75:5:20. Phospholipids were dissolved in chloroform/methanol at a ratio of 5:1 V/V and transferred to a 100 mL round bottom flask. The solvent was removed using a rotary evaporator (Rotavapor RE111, Buchi, Switzerland) while applying vacuum and heat (Starting at 37 °C and then increasing the temperature to around 50°C or before the solvents start boiling). After the formation of the thin lipid layer, the flask was kept in a vacuum oven at room temperature overnight, to make sure there is no trace of organic solvent left. The thin lipid layer was then hydrated with 200mM of citrate buffer (pH 3.5), to achieve a final lipid concentration of 10 mM. For some samples, the thin lipid film was hydrated in 200 mM citrate buffer (pH 5) or 200-mM phosphate buffer (pH 6.5). The buffers were heated to 85 °C.

A water bath sonicator (Elma Elmasonic S10H Heated Ultrasonic Water Bath, Elma Schmidbauer GmbH, Germany) preheated to ~ 80°C set at 100% power and 37KHz frequency was used to downsize the liposome. The desirable size and quality of lipids are usually reached within 4 to 5

rounds of 20 minutes of sonication while applying heat (108,109). The buffer outside was replaced by PBS using Sepharose column, creating a pH gradient formulation with an acidic pH inside and a neutral pH of 7.4 outside of the liposomes.

### 3.2.3. Encapsulation of Drugs in Liposomes

The molar ratio between liposome and drug should be 10:1. A 1.5 mg of pyronaridine tetraphosphate was then added to the liposomal solution. The drug and the liposomes were incubated at room temperature for about 17 h. The unencapsulated drug was separated from the loaded liposomes by pelleting drug-loaded liposomes via ultracentrifugation (150,000 x g, 4°C, 2.5h). The supernatant was then discarded and replaced with fresh PBS solution.

### 3.2.4. Characterization of loaded and unloaded liposomes

The average size (Z-average), the polydispersity Index (PDI), and the zeta potential (ZP) of liposomes were assessed by dynamic light scattering (DLS) using a Zetasizer Malvern Zetasizer 3000 (Malvern Instruments Ltd., Malvern, UK).

The encapsulated drug levels were measured by disrupting the liposomes using a 4% SDS solution. Pyronaridine absorbance at 426nm was used to assess encapsulated drug levels in a plate reader (Synergy H1 Hybrid Reader Biotek, Software Gene5 11.1). The loading and encapsulation efficiency of the loaded liposomes were calculated with based on the following equations.

$$\text{Pyronaridine loading (\%)} = \frac{\text{Weight of the encapsulated A4 in Nps}}{\text{Total weight of the polymer in NPs}} \times 100$$

$$\text{Pyronaridine Encapsulation efficiency (\%)} = \frac{\text{Weight of the encapsulated A4}}{\text{Initial weight of the A4 added}} \times 100$$

The morphology of the liposomes was checked with Transmission Electron Microscopy TEM. Sample preparation for TEM was done using a drop of liposome dispersion with the concentration of 10 mM transferred to a copper coated grid and incubated at room temperature for 20 minutes so that the liposomes settle on the membrane on the grid. The samples are then rinsed through 8 drops of water over parafilm each for almost 1 minute. The samples sat on 9:1 ratio of 2% methyl cellulose: 4% of uranyl acetate on ice for 10 minutes. After all the steps were done then it was lifted the grid and dry if off with Whatman paper to remove the excess liquid before imaging. The samples were observed under the electron microscope at 80kv (110). The prepared TEM specimens were then analyzed in a Morgagni 268 TEM microscope (Philips/field emission). The inserted camera was Gatan a CCD camera (111).

### 3.2.5. In vitro drug release

The *in vitro* release of the encapsulated pyronaridine from the liposomes was investigated using a dialysis-bag diffusion method. Each dialysis bag (Spectrapor dialysis tubing, MWCO = 3.5 kD, Spectrum Laboratories, Rancho Dominguez, CA, U.S.A.) only permeable to the drug, containing 2 mL of the liposomal formulation or free drug dissolved in PBS, was placed into 20 mL of PBS maintained at 37 °C in a shaking water bath (90 rpm, Julabo SW 22 shaking water bath, Seelbach, Germany). At selected time intervals, 0, 1, 3, 6, 9, 12, 24, 36, 48, 72, and 96 hours, aliquots of 0.5 mL from the continuous phase of the dialysis bag (release medium) were collected



and replaced with an equal volume of fresh release media (PBS). The concentrations of released drugs in collected samples were determined using a UV–Vis Plate reader (BioTek Synergy H1, hybrid reader, BioTek Instruments, Inc., Winooski, VT, USA). Detection was performed at a wavelength of 260 nm. All experiments were carried out in triplicate. Due to the media dilution during the release process, the amount of pyronaridine released was corrected by the correction factor as shown in the following equation:

$$R_n^a = R_n^b + \frac{V_w}{V_m} \sum_{i=1}^{n-1} R_{n-1}$$

where,  $R_n^a$  is percent drug released at time point n after correction;  $R_n^b$ , percent drug released at time point n before correction;  $R_{n-1}$  percent drug released at time point n-1;  $V_w$ , the volume of sample withdrew (mL);  $V_m$  volume the release medium (mL). Finally, the release profiles of the formulations were plotted, and their mean release time (MRT) was calculated using the equation below:

$$MRT = \frac{\sum_{i=1}^n t_{mid} \Delta M_i}{\sum_{i=1}^n \Delta M_i}$$

where i is the sampling number, n is the last sampling number,  $t_{mid}$  is the time at the midpoint between  $t_i$  and  $t_{i-1}$  (calculated as  $(t_i + t_{i-1})/2$ ) and  $\Delta M_i$  is the additional amount of drug released between  $t_i$  and  $t_{i-1}$ .

In vitro drug release of the encapsulated pyronaridine in the DSPC: DSPE\_PEG2000: Cholesterol liposomal formulation with an interior pH of 3.5 induced by encapsulation of citrate buffer at this pH was also assessed against BSA/buffer media that mimics in vivo conditions better. Each

dialysis bag (Spectrapor dialysis tubing, MWCO = 3.5 KD, Spectrum Laboratories, Rancho Dominguez, CA, U.S.A.) contained 2 mL of the liposomal formulation or free drug in PBS. The dialysis bag was then emersed in 300 mL of PBS and 10 % BSA and maintained in 37 °C in a shaking water bath (90 rpm, Julabo SW 22 shaking water bath, Seelbach, Germany). At selected time points, 0, 1, 3, 4, 6, 8, 24, 48, 72h, 150 µL sample was taken from each dialysis bag and replaced with fresh PBS. The concentration remaining in the bag was quantified by plate reader at 426nm as described above and subtracted from the total drug concentration and used as the released drug concentration (89).

### **3.2.6. Liposome stability Assay**

For stability assay, liposomes that were hydrated with citrate buffer, holding a pH of 3.5 or 5.0 inside were kept in the fridge (4 °C) and at room temperature (22 °C). After a period of 16 days, all the samples went through ultracentrifugation (150,000 x g, 4 °C, for 2.5 h) to separate the portion of the drug that was still loaded from the portion that has leaked out of the liposomal formulations. The supernatant was discarded and replaced with fresh PBS. The resuspended liposomal pellets were then disrupted by 4% SDS and the amount drug that was still trapped in the liposomes was measured at 426 nm as explained above (108).

### **3.2.7. Cell lines**

Two human colorectal cancer cell lines HCT116, SW620 were obtained from American Type Culture Collection (ATCC). The cells were grown in DMEM which was supplemented by 10% FBS and 1% penicillin streptomycin (90).

### **3.2.8. Assessing the Cell toxicity of Pyronaridine and determining its IC50 in colorectal cancer model**

The The 3-(4,5-dimethylthiazol-2-yl)-2,5-diphenyl-2H-tetrazolium bromide (MTT) assay was used to assess the cytotoxicity of pyronaridine as a free compound and its liposomal formulation in DSPC: DSPE-PEG2000: cholesterol against HCT116 and SW620 cell line. Briefly  $2 \times 10^3$  cells were seeded in 96 well plates (100  $\mu$ M). The plates were incubated for 24 hours so that the cells adhere to the plate. The day after cells are treated with 12 different concentrations of pyronaridine. The cytotoxicity of the compound is assessed at 72h time point. After the mentioned time, the cells are given a 20  $\mu$ L of MTT solution (5 mg/ml) of MTT solution and incubated for 1.5 hours. The culture media was removed and replaced with 100  $\mu$ L of DMSO and after all the crystals are dissolved the percentage of viability is calculated based on the amount of light absorption of the dissolved crystals at 570 nm. The viability of all groups are calculated based on the media only treated cells.

### **3.2.9. Assessing the Cell toxicity assay in Combenefit format**

In a typical experiment,  $2 \times 10^3$  cells were seeded in each well of 96 well plate, 24 hours prior to the beginning of the test. The cells were kept in the incubator to give them enough time to adhere to the plates. The seeded cells were first treated with 11 different concentrations of Pyronaridine. After a 4-difference interval, the cells were treated with 8 different concentrations of the chemotherapeutic agent (carboplatin or oxaliplatin). The cells were kept in the incubator for 72 h. This was followed by addition of 20  $\mu$ L of the MTT solution (5  $\mu$ g/mL) which was exposed for 1.5 h to the cells. The media was then removed and the MTT crystals were dissolved in 100

$\mu\text{L}$  of DMSO. Absorption at 570 nm in each well was used to measure cell viability for drug treated cells compared to the ones treated with media as the negative control (93).

### **3.2.10. Colony formation assay**

For this test, 100 cells are seeded in petri dishes and kept in incubator for 24 h. The cells were then treated with 100  $\mu\text{L}$  of pyronaridine as the chemosensitizer. Four hours after, the cells received 100  $\mu\text{L}$  of chemotherapeutic agent. The media was changed with fresh media every 72 h after. The test duration for different cell lines varied between 7 to 14 days. At the end point of the test, the media was removed, cells were washed with PBS, fixed with freezing cold methanol, and stained with 0.5% crystal violet solution. The number of colonies were counted and after normalizing data the fraction of surviving cells was calculated (94).

### **3.2.11. Statistical Analysis**

Tests were repeated at least three times and the data are shown as mean  $\pm$  standard deviation. Statistical analysis of data was carried out using Graph Pad Prism 9 Software (GraphPad Software Inc., La Jolla, CA, USA). The significant difference was assessed with One-way ANOVA or two-way ANOVA followed by Tukey's post-hoc analysis. If a significant difference were seen between groups, they were compared using the Mann-Whitney U test. A value of  $p \leq 0.05$  was considered as significantly different in all experiments.

## **3.3. Results**

### **3.3.1. Optimization of the Liposomal formulation of pyronaridine**

The characteristics of the developed liposomal formulations are summarised in **Table 3.1** and **Table 3.2** The characterization of particle average diameter showed a mean Z-average

diameter at a range of ~ 80-110 nm, irrespective of the lipid composition and interior pH. The Polydispersity index of all formulations was below 0.264, which indicates a uniform size distribution.

**Table 3.1:** Characteristics of pyronaridine-loaded liposomal formulations prepared from various phospholipids with an interior pH of 3.5.

Formulation	Z average diameter (nm)	PDI	EE (%)	MRT (h)
DOPC	83.09 ± 0.469	0.219 ± 0.011	97.9 ± 1.38	37.85 ± 2.49
POPC	84.05 ± 0.228	0.211 ± 0.003	95.4 ± 1.22	7.51 ± 0.31
DPPC	90.46 ± 0.383	0.247 ± 0.010	93.6 ± 1.32	4.60 ± 1.38
DSPC	107.6 ± 1.67	0.193 ± 0.009	99.24 ± 1.76	247.7 ± 16.3

**Table 3.2:** Characteristics of empty and pyronaridine-loaded liposomal formulations prepared from DSPC/DSPE-PEG and cholesterol with different interior pH.

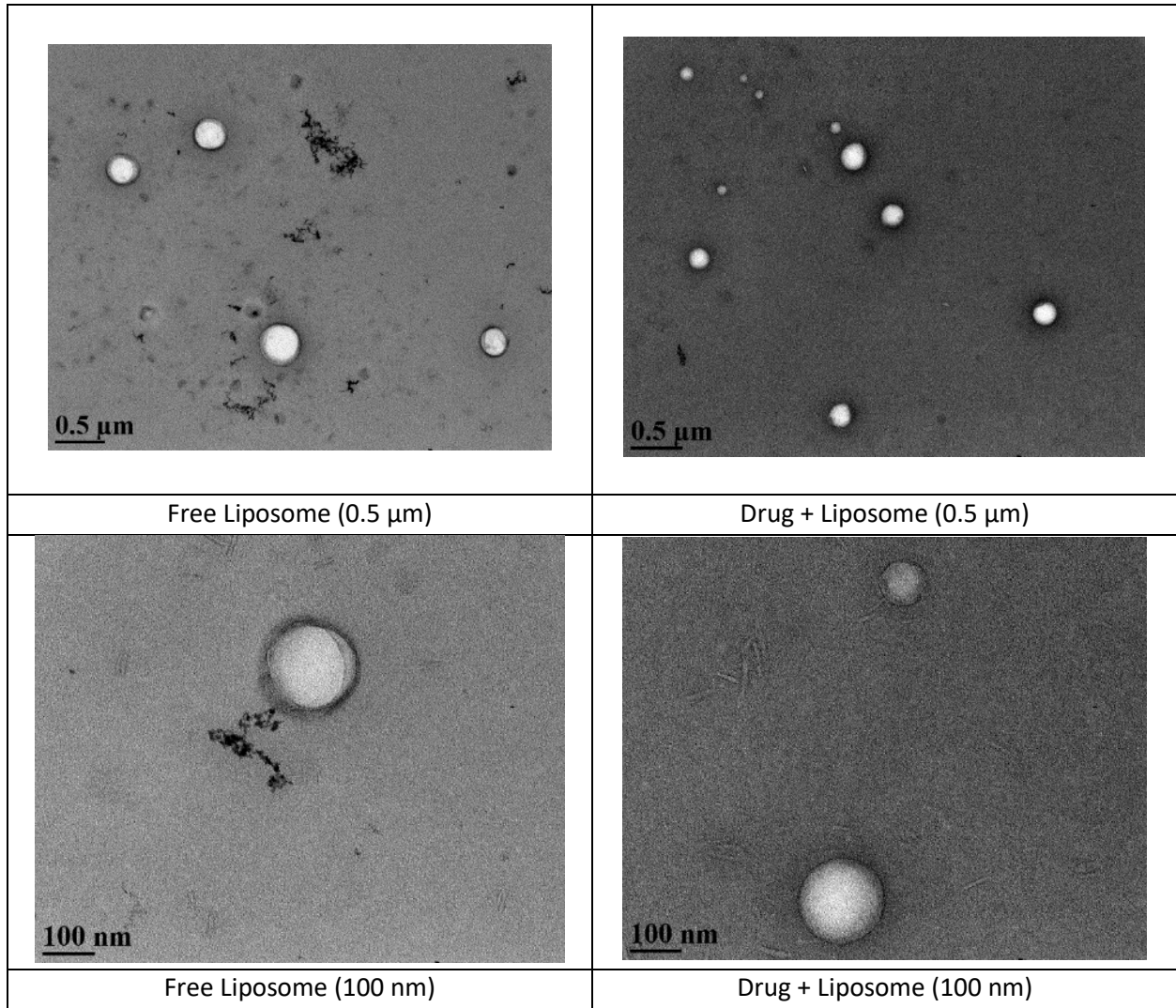
Formulation	Z average diameter (nm)	PDI	EE (%)	MRT (h)
Drug-loaded, pH 6.5	106.3 ± 0.95	0.216 ± 0.011	34.85 ± 1.29	16.63 ± 1.91
Drug-loaded, pH 5.0	103.8 ± 0.67	0.218 ± 0.009	97.51 ± 2.49	144.9 ± 5.62
Drug-loaded pH 3.5	107.6 ± 1.67	0.193 ± 0.009	99.24 ± 1.76	247.7 ± 16.3
Plain, pH 6.5	92.23 ± 0.752	0.226 ± 0.008		
Plain, pH 5.0	90.25 ± 0.123	0.199 ± 0.003		
Plain, pH 3.5	90.62 ± 0.286	0.225 ± 0.005		

MRT: Mean Release Time

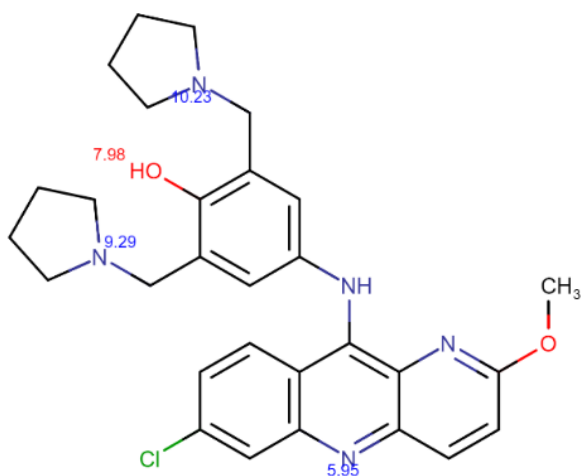
The type of phospholipid structure used in the preparation of liposomes did not affect encapsulated levels of pyronaridine in the liposomes at an interior pH of 3.5 (**Table 3.1**). However, Elevating the pH of the liposomal interior to 6.5 lowered the encapsulation efficiency of pyronaridine significantly. (**Table 3.2**).

Among all the developed formulations, DSPC, DSPE-PEG, and cholesterol holding a pH of 3.5 inside and 7.4 outside with a molar ratio of 10:1 (Lipid: Drug) demonstrated the highest encapsulation efficiency of higher than 99 percent. At pH 6.5 however, the encapsulated fraction was proportionally lower (35%). Testing different acidic pHs inside the liposomes demonstrated

that a sufficient pH gradient is necessary for reaching the desired loading and its disturbance would result in the lack of Pyronaridine encapsulation.



**Figure 3.1:** TEM pictures of DSPC with luminal pH of 3.5 Liposomal formulations (loaded and unloaded with pyronaridine). Images were obtained at 80 kV and two different magnifications of 18000x and 22000x and 89000x



*Figure 3.2: Pyronaridine structure, showing the pKa of different protonable groups*

There is a considerable variation between the sizes that were obtained by TEM microscopy and by Dynamic light scattering. Which could be due to a variety of reasons including the fact that the number of particles that are assessed and measured with microscopy is too low and inconclusive. Yet it is an adequate approach to confirm the formation of the free and loaded liposomes. The pictures are taken at 3 different magnifications as both free and encapsulated ones, and it is demonstrated in **Figure 3.1**. The formulation that was analyzed were DSPC based liposomes with luminal pH of 3.5.

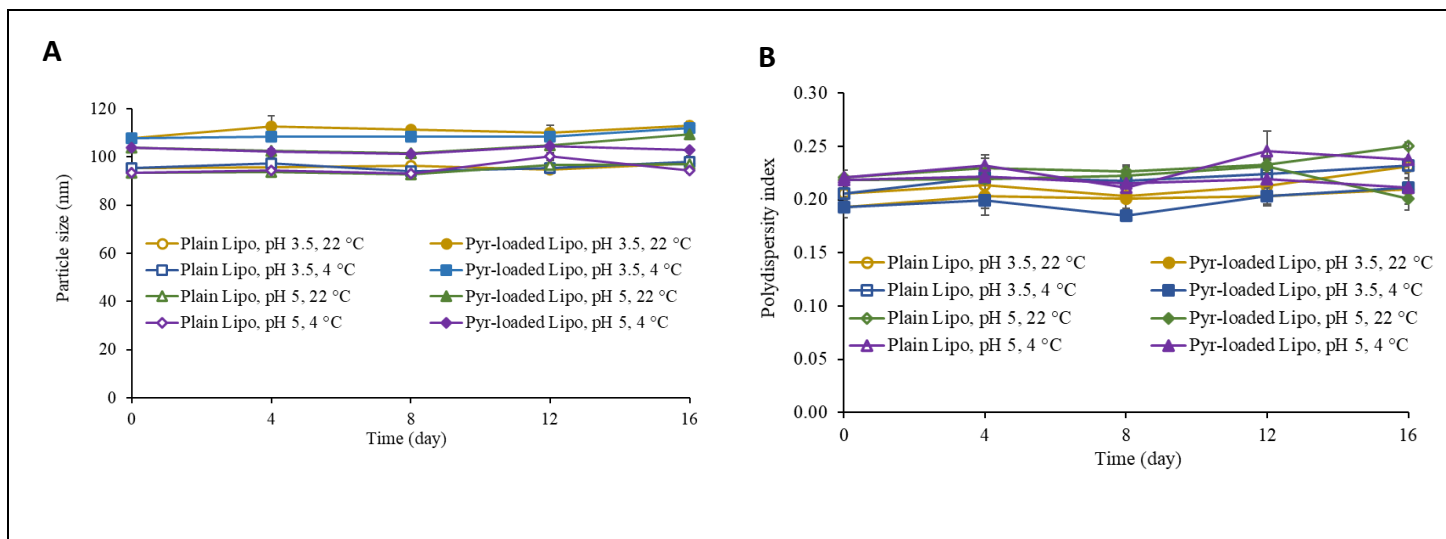
In pictures with higher magnification, it was also possible to visualize the bilayer structure of liposomes.

### 3.3.2. Stability of prepared liposomal formulations

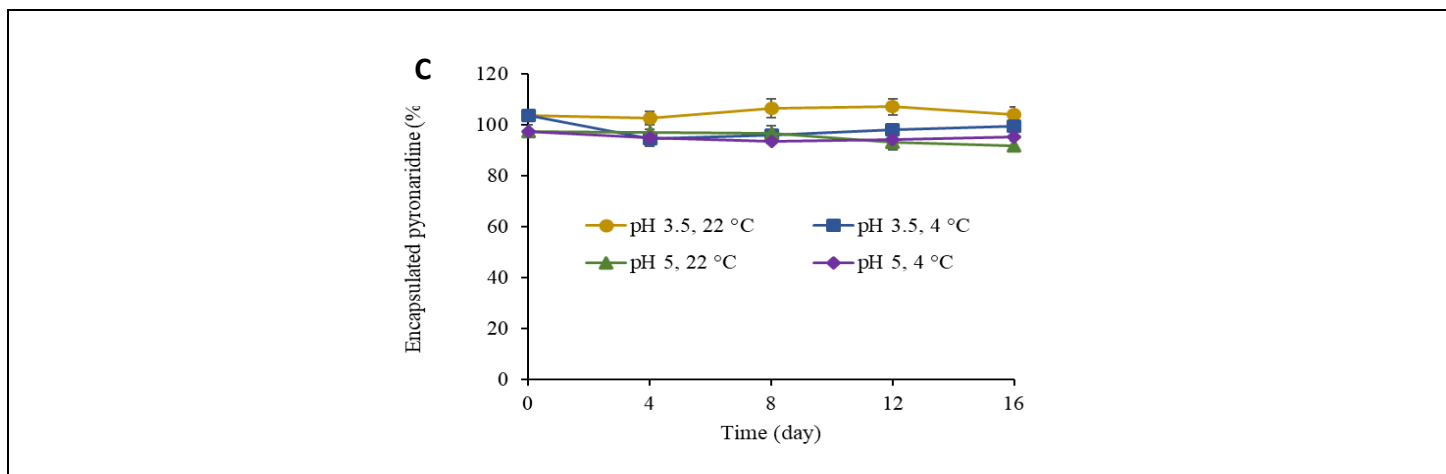
The concept of how drug gets loaded in the liposomes is based on the degree of lipophilicity of the drug at different pH. As the result of drug being entrapped in the acidic pH and

getting protonated, the level of lipophilicity drug decreases significantly. Yet as the more drug gets loaded, the reaction shifts toward consumption of [H+] and production of protonated pyronaridine until, eventually, the pH gradient is canceled. To investigate if this phenomenon would result in drug leakage from the liposomes, the amount of pyronaridine that remained encapsulated in the samples were measured following 16-day storage at both room temperature (22 °C) and fridge (4°C). Our results showed that the percentage of the encapsulated drug was maintained for the duration of the assay for all liposomal formulations under study **Figure 3.3.C** Vesicles appeared to maintain their integrity upon storage based on the assessment of changes in their size and polydispersity index during storage for 16 days **Figure 3.3.A** and **Figure 3.3.B**

The following graphs demonstrate the size and Polydispersity index of the DSPC, DSPE-PEG 2000, Cholesterol formulation, both loaded and unloaded with two different pH's over 16 days.







**Figure 3.3:** Stability of DSPC-based liposomal formulations of pyronaridine in terms of (A) Average diameter, (B) Polydispersity index, and (C) Encapsulation efficiency formulations with different lumen pH (3.5 and 5) following storage at 22 or 4 °C.

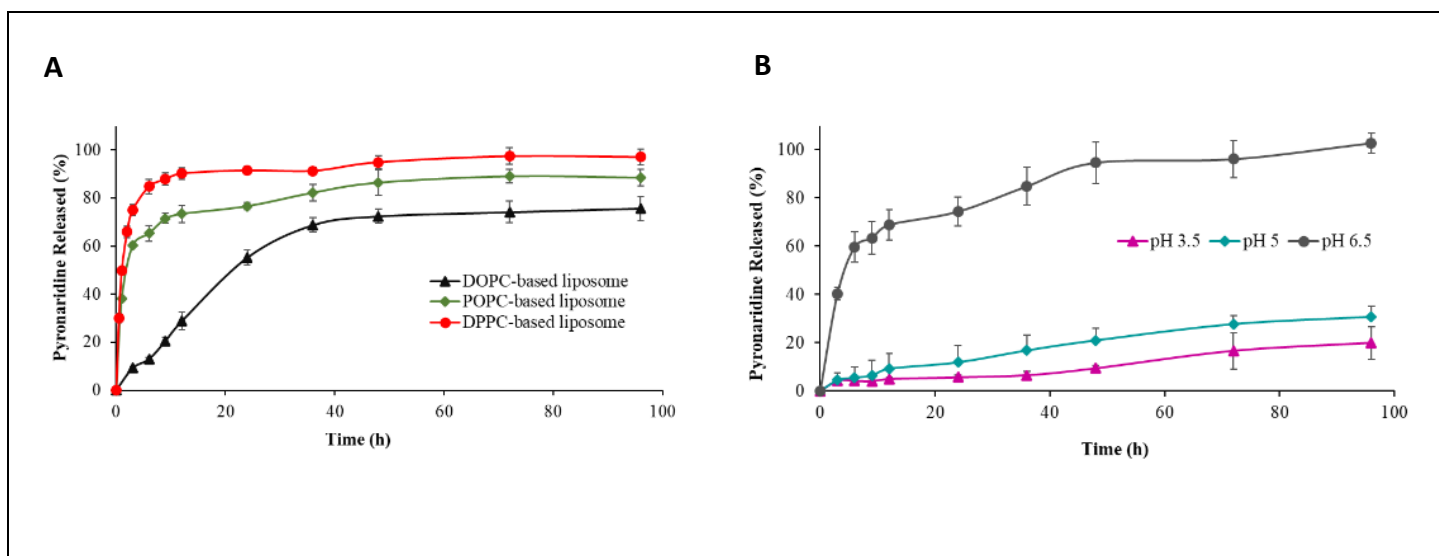
### 3.3.3. Release Study

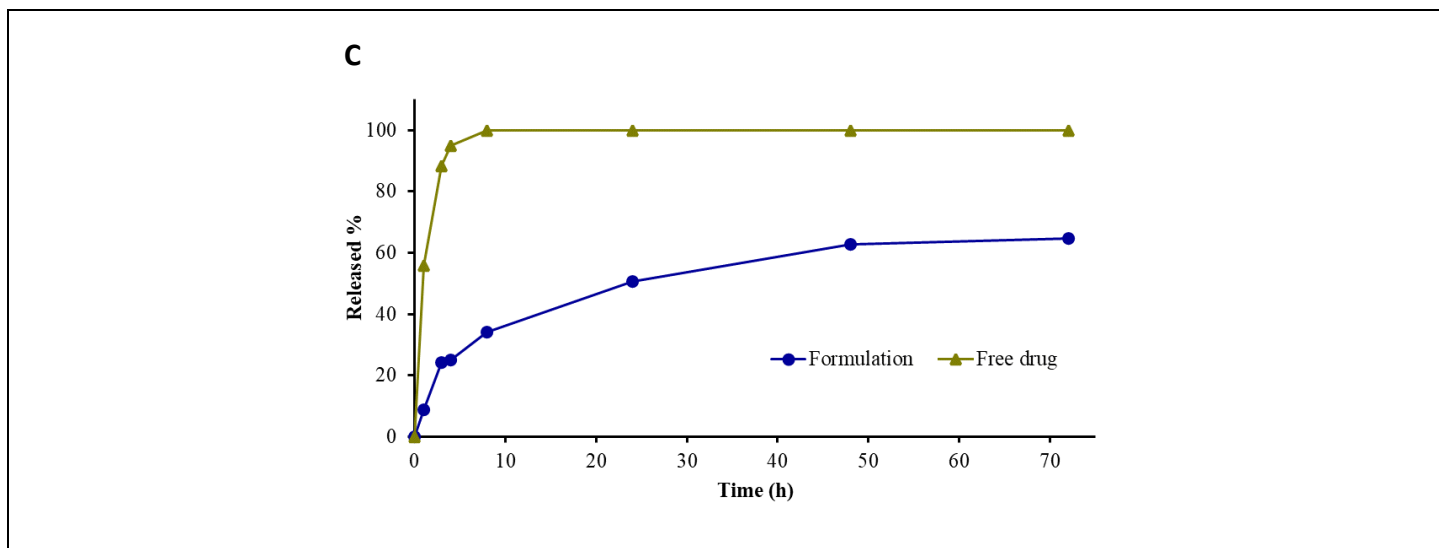
The result of the in vitro release of pyronaridine from DOPC-, POPC-, and DPPC- based liposomes with an interior pH of 3.5 are presented in **Figure 3.4.A**. The calculated corresponding MRTs (Mean Release Time) are presented in **Table 3.1**. Evidently, the drug release rate from the drug-loaded liposomes composed of DPPC and POPC was much faster than that of DOPC- based liposomes, reaching 60% of the release in less than 6h. The data did not show a sustained release pattern of the drug loaded in POPC and DPPC liposomes. The sustained release of the drug from DOPC liposomes resulted in an MRT (Mean Release Time) which was respectively 8 and 5 times longer than DPPC and POPC-based liposomes. Among different liposomal formulations of pyronaridine using an interior pH of 3.5 in DSPC based formulations showed the slowest release profile (MRT of 247.7 hrs).

**Figure 3.4.B** shows the effect of liposomes' interior pH on in vitro drug release at 37 °C for liposomes made from DSPC. The data suggest that increasing the pH accelerated the rate of drug

release. The MRTs of liposomes prepared at 3.5 (247.7h) and pH 5 (144.9h) were far different from DSPC liposomes prepared by hydrating at pH 6.5 (16.6h). Longer MRTs indicate slower release rates from the formulations. The mentioned data are presented in **Table 3.2:** Characteristics of empty and pyronaridine-loaded liposomal formulations prepared from DSPC/DSPE-PEG and cholesterol with different interior pH. Complete drug release was observed for liposomal formulation with inside pH of 6.5 after 96 hours, while only about 20 and 30% of the drug was released from DSPC liposomes with luminal pH of 3.5 and 5, respectively, at the same time.

Among all the developed formulations, DSPC, DSPE-PEG, and Cholesterol holding a pH of 3.5 inside demonstrated the best properties in terms of drug encapsulation and release.





**Figure 3.4:** The effect of (A) phospholipid type and (B) interior pH of liposomal formulations on the in vitro release of pyronaridine. (C) The in vitro release profile of free versus encapsulated pyronaridine at set time points during 72h test. Release media: PBS+10 %BSA

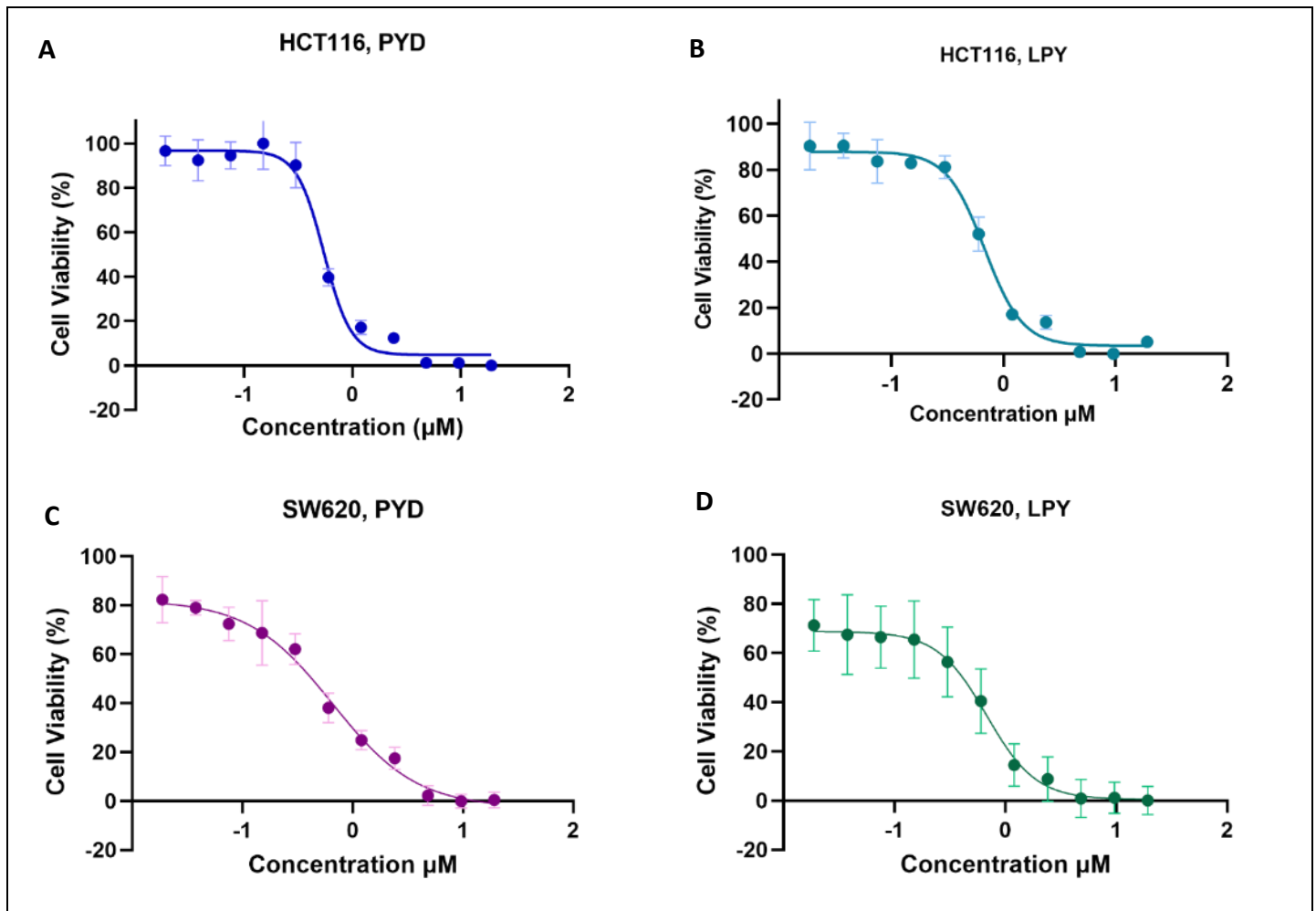
The release profile of free pyronaridine versus the DSPC based liposomal formulation is demonstrated in **Figure 3.4.C**. During the first 4 hours of the study, more than 90% of the free pyronaridine (95%) is released from the dialysis bag, while only 25% of the loaded drug is released from the liposomal formulation into the release media. After 24 hours, while all the free drugs are released into the released media (100% released), about 50% of drug-loaded liposomes were released from the carrier. After the first 24 hours the rate of release would decrease significantly until after 72h there is only an extra 15% is released from the liposomal formulation reaching to almost 65% release of the pyronaridine from the carrier. Among all the different liposomal conformations, and different luminal pHs, DSPC: DSPE-PEG 2000, Cholesterol with the pH: 3.5 has the best loading efficiency and drug release profile. As a result, all the further studies are done with DSPC: DSPE-PEG2000: cholesterol holding a pH gradient of 3.5 inside and 7.4 outside of the liposomes.

### 3.3.4. In vitro nonspecific cytotoxicity of Pyronaridine and its liposomal formulation against CRC cells:

The level of cytotoxicity of the compound was assessed against two different colorectal cancer cell lines. HCT116 and SW620. The cells were seeded 24 hours prior to the treatment and then treated with the 12 different concentrations and then incubated with the treatment for 72h, and then assessed with MTT assay. The data on the IC50 values are demonstrated in **Table 3.3** below. Also, the sigmoidal graphs of the cytotoxic effect of pyronaridine are shown in **Figure 3.5**.

*Table 3.3: The IC50 (mean ± SD) of free PYD and LPY against colorectal cancer cell lines measured by MTT (n=3)*

<b>(72 h)</b>	<b>IC50 of PYD (μM)</b>	<b>IC50 iof LPY (μM)</b>
<b>HCT116</b>	<b>0.558 ± 0.05</b>	<b>0.499 ± 0.33</b>
<b>SW620</b>	<b>0.758 ± 0.121</b>	<b>0.669 ± 0.212</b>



*Figure 3.5: The sigmoidal curves demonstrate half maximum inhibitory value (IC<sub>50</sub>) in **A**) HCT116 cell line free pyronaridine, **B**) liposomal formulation of pyronaridine, **C**) in SW620 cell line free pyronaridine, **D**) liposomal formulation of it*

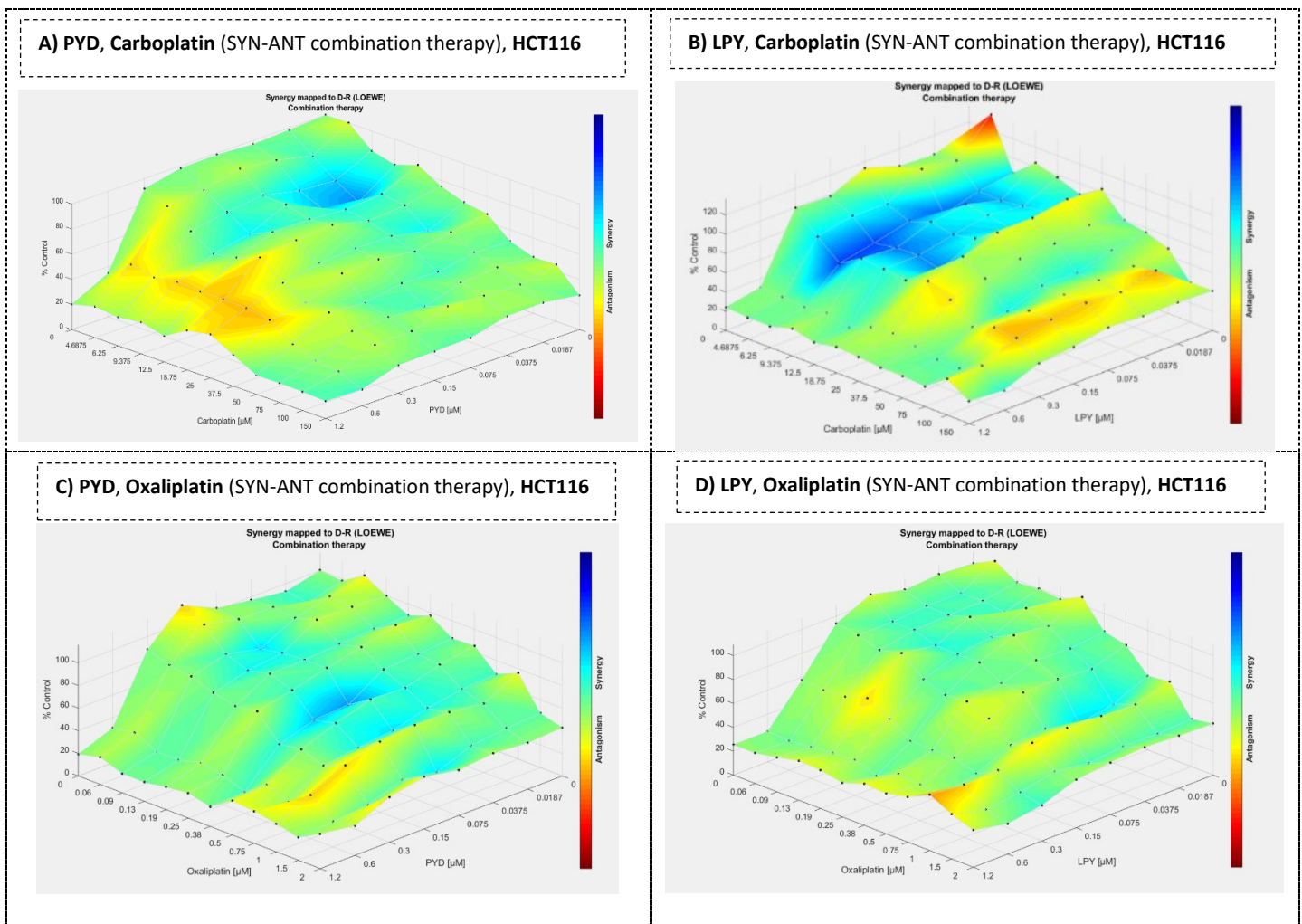
As it can be observed in the results, the HCT116 cell line is more sensitive to the effect of pyronaridine than SW620. Moreover, it seems that the formulation does not change the level of toxicity of the compound.

### 3.3.5. Sensitization of CRC to Carboplatin by Pyronaridine and its liposomal formulation and assessing the possibility of synergism

This test was designed based on the format that was necessary to analyze the results of the Combenefit application. In this set of tests, pyronaridine was given to the seeded cells 4 hours

prior to the chemotherapeutic agent (112). In this series of tests, we are using the combination approach, which is using the noneffective doses of drugs to analyze the possibility of getting significant results (113). Four concentrations of pyronaridine and all concentrations of the chosen chemotherapeutic agents were below the IC50 in both HCT116 and SW620 cell line.

The possibility of synergism was also assessed using the same application. Loewe model was chosen for analyzing the effects that drugs had on each other. Loewe model not only considers the dose equivalence principle but also the sham combination principle, which would make it the best approach for analyzing synergism in this study (113).

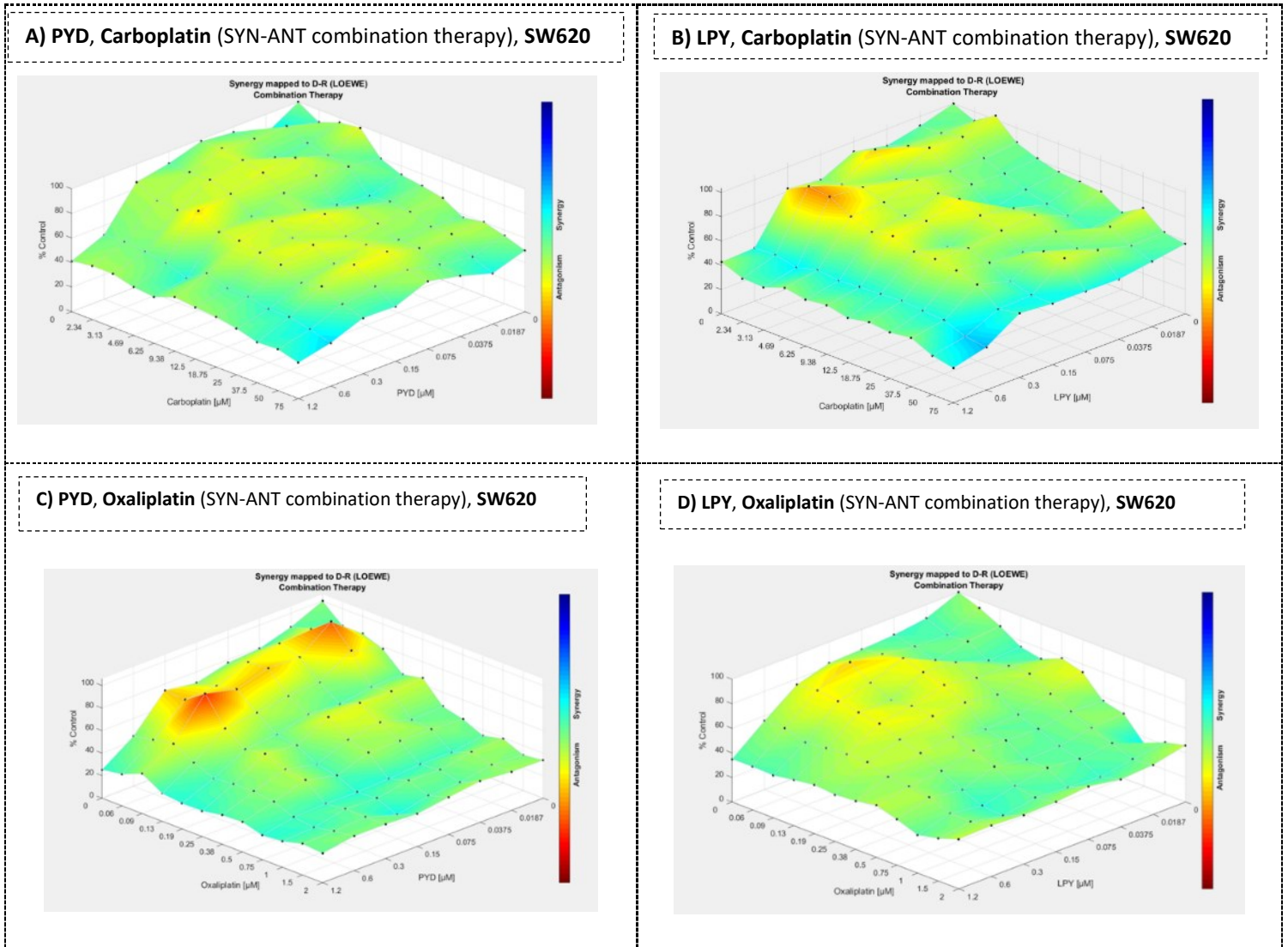


*Figure 3.6: Combeneft format of presenting synergism data on HCT116 cell line treated with A) Pyronaridine as free and B) liposomal formulation with Carboplatin. C) HCT116 cell line treated with Pyronaridine as free and D) liposomal formulation in combination with Oxaliplatin*

The results showed a chemosensitization of HCT116 cell line to the effect of carboplatin after treating with free and liposomal pyronaridine. HCT116 cell line were showing a minor synergism toward a combination therapy with Free pyronaridine in [0.0187-0.0375]  $\mu\text{M}$  concentration and Carboplatin in [6.25-12.5]  $\mu\text{M}$  concentration. On the other hand, liposomal formulation of pyronaridine were able to demonstrate a stronger synergism to the effect of carboplatin. Liposomal pyronaridine in the concentration range of [0.075-0.3]  $\mu\text{M}$  and Carboplatin in the concentration range of [6.25-18.75]  $\mu\text{M}$  (same as in the free treatment group) shows a high level of synergism which would indicate the potential for further cell studies and helps with choosing the concentration range.

The results on the combination therapy with pyronaridine (as free and liposomal formulation) are not as promising as the results we had on carboplatin yet in 0.15  $\mu\text{M}$  of pyronaridine and Oxaliplatin in the concentration range of [0.25-1]  $\mu\text{M}$  a slight level of synergism can be witnessed. These concentrations are used to further investigate the effects of chemosensitization on the HCT116 cell line while being treated with Oxaliplatin.

Same series of tests were done on SW620 cell line.



**Figure 3. 7:** Combeneft format of presenting synergism data on **SW620** cell line treated with **A) Pyronaridine** as free and **B) liposomal formulation** with **Carboplatin**. **C) SW620** cell line treated with Pyronaridine as free and **D) liposomal formulation** in combination with **Oxaliplatin**

As the results are indicating SW620 is less sensitive to the effect of chemosensitization yet on higher concentration of pyronaridine (0.6  $\mu\text{M}$ ) some synergisms can be seen. Loaded pyronaridine is demonstrating a higher-level effect in comparison to free drug. Also 0.6  $\mu\text{M}$  of



pyronaridine were able to sensitize SW620 to a broad concentration of Carboplatin [2.34-75]  $\mu\text{M}$  which would make it a desirable candidate for further studies.

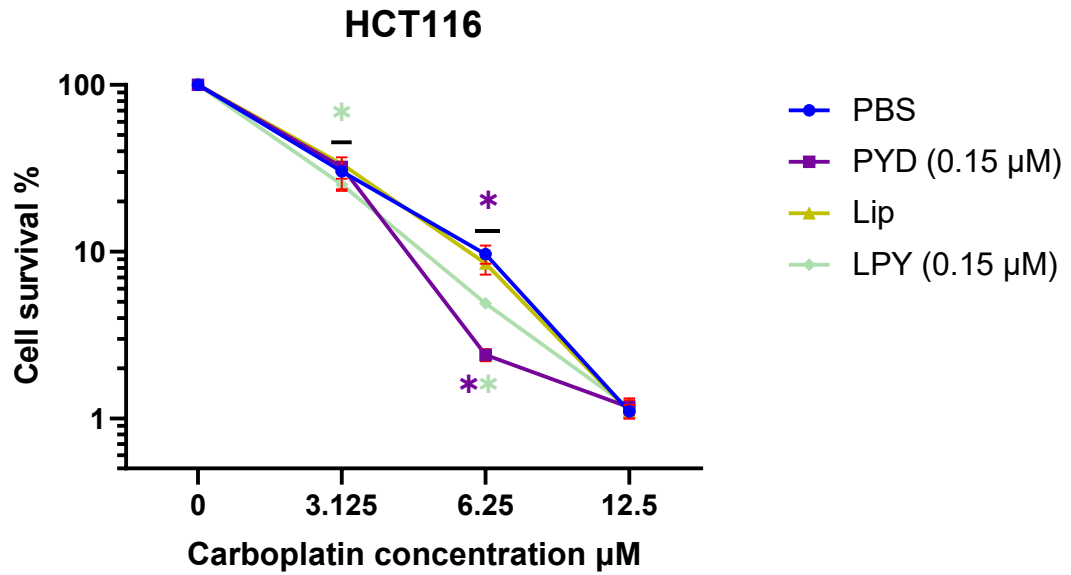
Both cell lines show better sensitivity to the effect of carboplatin in comparison to oxaliplatin. Although all in all HCT116 shows a stronger effect to chemosensitization compared to SW620. Also same as the group that were treated with carboplatin, SW620 cell line demonstrates an antagonistic effect to 0.15  $\mu\text{M}$  of pyronaridine while 0.6  $\mu\text{M}$  was able to sensitize SW620 to the effect of Carboplatin and at minimum have an additive effect to Oxaliplatin. A further series of colony formation assay were done to see if we could witness an aligned results to what we have in Combeneft sets.

### **3.3.6. Colony Forming Assay**

#### *3.3.6.1. HCT116*

The next step after assessing the effect combination therapy on both cell lines is colony forming assay. (All the subsequent data are normalized)

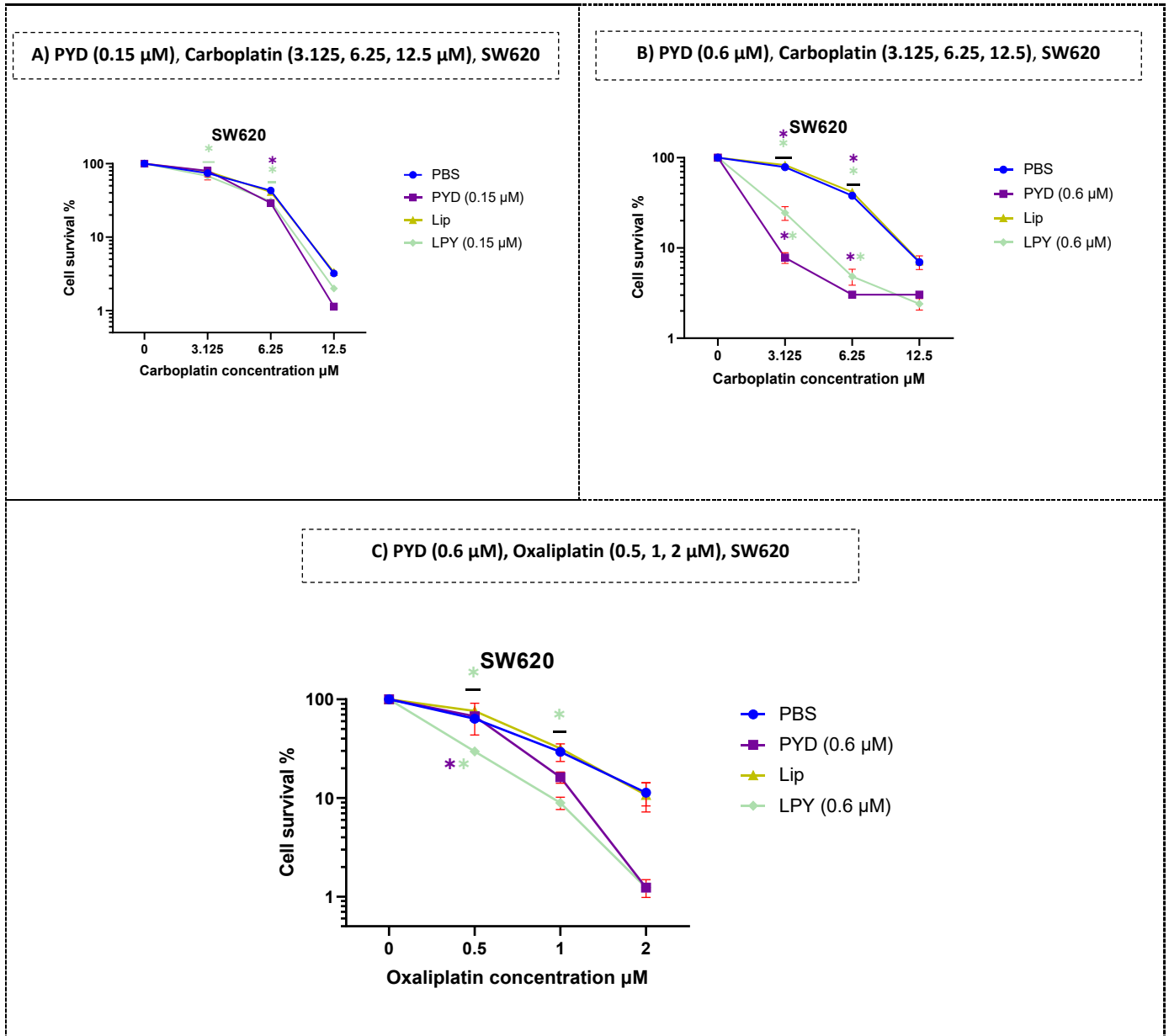
The concentrations were chosen based on the previous studies. The Combeneft studies demonstrated that 0.15  $\mu\text{M}$  of pyronaridine and a range of [2-18  $\mu\text{M}$ ] carboplatin in the HCT116 cell line could have a synergistic effect (Method of statistical analysis on the results: Two-way ANOVA, Tukey's multiple comparison test) (n=3)



**Figure 3. 8:** Clonogenic assay in HCT116 (0.15 µM) and Carboplatin (3.125, 6.25, 12.5 µM) (n=3). (\*Purple) Shows statistically significant differences from PBS as a control and PYD. \* Shows statistically significant difference from Lip as a control and LPY. (Two-way ANOVA, Tukey's multiple comparison test)

### 3.3.6.2. SW620

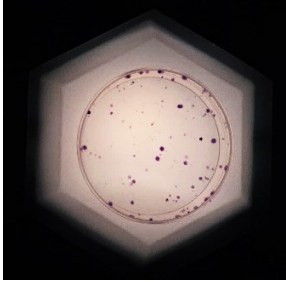
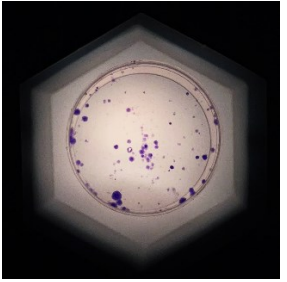
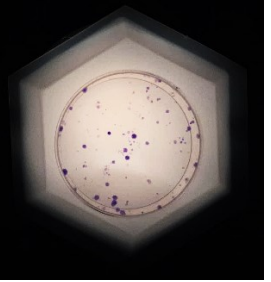
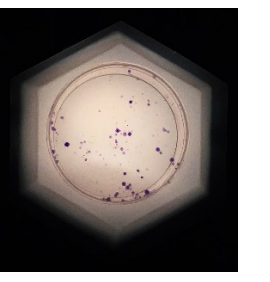
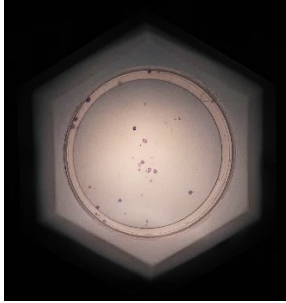
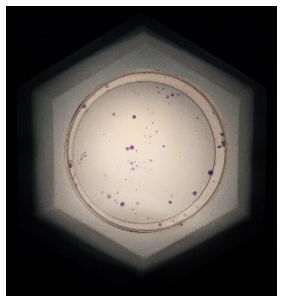
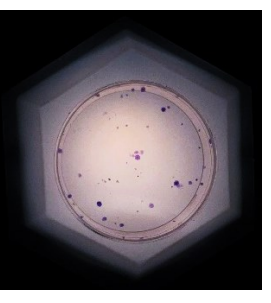
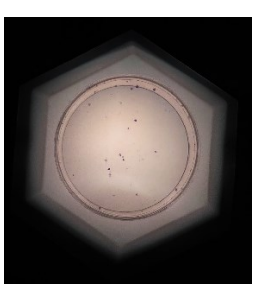
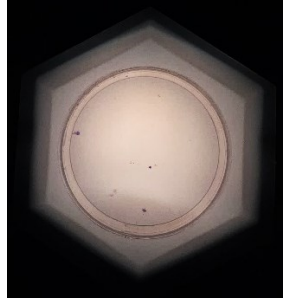
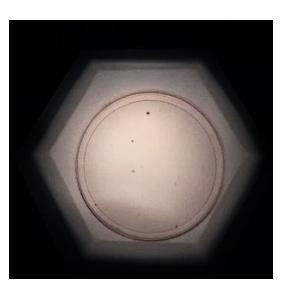
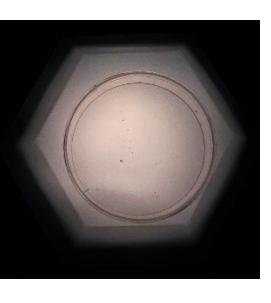
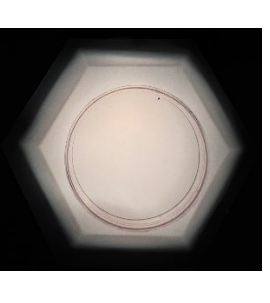
In comparison to HCT116 cell line, in SW620 cell line, the cells showed a considerably lower level of sensitivity to the chemotherapeutic agents. Although as it was observed before in the A4 project, the higher concentration of the chemosensitizer while demonstrating a level of cytotoxicity on its own also has a higher potential in sensitizing the cell to the effect of chemotherapeutic agents.



**Figure 3. 9.** The results of clonogenic assay following combination of PYD (0.15, 0.6  $\mu\text{M}$ ) and LPY with Carboplatin (3.125, .25, 12.5  $\mu\text{M}$ ) and Oxaliplatin (0.5, 1, 2  $\mu\text{M}$ ) against HCT116 and SW620. \* Shows statistically significant differences from the PBS as control and PYD. \* Shows statistically significant differences from the Lip as control and LPY. (Two-way ANOVA, Tukey's multiple comparison test)

### HCT116 Colony Pictures

PYD:0.15, Carboplatin:3.125, 6.25, 12.5  $\mu\text{M}$

HCT116	PBS	PYD (0.15)	Lip	LPY (0.15)
Carboplatin: 0 $\mu\text{M}$				
Carboplatin: 3.125 $\mu\text{M}$				
Carboplatin: 6.25 $\mu\text{M}$				

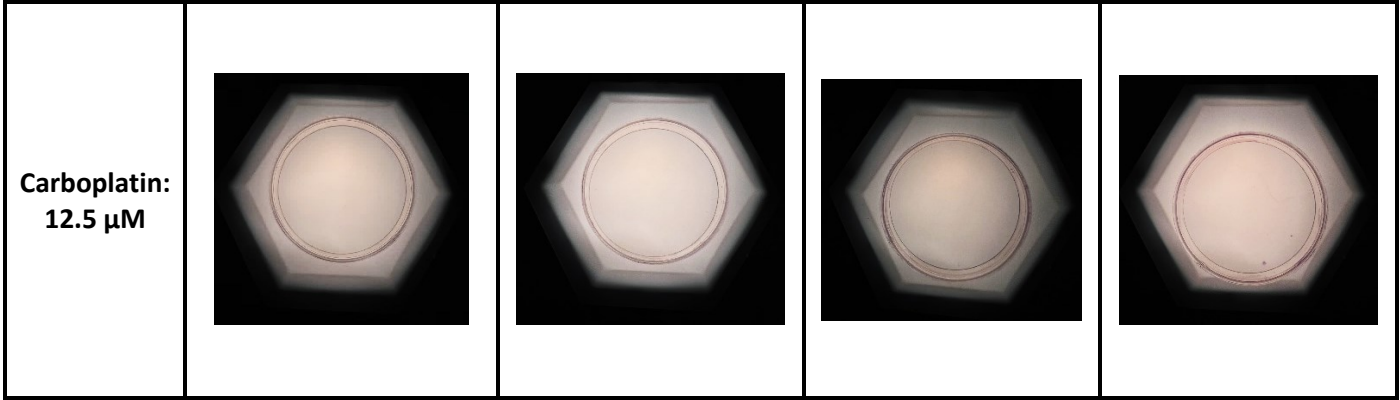
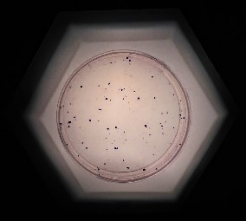
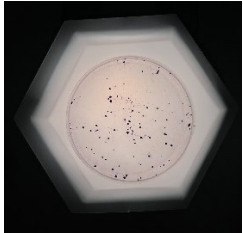
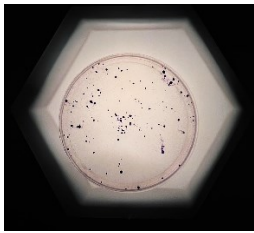
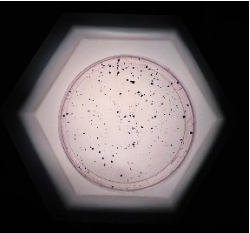
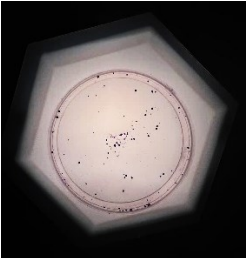
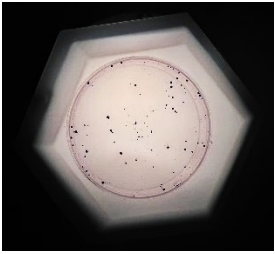

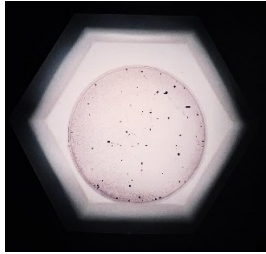


Figure 3.10: Clonogenic assay in HCT116, PYD (0.15  $\mu$ M) and Carboplatin (3.125, 6.25, 12.5  $\mu$ M) (n=3)

**SW620 Colony Pictures**

**PYD:0.15, Carboplatin:3.125, 6.25, 12.5  $\mu$ M**

HCT116	PBS	PYD (0.15)	Lip	LPY (0.15)
<p><b>Carboplatin: 0 <math>\mu</math>M</b></p>				
<p><b>Carboplatin: 3.125 <math>\mu</math>M</b></p>				

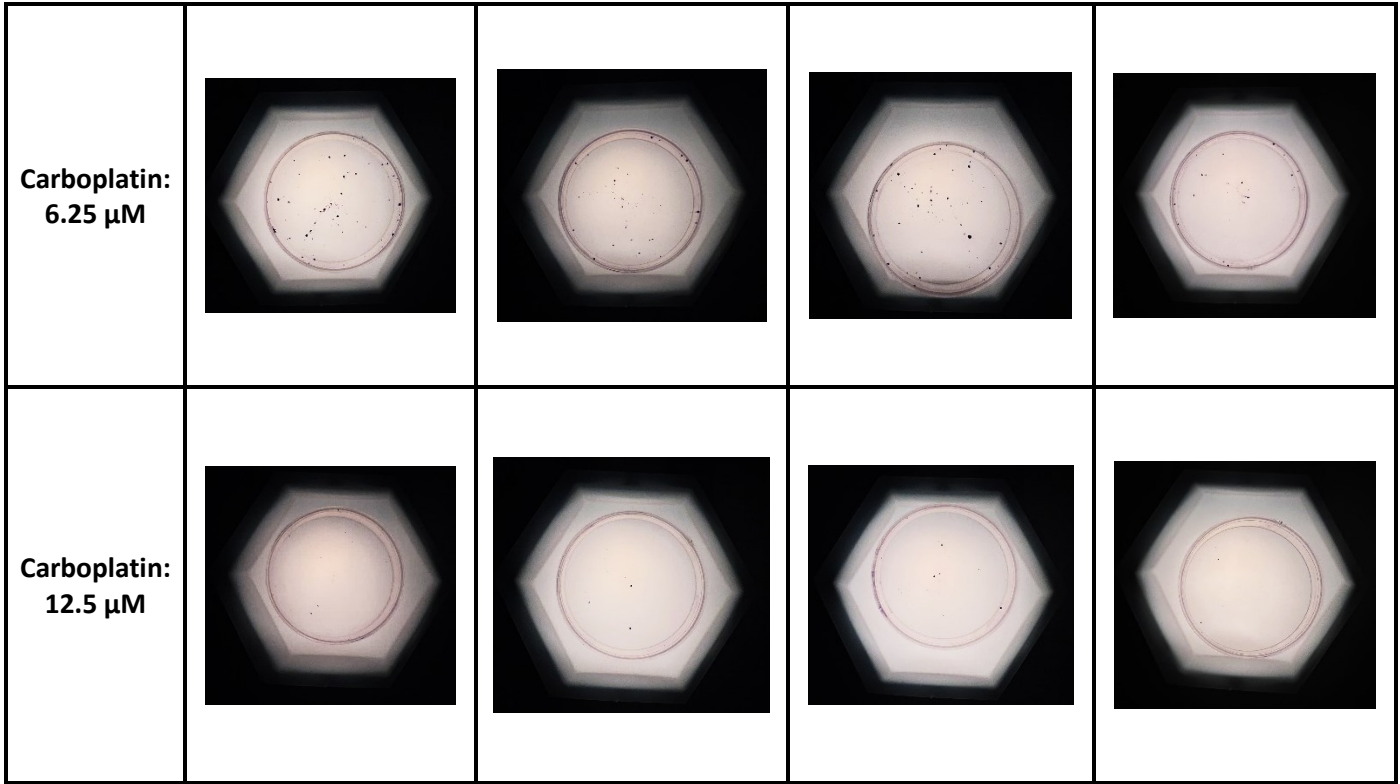
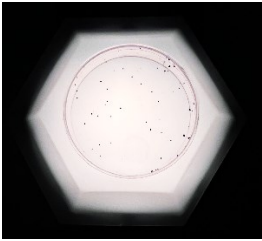
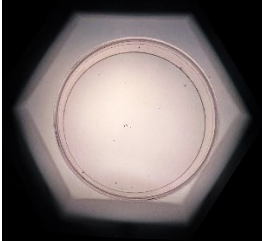
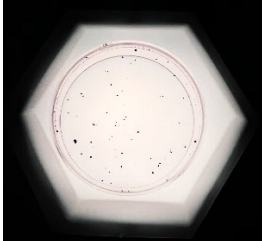
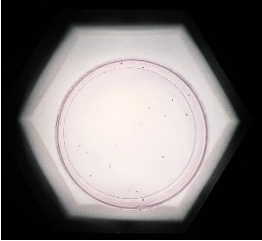

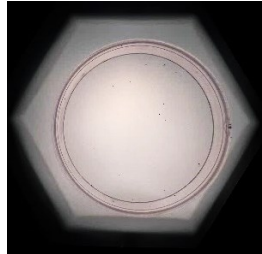
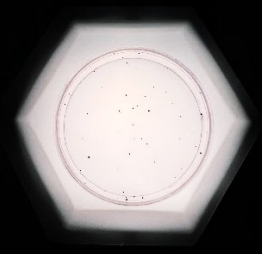
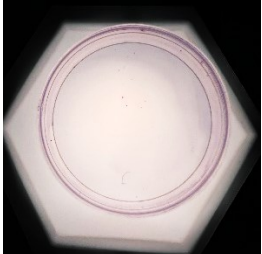
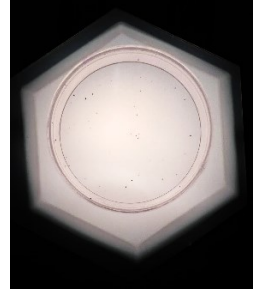

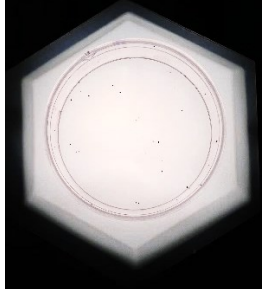
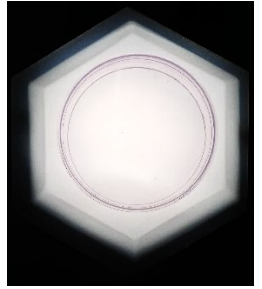


Figure 3.11: Clonogenic assay in SW620, PYD (0.15  $\mu$ M) and Carboplatin (3.125, 6.25, 12.5  $\mu$ M) (n=3)

### SW620 Colony Pictures

PYD:0.6, Oxaliplatin :0.5, 1, 2  $\mu\text{M}$

HCT116	PBS	PYD (0.6)	Lip	LPY (0.6)
Oxaliplatin: 0 $\mu\text{M}$				
Oxaliplatin: 0.5 $\mu\text{M}$				
Oxaliplatin: 1 $\mu\text{M}$				

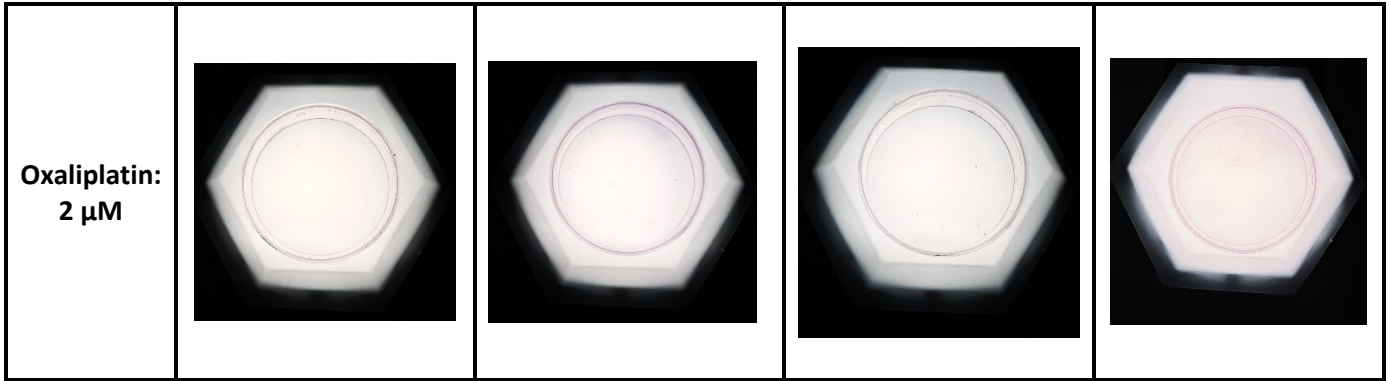
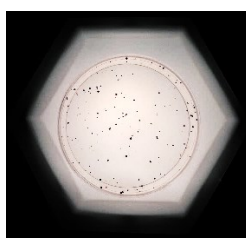
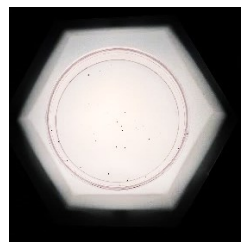
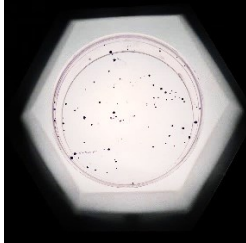
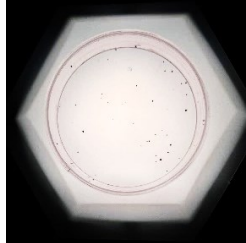
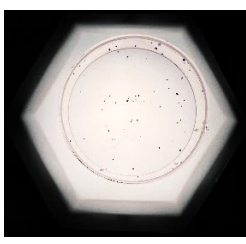
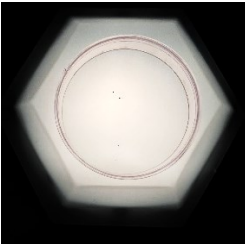
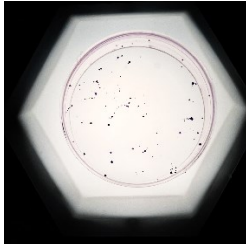
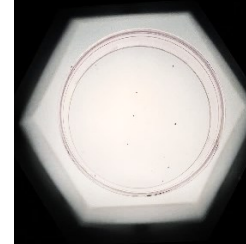


Figure 3.12: Clonogenic assay in SW620, PYD (0.6  $\mu$ M) and Oxaliplatin (0.5, 1, 2  $\mu$ M) (n=3)

**SW620 Colony Pictures**

**PYD:0.6, Carboplatin:3.125, 6.25, 12.5  $\mu$ M**

HCT116	PBS	PYD (0.6)	Lip	LPY (0.6)
<p><b>Carboplatin: 0 <math>\mu</math>M</b></p>				
<p><b>Carboplatin: 3.125 <math>\mu</math>M</b></p>				



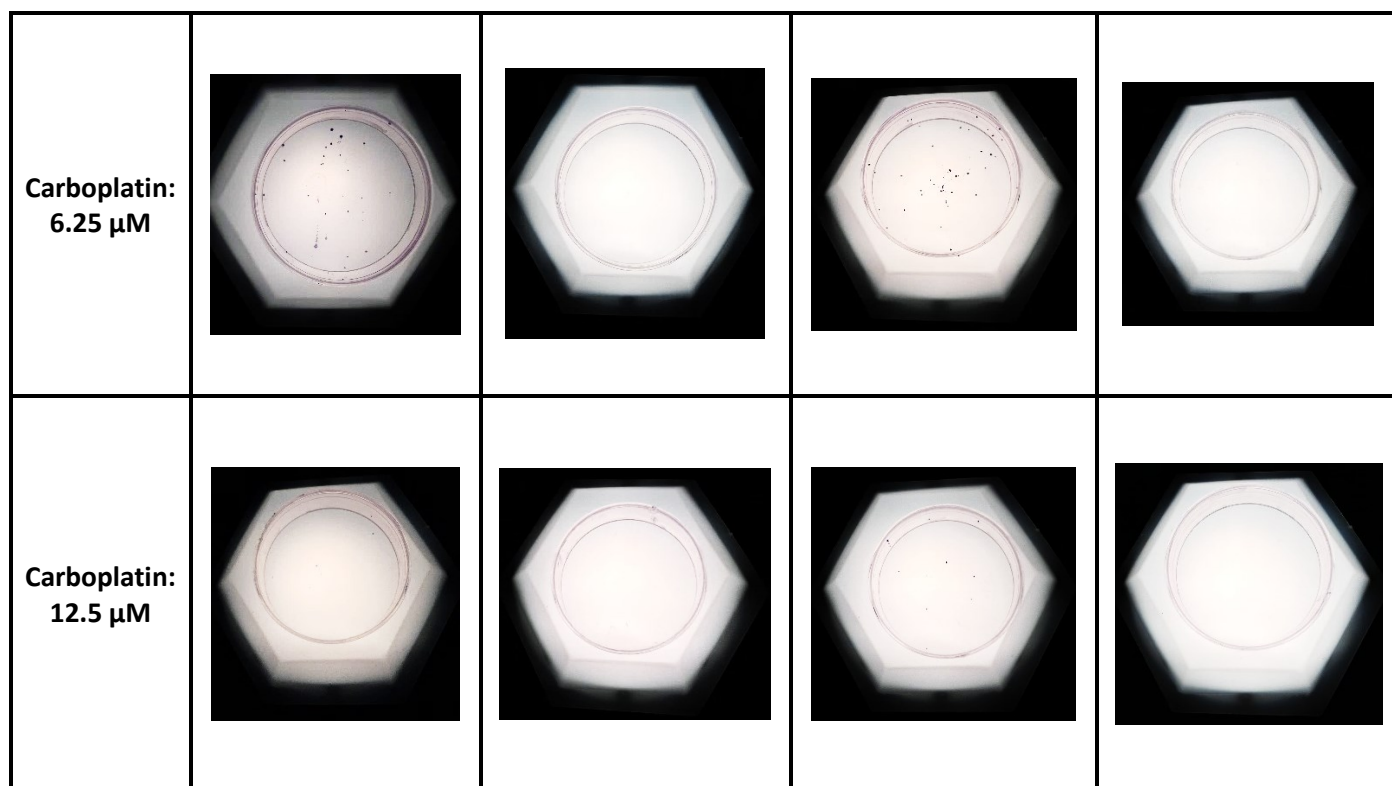


Figure 3.13: Clonogenic assay in SW620, PYD (0.6  $\mu$ M) and Carboplatin (3.125, 6.25, 12.5  $\mu$ M) (n=3)

### 3.4. Discussion

In this project, two objectives were followed. First, to find the most desirable delivery system for pyronaridine, which would provide a high encapsulation and a controlled release in biologically relevant media. Second to assess the effectiveness of pyronaridine as a chemosensitizer in combination with platinum-based drugs against colorectal cancer cell lines. Pyronaridine is an antimalaria drug clinically used since the 1970s. It has shown cytotoxicity against multiple cancer cell lines (104). Our research group has been interested in the repurposing of PYD as a novel inhibitor of ERCC1/XPF (71,91). The ERCC1/XPF complex plays a pivotal role in the nucleotide excision repair pathway, which is involved in the repair of DNA caused by alkylating agents, *i.e.* methylating agents that form adducts (34,71,114).

Inhibitors of DNA repair can make cancer cells more sensitive to the effect of DNA damaging agents but may show the same function in normal cells. This can lead to increased normal cell toxicity when used in combination with DNA damaging chemotherapeutics. In order to decrease the possibility of adverse side effects on normal cells, specifically when combined with DNA-damaging agents, this study focused on designing an optimum nano-delivery system with potential for preferential delivery of PYD to solid tumor over normal tissues. Such delivery system is expected to show high levels of PYD loading while reducing PYD release in vitro. Nano-delivery systems of proper size and stealth properties that can retain their drug content are expected to be able to change the pharmacokinetics and biodistribution of the cargo, redirecting its distribution from normal tissue to solid tumors, by EPR effect. Considering that PYD is a water-soluble compound, a liposomal formulation was considered to be the best option for this purpose (105).

Many cancers, including bladder, head and neck, ovarian and colorectal cancer, have been treated with carboplatin and oxaliplatin. Both chemotherapeutic drugs have the capability to damage the DNA of the cells (29). Adverse side effects, high toxicity, and drug resistance are among the reasons that limit the use of these groups of chemotherapeutics to a great extent. (27) ERCC1/XPF is a DNA repair enzyme that has shown to play a major role in the repair of DNA damage by platinum-based chemotherapeutics (29). In the current study, PYD and its liposomal formulation were hypothesized to act as effective chemosensitizers for carboplatin and oxaliplatin in colorectal cancer cells.

Among all the developed formulations with different luminal pHs, DSPC/DSPE-PEG200/Cholesterol with luminal pH of 3.5 demonstrated the best physicochemical

characteristics (107). The formulation achieved 99% encapsulation efficiency while only releasing 50% of the entrapped drug after 72h immersed in biologically relevant media. The modifications that were done in the formulation in comparison to what reported in the literature enabled higher encapsulation and an improved release profile got PYD (107). (Table 3.1, Table 3.2, Figure 3.4.)

Depending on the environment's pH, pyronaridine can be present in different ionization states. This is owed to the pKas of its hydroxyl and three Amin groups (7.98, 5.95, 9.29, 10.23) (The figure 3.2 demonstrates structure of PYD compound and the pKas of different protonable group) (107,115).

At pH 7.4, the pH of outside media for liposomal encapsulation, PYD is mainly present in an unionized form and is highly lipophilic (logD 0.34) (107,116,117). The higher lipophilicity will make the drug more prone to pass the lipid bilayer, entering the core of liposomes that hold an acidic pH of 3.5. The lipophilicity of the drug changes significantly when facing an acidic environment (117). At pH 3.5, 99.6% of pyronaridine molecules are protonated in all three amino groups (107) making PYD to get trapped within the liposomes effectively. Under this condition, more PYD gets loaded, the reaction shifts toward consumption of [H+] and production of protonated pyronaridine until, eventually, the pH gradient is canceled.

Higher values of pH in the liposome core (pH 5.0) decreased the drug loading and increased the rate of drug release for liposomes. This was due to the lower proportion of ionized PYD in pH 5.0 compared to that of pH 3.5 that can enhance the chance of PYD release and leakage or reduce the driving force for partition of PYD to the liposomal core during the encapsulation process.

Due to the significance of lipid phase transition temperature (TC) on liposome stability, drug release and apparent circulation lifetimes, we examined the effect of lipids with varying TC in the liposome composition on the release and encapsulation of PYD, as well. Our results showed that the level of drug encapsulation, increased with increasing degree of lipid unsaturation but decreased with increasing TC of the lipid composition.

Figures 3.4 show the time course of cumulative percent drug release for liposomes made from unsaturated DOPC lipid and saturated DSPC lipid. Liposomes made from the unsaturated DOPC (lowest T<sub>c</sub> of -15°C) exhibited a much higher rate of drug release (MRT 37.85h) (Table 3.1 and Table 3.2). This formulation released most of its drug (70%) within 48h and there was no further release after 48h. Liposomes made from the fully saturated DSPC (with the highest TC (54 °C) exhibited extremely lower rate of PYD release (MRT 247.7h). The lipid formulations made from POPC (TC= -5°C) had intermediate rate and duration of drug release between that of DSPC and DOPC liposomes. DSPC and DOPC have similar headgroup and both have two acyl chains of equal lengths (18 carbon). Higher drug release rate from DPPC liposomes might be due to shorter acyl chains (16 carbons) compared to other tested lipids and significant lower TC (41 °C) as apposed to DSPC (54 °C). The rate of drug release was inversely related to the chain length of the constituent lipid chains. In addition to having higher encapsulation capacity for hydrophobic drugs as, liposomes made from lipids with longer acyl chains. While these observations may suggest that the observed differences in drug release for the formulations was due to differences in TC as well as the degree of saturation, the generalization may not hold for all lipids.

We next checked the possibility of synergy between PYD and its liposomal formulation with carboplatin and oxaliplatin in two different colorectal cancer cell lines using MTT assay. Loewe

models were chosen for this analysis because Loewe model not only considers the dose equivalence principal, but also the sham combination principal which would make it the best approach for analyzing synergism in this study (113).

Our results showed that the HCT116 cell lines was more sensitive to the effect of combination therapy and interestingly the loaded drug demonstrated a higher level of synergism in comparison to the free dug. This was in line with previous observations and may be due to the effect of formulation in increasing PYD access to its intracellular target by its liposomal formulation. (118–123). Well

**Conclusions:**

The results points to liposomal formulation of pyronaridine as a nano-formulation for this novel inhibitor of ERCC1/XPF capable of sensitization of CRC cells to the anticancer activity of platinum-based chemotherapeutics.

## **Chapter four: conclusion and future work**

#### 4.1. Conclusions

The results of this study pointed to the potential of polymeric micellar formulation of A4 (PM/A4) as well as liposomal formulation of PYD as nano-chemosensitizers in the treatment of colorectal cancer when combined with carboplatin.

Our studies showed that polymeric micelles based on PEO-PBCL to be the best systems for the delivery of A4. This formulation, not only tackle the solubility issue of this compound but also controlled its release from the formulation in a biologically relevant media. The PLA assay demonstrated that 2 $\mu$ M of the A4 compound can inhibit the interaction between the ERCC1 and XPF at 24h time point. Micellar formulation of A4 compound was able to decrease the non-specific cytotoxicity of the compound to a considerable extent. Both cell lines showed a higher level of sensitivity toward carboplatin treatment in combination with either free or PM/A4. In colony forming assay, both cell lines were sensitized to the effect of Carboplatin when they received a lower concentration of A4 compound, but to show sensitivity to the effect of Oxaliplatin, they needed a higher concentration of A4 compound both as free and PM/A4.

Liposomal delivery system is the ideal way for the delivery of Pyronaridine compound. Among all the developed liposomal formulations, DSPC, DSPE-PEG200, Cholesterol with a luminal pH of 3.5 showed a considerably high encapsulation efficiency and the most desirable release profile. Based on the recent work of our colleagues, it was shown that 2 $\mu$ M of pyronaridine compound is able to inhibit the dimerization of ERCC1 and XPF (91). IC50 of both free pyronaridine and liposomal formulation of pyronaridine was assessed. Combination treatment of LPY and

Carboplatin showed a considerable level of synergism in the HCT116 cell line, while in SW620, a higher concentration of PYD demonstrated a lower level of synergism.

#### **4.2. Future works**

In the short term the following experiments should be conducted to supplement the current data: Considering that the higher concentration of PYD were able to demonstrate a considerable sensitization result in SW620 cell line, the same test will be repeated in HCT116 cell line with a higher concentration of PYD and its liposomal formulation. In order to assess if the level of sensitivity that we are observing is due to inhibition of ERCC1 and XPF interactions or potential off target activities of the compounds under study, the same set of cytotoxicity tests should be repeated in ERCC1/XPF<sup>-/-</sup> HCT116 cells available to our research group. In order to investigate if the inhibition of dimerization leads to degradation of the two proteins, a western blot test will be performed.

In the long term, conduction of pharmacokinetics and anticancer studies for both formulations in relative tumor bearing animal models of CRC alone and in combination with carboplatin is suggested.



## References:

1. International Agency for research cancer. Available from: <https://www.iarc.who.int/cancer-topics/>
2. Fouad YA, Aanei C. Revisiting the hallmarks of cancer. *Am J Cancer Res.* 2017;7(5):1016–36.
3. Kuipers EJ, Grady WM, Lieberman D, Seufferlein T, Sung JJ, Boelens PG, et al. Colorectal cancer. *Nat Rev Dis Primers.* 2015 Dec 17;1(1):15065.
4. Xi Y, Xu P. Global colorectal cancer burden in 2020 and projections to 2040. *Translational Oncology.* 2021 Oct;14(10):101174.
5. De Falco V, Napolitano S, Roselló S, Huerta M, Cervantes A, Ciardiello F, et al. How we treat metastatic colorectal cancer. *ESMO Open.* 2019;4:e000813.
6. Dekker E, Tanis PJ, Vleugels JLA, Kasi PM, Wallace MB. Colorectal cancer. *The Lancet.* 2019 Oct;394(10207):1467–80.
7. Fiori E, Lamazza A, Schillaci A, Femia S, DeMasi E, DeCesare A, et al. Palliative management for patients with subacute obstruction and stage IV unresectable rectosigmoid cancer: colostomy versus endoscopic stenting: final results of a prospective randomized trial. *The American Journal of Surgery.* 2012 Sep;204(3):321–6.
8. De Graaf EJR, Doornebosch PG, Tollenaar RAEM, Meershoek-Klein Kranenbarg E, de Boer AC, Bekkering FC, et al. Transanal endoscopic microsurgery versus total mesorectal excision of T1 rectal adenocarcinomas with curative intention. *European Journal of Surgical Oncology (EJSO).* 2009 Dec;35(12):1280–5.
9. Doornebosch PG, Zeestraten E, de Graaf EJR, Hermsen P, Dawson I, Tollenaar RAEM, et al. Transanal endoscopic microsurgery for T1 rectal cancer: size matters! *Surg Endosc.* 2012 Feb;26(2):551–7.
10. van Gijn W, Marijnen CA, Nagtegaal ID, Kranenbarg EMK, Putter H, Wiggers T, et al. Preoperative radiotherapy combined with total mesorectal excision for resectable rectal cancer: 12-year follow-up of the multicentre, randomised controlled TME trial. *The Lancet Oncology.* 2011 Jun;12(6):575–82.
11. Sauer R, Becker H, Hohenberger W, Rödel C, Wittekind C, Fietkau R, et al. Preoperative versus Postoperative Chemoradiotherapy for Rectal Cancer. *N Engl J Med.* 2004 Oct 21;351(17):1731–40.

12. Labianca R, Nordlinger B, Beretta GD, Mosconi S, Mandalà M, Cervantes A, et al. Early colon cancer: ESMO Clinical Practice Guidelines for diagnosis, treatment and follow-up. *Annals of Oncology*. 2013 Oct;24:vi64–72.
13. Lombardi L, Morelli F, Cinieri S, Santini D, Silvestris N, Fazio N, et al. Adjuvant colon cancer chemotherapy: where we are and where we'll go. *Cancer Treatment Reviews*. 2010 Nov;36:S34–41.
14. Gill S, Thomas RR, Goldberg RM. Colorectal cancer chemotherapy: REVIEW: COLORECTAL CANCER CHEMOTHERAPY. *Alimentary Pharmacology & Therapeutics*. 2003 Oct;18(7):683–92.
15. Engstrom PF, Arnoletti JP, Benson AB, Chen YJ, Choti MA, Cooper HS, et al. Colon Cancer. *J Natl Compr Canc Netw*. 2009 Sep;7(8):778–831.
16. Gustavsson B, Carlsson G, Machover D, Petrelli N, Roth A, Schmoll HJ, et al. A Review of the Evolution of Systemic Chemotherapy in the Management of Colorectal Cancer. *Clinical Colorectal Cancer*. 2015 Mar;14(1):1–10.
17. Dilruba S, Kalayda GV. Platinum-based drugs: past, present and future. *Cancer Chemother Pharmacol*. 2016 Jun;77(6):1103–24.
18. Calvert AH, Harland SJ, Newell DR, Siddik ZH, Jones AC, McElwain TJ, et al. Early clinical studies with cis-diammine-1,1-cyclobutane dicarboxylate platinum II. *Cancer Chemother Pharmacol*. 1982 Dec;9(3):140–7.
19. Abdulsalam Alharbi. Development of Novel Polymeric Micellar DACHPt for Enhanced Platinum Based Chemotherapy in Colorectal Cancer. 2019 [cited 2022 Nov 24]; Available from: <https://era.library.ualberta.ca/items/3df4e36e-00f6-492f-b26b-fe558bd22b90>
20. Ken R. Harrap. Initiatives with platinum and quinazoline-based antitumor molecules fourteenth bruce F. cain memorial award lecture. Available from: <https://aacrjournals.org/cancerres/article/55/13/2761/501203/Initiatives-with-Platinum-and-Quinazoline-based>
21. Calvert AH, Newell DR, Gumbrell LA, O'Reilly S, Burnell M, Boxall FE, et al. Carboplatin dosage: prospective evaluation of a simple formula based on renal function. *J Clin Oncol*. 1989 Nov;7(11):1748–56.
22. Kim R, Byer J, Fulp WJ, Mahipal A, Dinwoodie W, Shibata D. Carboplatin and Paclitaxel Treatment Is Effective in Advanced Anal Cancer. *Oncology*. 2014;87(2):125–32.
23. van Hagen P, Hulshof MCCM, van Lanschot JJB, Steyerberg EW, Henegouwen MI van B, Wijnhoven BPL, et al. Preoperative Chemoradiotherapy for Esophageal or Junctional Cancer. *N Engl J Med*. 2012 May 31;366(22):2074–84.

24. Gadgeel SM, Shields AF, Heilbrun LK, Labadidi S, Zalupski M, Chaplen R, et al. Phase II Study of Paclitaxel and Carboplatin in Patients With Advanced Gastric Cancer: American Journal of Clinical Oncology. 2003 Feb;26(1):37–41.
25. O’Dwyer PJ, Stevenson JP, Johnson SW. Clinical Status of Cisplatin, Carboplatin, and Other Platinum-Based Antitumor Drugs. In: Lippert B, editor. Cisplatin [Internet]. Zürich: Verlag Helvetica Chimica Acta; 2006 [cited 2022 Nov 24]. p. 29–69. Available from: <https://onlinelibrary.wiley.com/doi/10.1002/9783906390420.ch2>
26. Rabik CA, Dolan ME. Molecular mechanisms of resistance and toxicity associated with platinating agents. Cancer Treatment Reviews. 2007 Feb;33(1):9–23.
27. Lebwohl D, Canetta R. Clinical development of platinum complexes in cancer therapy: an historical perspective and an update. European Journal of Cancer. 1998 Sep;34(10):1522–34.
28. Agarwal R, Kaye SB. Ovarian cancer: strategies for overcoming resistance to chemotherapy. Nat Rev Cancer. 2003 Jul 1;3(7):502–16.
29. Martin LP, Hamilton TC, Schilder RJ. Platinum Resistance: The Role of DNA Repair Pathways. Clinical Cancer Research. 2008 Mar 1;14(5):1291–5.
30. Erasmus H, Gobin M, Niclou S, Van Dyck E. DNA repair mechanisms and their clinical impact in glioblastoma. Mutation Research/Reviews in Mutation Research. 2016 Jul;769:19–35.
31. Lewis T, Dimri M. Biochemistry, DNA Repair. In: StatPearls [Internet]. Treasure Island (FL): StatPearls Publishing; 2022 [cited 2022 Nov 25]. Available from: <http://www.ncbi.nlm.nih.gov/books/NBK560563/>
32. Sadat, Sams MA. Nanodelivery of novel inhibitors of DNA repair for enhanced cancer therapy. [cited 2022 Nov 25]; Available from: <https://era.library.ualberta.ca/items/edfcb9c9-d864-4016-aa30-0cb8f6a18177>
33. Chen Q, Van der Sluis PC, Boulware D, Hazlehurst LA, Dalton WS. The FA/BRCA pathway is involved in melphalan-induced DNA interstrand cross-link repair and accounts for melphalan resistance in multiple myeloma cells. Blood. 2005 Jul 15;106(2):698–705.
34. Elmenoufy AHM. Design, Synthesis, and Biological Evaluation of Compounds for DNA Targeted Therapy. 2020 [cited 2022 Nov 25]; Available from: <https://era.library.ualberta.ca/items/b8a0a772-df2b-4ba9-84fd-f95f99e99a81>
35. Lehmann A, Niimi A, Ogi T, Brown S, Sabbioneda S, Wing J, et al. Translesion synthesis: Y-family polymerases and the polymerase switch. DNA Repair. 2007 Jul 1;6(7):891–9.
36. Albertella MR, Lau A, O’Connor MJ. The overexpression of specialized DNA polymerases in cancer. DNA Repair. 2005 May;4(5):583–93.

37. Kelland LR, Mistry P, Abel G, Freidlos F, Loh SY, Roberts JJ, et al. Establishment and Characterization of an in Vitro Model of Acquired Resistance to Cisplatin in a Human Testicular Nonseminomatous Germ Cell Line1. *Cancer Research*. 1992 Apr 1;52(7):1710–6.
38. Scharer OD. Nucleotide Excision Repair in Eukaryotes. *Cold Spring Harbor Perspectives in Biology*. 2013 Oct 1;5(10):a012609–a012609.
39. Rosell R, Mendez P, Isla D, Taron M. Platinum Resistance Related to a Functional NER Pathway. *Journal of Thoracic Oncology*. 2007 Dec;2(12):1063–6.
40. Nospikel T. Nucleotide excision repair and neurological diseases. *DNA Repair*. 2008 Jul;7(7):1155–67.
41. Shuck SC, Short EA, Turchi JJ. Eukaryotic nucleotide excision repair: from understanding mechanisms to influencing biology. *Cell Res*. 2008 Jan;18(1):64–72.
42. Costa R. The eukaryotic nucleotide excision repair pathway. *Biochimie*. 2003 Nov;85(11):1083–99.
43. Fousteri M, Mullenders LH. Transcription-coupled nucleotide excision repair in mammalian cells: molecular mechanisms and biological effects. *Cell Res*. 2008 Jan;18(1):73–84.
44. Kartalou M, Essigmann JM. Mechanisms of resistance to cisplatin. *Mutation Research/Fundamental and Molecular Mechanisms of Mutagenesis*. 2001 Jul;478(1–2):23–43.
45. Lans H, Marteijn JA, Vermeulen W. ATP-dependent chromatin remodeling in the DNA-damage response. *Epigenetics & Chromatin*. 2012 Jan 30;5(1):4.
46. Tsodikov OV, Enzlin JH, Schärer OD, Ellenberger T. Crystal structure and DNA binding functions of ERCC1, a subunit of the DNA structure-specific endonuclease XPF–ERCC1. *Proc Natl Acad Sci USA*. 2005 Aug 9;102(32):11236–41.
47. Tripsianes K, Folkers G, Ab E, Das D, Odijk H, Jaspers NGJ, et al. The Structure of the Human ERCC1/XPF Interaction Domains Reveals a Complementary Role for the Two Proteins in Nucleotide Excision Repair. *Structure*. 2005 Dec;13(12):1849–58.
48. Choi YJ, Ryu KS, Ko YM, Chae YK, Pelton JG, Wemmer DE, et al. Biophysical Characterization of the Interaction Domains and Mapping of the Contact Residues in the XPF-ERCC1 Complex. *Journal of Biological Chemistry*. 2005 Aug;280(31):28644–52.
49. Moghimi SM, Hunter AC, Murray JC. Nanomedicine: current status and future prospects. *FASEB j*. 2005 Mar;19(3):311–30.
50. Soleymani Abyaneh H. Rational Design and Development of Nanodelivery Systems and Combination Treatments for Overcoming Chemoresistance in Solid Tumors. 2017 [cited 2022 Nov 29]; Available from: <https://era.library.ualberta.ca/items/82817f9d-0fbd-482d-a9a8-f519541231c9>

51. Phillips MA, Gran ML, Peppas NA. Targeted nanodelivery of drugs and diagnostics. *Nano Today*. 2010 Apr;5(2):143–59.
52. Dawidczyk CM, Kim C, Park JH, Russell LM, Lee KH, Pomper MG, et al. State-of-the-art in design rules for drug delivery platforms: Lessons learned from FDA-approved nanomedicines. *Journal of Controlled Release*. 2014 Aug;187:133–44.
53. Matsumura Y, Kataoka K. Preclinical and clinical studies of anticancer agent-incorporating polymer micelles. *Cancer Science*. 2009 Apr;100(4):572–9.
54. Houdaihed L, Evans JC, Allen C. Overcoming the Road Blocks: Advancement of Block Copolymer Micelles for Cancer Therapy in the Clinic. *Mol Pharmaceutics*. 2017 Aug 7;14(8):2503–17.
55. Estanqueiro M, Amaral MH, Conceição J, Sousa Lobo JM. Nanotechnological carriers for cancer chemotherapy: The state of the art. *Colloids and Surfaces B: Biointerfaces*. 2015 Feb;126:631–48.
56. Balogh LP, editor. *Nano-enabled medical applications*. Singapore: Jenny Stanford Publishing Pte. Ltd.; 2021.
57. Torchilin VP. Multifunctional, stimuli-sensitive nanoparticulate systems for drug delivery. *Nat Rev Drug Discov*. 2014 Nov;13(11):813–27.
58. Pérez-Herrero E, Fernández-Medarde A. Advanced targeted therapies in cancer: Drug nanocarriers, the future of chemotherapy. *European Journal of Pharmaceutics and Biopharmaceutics*. 2015 Jun;93:52–79.
59. Lee J, Lee H, Andrade J. Blood compatibility of polyethylene oxide surfaces. *Progress in Polymer Science*. 1995;20(6):1043–79.
60. Torchilin VP, Papisov MI. Why do Polyethylene Glycol-Coated Liposomes Circulate So Long?: Molecular Mechanism of Liposome Steric Protection with Polyethylene Glycol: Role of Polymer Chain Flexibility. *Journal of Liposome Research*. 1994 Jan;4(1):725–39.
61. Kommareddy S, Tiwari SB, Amiji MM. Long-Circulating Polymeric Nanovectors for Tumor-Selective Gene Delivery. *Technol Cancer Res Treat*. 2005 Dec;4(6):615–25.
62. Soleymani Abyaneh H, Vakili MR, Zhang F, Choi P, Lavasanifar A. Rational design of block copolymer micelles to control burst drug release at a nanoscale dimension. *Acta Biomaterialia*. 2015 Sep;24:127–39.
63. Aliabadi HM, Lavasanifar A. Polymeric micelles for drug delivery. *Expert Opinion on Drug Delivery*. 2006 Jan;3(1):139–62.
64. Bozzuto G, Molinari A. Liposomes as nanomedical devices. *IJN*. 2015 Feb;975.

65. Lasic DD, Frederik PM, Stuart MCA, Barenholz Y, McIntosh TJ. Gelation of liposome interior A novel method for drug encapsulation. *FEBS Letters*. 1992 Nov 9;312(2–3):255–8.
66. Zamboni WC. Liposomal, Nanoparticle, and Conjugated Formulations of Anticancer Agents. *Clinical Cancer Research*. 2005 Dec 1;11(23):8230–4.
67. Drummond DC, Meyer O, Hong K, Kirpotin DB, Papahadjopoulos D. Optimizing Liposomes for Delivery of Chemotherapeutic Agents to Solid Tumors. *Pharmacol Rev*. 1999 Dec 1;51(4):691.
68. Papahadjopoulos D, Allen TM, Gabizon A, Mayhew E, Matthay K, Huang SK, et al. Sterically stabilized liposomes: improvements in pharmacokinetics and antitumor therapeutic efficacy. *Proc Natl Acad Sci USA*. 1991 Dec 15;88(24):11460–4.
69. Barenholz Y. Relevancy of Drug Loading to Liposomal Formulation Therapeutic Efficacy. *Journal of Liposome Research*. 2003 Jan;13(1):1–8.
70. Allen TM, Hansen C. Pharmacokinetics of stealth versus conventional liposomes: effect of dose. *Biochimica et Biophysica Acta (BBA) - Biomembranes*. 1991 Sep;1068(2):133–41.
71. Elmenoufy AH, Gentile F, Jay D, Karimi-Busheri F, Yang X, Soueidan OM, et al. Targeting DNA Repair in Tumor Cells via Inhibition of ERCC1–XPF. *J Med Chem*. 2019 Sep 12;62(17):7684–96.
72. Wang Y, Zhang Z, Xu S, Wang F, Shen Y, Huang S, et al. pH, redox and photothermal tri-responsive DNA/polyethylenimine conjugated gold nanorods as nanocarriers for specific intracellular co-release of doxorubicin and chemosensitizer pyronaridine to combat multidrug resistant cancer. *Nanomedicine: Nanotechnology, Biology and Medicine*. 2017 Jul;13(5):1785–95.
73. Qi J, Wang S, Liu G, Peng H, Wang J, Zhu Z, et al. Pyronaridine, a novel modulator of P-glycoprotein-mediated multidrug resistance in tumor cells in vitro and in vivo. *Biochemical and Biophysical Research Communications*. 2004 Jul;319(4):1124–31.
74. Biller LH, Schrag D. Diagnosis and Treatment of Metastatic Colorectal Cancer: A Review. *JAMA*. 2021 Feb 16;325(7):669.
75. Buyana B, Naki T, Alven S, Aderibigbe BA. Nanoparticles Loaded with Platinum Drugs for Colorectal Cancer Therapy. *IJMS*. 2022 Sep 24;23(19):11261.
76. Hector S, Bolanowska-Higdon W, Zdanowicz J, Hitt S, Pendyala L. In vitro studies on the mechanisms of oxaliplatin resistance. *Cancer Chemother Pharmacol*. 2001 Nov;48(5):398–406.
77. Shen B, Mao W, Ahn J, Chung P, He P. Mechanism of HN-3 cell apoptosis induced by carboplatin: Combination of mitochondrial pathway associated with Ca<sup>2+</sup> and the nucleus

pathways. Mol Med Report [Internet]. 2018 Sep 24 [cited 2022 Dec 20]; Available from: <http://www.spandidos-publications.com/10.3892/mmr.2018.9507>

78. Hall MD, Okabe M, Shen DW, Liang XJ, Gottesman MM. The Role of Cellular Accumulation in Determining Sensitivity to Platinum-Based Chemotherapy. *Annu Rev Pharmacol Toxicol*. 2008 Feb 1;48(1):495–535.
79. Knipp M. Metallothioneins and Platinum(II) Anti-Tumor Compounds. *CMC*. 2009 Feb 1;16(5):522–37.
80. McNeil EM, Astell KR, Ritchie AM, Shave S, Houston DR, Bakrania P, et al. Inhibition of the ERCC1–XPF structure-specific endonuclease to overcome cancer chemoresistance. *DNA Repair*. 2015 Jul 1;31:19–28.
81. de Laat WL, Appeldoorn E, Jaspers NGJ, Hoeijmakers JHJ. DNA Structural Elements Required for ERCC1-XPF Endonuclease Activity. *Journal of Biological Chemistry*. 1998 Apr;273(14):7835–42.
82. Gaillard PHL. Activity of individual ERCC1 and XPF subunits in DNA nucleotide excision repair. *Nucleic Acids Research*. 2001 Feb 15;29(4):872–9.
83. Jordheim LP, Barakat KH, Heinrich-Balard L, Matera EL, Cros-Perrial E, Bouledrak K, et al. Small Molecule Inhibitors of ERCC1-XPF Protein-Protein Interaction Synergize Alkylating Agents in Cancer Cells. *Mol Pharmacol*. 2013 Jul;84(1):12–24.
84. Gentile F, Elmenoufy AH, Ciniero G, Jay D, Karimi-Busheri F, Barakat KH, et al. Computer-aided drug design of small molecule inhibitors of the ERCC1-XPF protein–protein interaction. *Chem Biol Drug Des*. 2020 Apr;95(4):460–71.
85. Ciniero G, Elmenoufy AH, Gentile F, Weinfeld M, Deriu MA, West FG, et al. Enhancing the activity of platinum-based drugs by improved inhibitors of ERCC1–XPF-mediated DNA repair. *Cancer Chemother Pharmacol*. 2021 Feb;87(2):259–67.
86. Mahmud A, Xiong XB, Lavasanifar A. Novel Self-Associating Poly(ethylene oxide)- *b* lock - poly( $\epsilon$ -caprolactone) Block Copolymers with Functional Side Groups on the Polyester Block for Drug Delivery. *Macromolecules*. 2006 Dec 1;39(26):9419–28.
87. Aliabadi HM, Mahmud A, Sharifabadi AD, Lavasanifar A. Micelles of methoxy poly(ethylene oxide)-*b*-poly( $\epsilon$ -caprolactone) as vehicles for the solubilization and controlled delivery of cyclosporine A. *Journal of Controlled Release*. 2005 May;104(2):301–11.
88. Saqr A, Vakili MR, Huang YH, Lai R, Lavasanifar A. Development of Traceable Rituximab-Modified PEO-Polyester Micelles by Postinsertion of PEG-phospholipids for Targeting of B-cell Lymphoma. *ACS Omega*. 2019 Nov 12;4(20):18867–79.

89. de Paiva IM, Vakili MR, Soleimani AH, Tabatabaei Dakhili SA, Munira S, Paladino M, et al. Biodistribution and Activity of EGFR Targeted Polymeric Micelles Delivering a New Inhibitor of DNA Repair to Orthotopic Colorectal Cancer Xenografts with Metastasis. *Mol Pharmaceutics*. 2022 Mar 10;acs.molpharmaceut.1c00918.
90. Sadat SMA, Vakili MR, Paiva IM, Weinfeld M, Lavasanifar A. Development of Self-Associating SN-38-Conjugated Poly(ethylene oxide)-Poly(ester) Micelles for Colorectal Cancer Therapy. *Pharmaceutics*. 2020 Oct 29;12(11):1033.
91. Jackson N, Alhussan A, Bromma K, Jay D, Donnelly JC, West FG, et al. Repurposing Antimalarial Pyronaridine as a DNA Repair Inhibitor to Exploit the Full Potential of Gold-Nanoparticle-Mediated Radiation Response. *Pharmaceutics*. 2022 Dec 14;14(12):2795.
92. Weilbeer C, Jay D, Donnelly JC, Gentile F, Karimi-Busheri F, Yang X, et al. Modulation of ERCC1-XPF Heterodimerization Inhibition via Structural Modification of Small Molecule Inhibitor Side-Chains. *Front Oncol*. 2022 Mar 17;12:819172.
93. Xiong XB, Ma Z, Lai R, Lavasanifar A. The therapeutic response to multifunctional polymeric nano-conjugates in the targeted cellular and subcellular delivery of doxorubicin. *Biomaterials*. 2010 Feb;31(4):757–68.
94. Franken NAP, Rodermond HM, Stap J, Haveman J, van Bree C. Clonogenic assay of cells in vitro. *Nat Protoc*. 2006 Dec;1(5):2315–9.
95. Florea AM, Büsselberg D. Cisplatin as an Anti-Tumor Drug: Cellular Mechanisms of Activity, Drug Resistance and Induced Side Effects. *Cancers*. 2011 Mar 15;3(1):1351–71.
96. Araghi M, Soerjomataram I, Jenkins M, Brierley J, Morris E, Bray F, et al. Global trends in colorectal cancer mortality: projections to the year 2035. *Int J Cancer*. 2019 Jun 15;144(12):2992–3000.
97. Kuipers EJ, Rösch T, Bretthauer M. Colorectal cancer screening—optimizing current strategies and new directions. *Nat Rev Clin Oncol*. 2013 Mar;10(3):130–42.
98. van de Velde CJH, Boelens PG, Borrás JM, Coebergh JW, Cervantes A, Blomqvist L, et al. EURECCA colorectal: Multidisciplinary management: European consensus conference colon & rectum. *European Journal of Cancer*. 2014 Jan;50(1):1.e1-1.e34.
99. van de Velde CJH, Boelens PG, Tanis PJ, Espin E, Mroczkowski P, Naredi P, et al. Experts reviews of the multidisciplinary consensus conference colon and rectal cancer 2012. *European Journal of Surgical Oncology (EJSO)*. 2014 Apr;40(4):454–68.
100. Quirke P, West NP, Nagtegaal ID. EURECCA consensus conference highlights about colorectal cancer clinical management: the pathologists expert review. *Virchows Archiv*. 2014;464(2):129–34.



101. Tudyka V, Blomqvist L, Beets-Tan RGH, Boelens PG, Valentini V, Van De Velde CJ, et al. EURECCA consensus conference highlights about colon & rectal cancer multidisciplinary management: the radiology experts review. *European Journal of Surgical Oncology (EJSO)*. 2014;40(4):469–75.
102. Valentini V, Glimelius B, Haustermans K, Marijnen CA, Rödel C, Gambacorta MA, et al. EURECCA consensus conference highlights about rectal cancer clinical management: the radiation oncologist's expert review. *Radiotherapy and Oncology*. 2014;110(1):195–8.
103. Van de Velde CJ, Aristei C, Boelens PG, Beets-Tan RG, Blomqvist L, Borrás JM, et al. EURECCA colorectal: multidisciplinary mission statement on better care for patients with colon and rectal cancer in Europe. *European Journal of Cancer*. 2013;49(13):2784–90.
104. Villanueva PJ, Martínez A, Baca ST, DeJesus RE, Larragoity M, Contreras L, et al. Pyronaridine exerts potent cytotoxicity on human breast and hematological cancer cells through induction of apoptosis. Tan M, editor. *PLoS ONE*. 2018 Nov 5;13(11):e0206467.
105. Adegoke O, Babalola C, Oshitade O, Famuyiwa A. Determination of the physicochemical properties of pyronaridine - a new antimalarial drug. *Pakistan journal of pharmaceutical sciences*. 2006 Feb 1;19:1–6.
106. Tenchov R, Bird R, Curtze AE, Zhou Q. Lipid Nanoparticles—From Liposomes to mRNA Vaccine Delivery, a Landscape of Research Diversity and Advancement. *ACS Nano*. 2021 Nov 23;15(11):16982–7015.
107. Biosca A, Dirscherl L, Moles E, Imperial S, Fernández-Busquets X. An ImmunoPEGLiposome for Targeted Antimalarial Combination Therapy at the Nanoscale. *Pharmaceutics*. 2019 Jul 16;11(7):341.
108. Biosca A, Dirscherl L, Moles E, Imperial S, Fernández-Busquets X. An ImmunoPEGLiposome for Targeted Antimalarial Combination Therapy at the Nanoscale. *Pharmaceutics*. 2019 Jul 16;11(7):341.
109. Dua JS, Rana AC, Bhandari AK. Liposome: methods of preparation and applications.
110. Théry C, Amigorena S, Raposo G, Clayton A. Isolation and Characterization of Exosomes from Cell Culture Supernatants and Biological Fluids. *Current Protocols in Cell Biology* [Internet]. 2006 Mar [cited 2022 Oct 19];30(1). Available from: <https://onlinelibrary.wiley.com/doi/10.1002/0471143030.cb0322s30>
111. Baxa U. Imaging of Liposomes by Transmission Electron Microscopy. In: McNeil SE, editor. *Characterization of Nanoparticles Intended for Drug Delivery* [Internet]. New York, NY: Springer New York; 2018 [cited 2022 Sep 15]. p. 73–88. (Methods in Molecular Biology; vol. 1682). Available from: [http://link.springer.com/10.1007/978-1-4939-7352-1\\_8](http://link.springer.com/10.1007/978-1-4939-7352-1_8)

112. Di Veroli GY, Fornari C, Wang D, Mollard S, Bramhall JL, Richards FM, et al. Combenefit: an interactive platform for the analysis and visualization of drug combinations. *Bioinformatics*. 2016 Sep 15;32(18):2866–8.
113. Foucquier J, Guedj M. Analysis of drug combinations: current methodological landscape. *Pharmacol Res Perspect*. 2015 Jun;3(3):e00149.
114. de Almeida LC, Calil FA, Machado-Neto JA, Costa-Lotufo LV. DNA damaging agents and DNA repair: From carcinogenesis to cancer therapy. *Cancer Genetics*. 2021 Apr;252–253:6–24.
115. Chemaxon [Internet]. Available from: <https://chemaxon.com/calculators-and-predictors>
116. Ruscoe JE, Tingle MD, O'Neill PM, Ward SA, Park BK. Effect of Disposition of Mannich Antimalarial Agents on Their Pharmacology and Toxicology. *Antimicrob Agents Chemother*. 1998 Sep;42(9):2410–6.
117. Croft SL, Duparc S, Arbe-Barnes SJ, Craft JC, Shin CS, Fleckenstein L, et al. Review of pyronaridine anti-malarial properties and product characteristics. *Malar J*. 2012 Dec;11(1):270.
118. Wong HL, Bendayan R, Rauth AM, Wu XY. Simultaneous delivery of doxorubicin and GG918 (Elacridar) by new Polymer-Lipid Hybrid Nanoparticles (PLN) for enhanced treatment of multidrug-resistant breast cancer. *Journal of Controlled Release*. 2006 Dec;116(3):275–84.
119. Hasenstein JR, Shin HC, Kasmerchak K, Buehler D, Kwon GS, Kozak KR. Antitumor Activity of Triolimus: A Novel Multidrug-Loaded Micelle Containing Paclitaxel, Rapamycin, and 17-AAG. *Molecular Cancer Therapeutics*. 2012 Oct 1;11(10):2233–42.
120. Shuhendler AJ, O'Brien PJ, Rauth AM, Wu XY. On the synergistic effect of doxorubicin and mitomycin C against breast cancer cells. *Drug metabolism and drug interactions*. 2007;22(4):201–34.
121. Harasym TO, Tardi PG, Harasym NL, Harvie P, Johnstone SA, Mayer LD. Increased preclinical efficacy of irinotecan and floxuridine coencapsulated inside liposomes is associated with tumor delivery of synergistic drug ratios. *Oncology Research Featuring Preclinical and Clinical Cancer Therapeutics*. 2006;16(8):361–74.
122. Zhang RX, Cai P, Zhang T, Chen K, Li J, Cheng J, et al. Polymer–lipid hybrid nanoparticles synchronize pharmacokinetics of co-encapsulated doxorubicin–mitomycin C and enable their spatiotemporal co-delivery and local bioavailability in breast tumor. *Nanomedicine: Nanotechnology, Biology and Medicine*. 2016;12(5):1279–90.
123. Zhang RX, Wong HL, Xue HY, Eoh JY, Wu XY. Nanomedicine of synergistic drug combinations for cancer therapy – Strategies and perspectives. *Journal of Controlled Release*. 2016 Oct;240:489–503.